Experimental research into the effect of freeboard on the stability of a crown wall on a rubble mound breakwater

M.Sc. Thesis

March 14, 2017

Experimental research into the effect of freeboard on the stability of a crown wall on a rubble mound breakwater

by

J.F. Bekker

in partial fulfillment of the requirements for the degree of

Master of Science

in Hydraulic Engineering

at the Delft University of Technology,

to be defended publicly on March 29, 2017 at 15:00 AM.

Chairman:	Prof.dr. ir. W.S.J. Uijttewaal,	TU Delft
Thesis committee:	Dr. ir. B. Hofland,	TU Delft
	Ir. H.J. Verhagen,	TU Delft
	Ir. G. Smith,	Van Oord

TU Delft Delft University of Technology

Van Oord Marine ingenuity

Preface

This Master Thesis has been carried out in order to obtain the degree of Master of Science at Delft University of Technology. The project has been accomplished in association with Dutch marine contractor Van Oord.
The experimental research took place in the Waterlab of the Faculty of Civil Engineering & Geosciences in Delft, the Netherlands. The writing of this thesis took place at the headquarters of Van Oord in Rotterdam.
The cooperation between the TU Delft and Van Oord has led to a knowledge expansion about the stability of a crown wall on top of a rubble mound breakwater.

In March 2016 I started working on this study. Now, a year later in March 2017 I can proudly present the final version of this thesis. This could not be established without the support and help of many persons.
First of all I would like to thank the members of my graduation committee, prof. dr. ir. W.S.J. Uijttewaal, dr. ir. B. Hofland, ir. H.J. Verhagen and ir. G. Smith. The committee meetings were inspiring and you provided useful information, insight, feedback and guidance. Special thanks go to my daily supervisor of the TU Delft, Bas Hofland, whose enthusiasm and profound knowledge were encouraging and always kept me motivating in doing this research. Thanks to my supervisor at Van Oord, Greg Smith, who provided useful practical insight and information with respect to scaled model tests.
I would like to thank the Waterlab-personnel for helping me with the set-up of the model and other practical challenges.

I express my gratitude to Dirk Hamer, who gave me the opportunity to graduate at Van Oord. Dirk has always been interested in this research, took time whenever this was needed and provided useful organizational guidance.

On a personal note, I would like to thank my good friends and study mates for having such a great time in Delft in which study and relaxation alternated in balance. I want to thank my family, especially my parents and brother who have supported me throughout my entire study and form the basis for me as a person.
Lastly but not least, I want to express my deep respect to my girlfriend, for her unconditional love, support and patience during this graduation period.

Rotterdam, March, 2017

Jeroen Bekker

Summary

In this thesis the stability of a crown wall on top of a rubble mound breakwater under influence of wave loading is examined. A crown wall is a gravity based L- shaped concrete structure which gains stability due to its own weight and friction between the base and contact surface of the rubble mound.
The main function of a crown wall is to reduce wave overtopping. Secondly, the flat surface enables transport on the breakwater for maintenance purposes and to place pipelines on top of the structure. From a economical prospective a crown wall gives the breakwater more height in a cheaper way than placing rubble mound up to that same height.

Marine contractor Van Oord was awarded to extend a breakwater with a crown wall on top in Constanta, Romania. The design of the breakwater, made by a local consultant, was reviewed by Van Oord, which led to the conclusion that the crown wall would be blown of the breakwater for that particular design in combination with the design wave conditions. Subsequently, physical scaled model tests were executed by Artelia in Grenoble, but, against all expectations the crown wall appeared to remain stable.

Based on the contradiction between stability calculations and the outcome of the scaled model tests, the hypothesis arose that currently used wave load calculation methods lead to designs that seem to be too conservative especially when freeboard increases. Freeboard can be defined as base freeboard R_b or armour crest freeboard R_{ca} which is shown in figure 1.

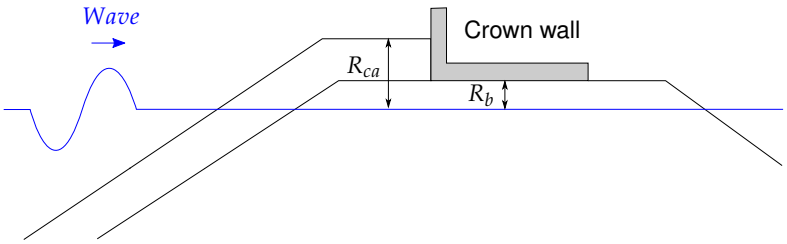

Figure 1: A wave approaches a crown wall on top of a rubble mound breakwater. The armour crest freeboard R_{ca} and base freeboard R_b are defined.

This hypothesis is the motivation for this thesis from which the following research question is defined:

'What causes current design methods to be not accurate enough in the design of the crown wall on top of a rubble mound breakwater?'

In order to answer this question, an experimental research is carried out in which a number of study steps must be reached. In first step the effect and shape of upward pressures acting on the base of the crown wall is described. Secondly, a relationship for the vertical loads as function of wave condition and freeboard is determined. Thirdly, the possible presence of phase lag between maximum horizontal- and vertical loads is investigated. Lastly, a dataset of critical weights is generated from which design guidelines are defined which could be used for a first estimate of the weight in designing the crown wall.

A physical scaled model (1:30) in a wave flume is used to execute experiments in which the stability of the crown wall is explored.
On top of a rubble mound breakwater, which includes a core and armour layer, three crown wall elements are placed which are loaded by swell waves and storm waves. Different test conditions are used in which freeboard, wave height and wave period are varied whereas geometric parameters remain unchanged. Tests are divided in the following three main subjects: pressure measurements, uplift stability and overall stability.

Based on pressure measurements it is concluded that the mostly used design method PEDERSEN [1996] and its extended version of NØRGAARD *et al.* [2013], assume an upward pressure distribution which is too conservative in shape and distance over which pressure is exerted against the base of the crown wall. These methods assume a linear pressure distribution, but seems to be conservative based on test results since S-shaped and parabolic upward pressure distributions are found. Furthermore, it is assumed that upward pressure acts over the full length of the base whatever wave conditions and freeboard are. However, a relation is found which indicates that the effective length of the upward pressure x_c actually depends on wave height and freeboard, see figure 2.

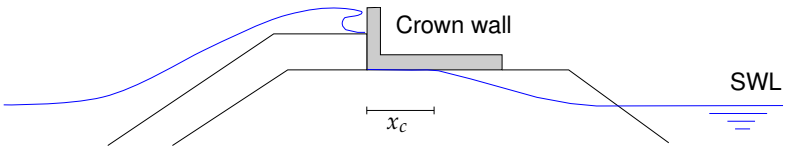

Figure 2: Wave impact on the crown wall, water hits the base over a length x_c

Comparing the predicted vertical loads based on the methods of PEDERSEN [1996] and NØRGAARD *et al.* [2013] to the found vertical loads derived from uplift stability in this research, it is observed that substantial overpredictions arise when $R_b > 0$, which is in accordance to the reduction of effective length x_c for increasing freeboard.

Generated data with respect to critical weights confirms that the conventional methods of PEDERSEN [1996] and NØRGAARD *et al.* [2013] are too conservative in

predicting overall stability with respect to sliding failure, especially when $R_b > 0$. By implementing the found relations for the effective length x_c, PEDERSEN [1996] but especially NØRGAARD *et al.* [2013] suddenly become more reliable with respect to the found critical weights.

The presented design guidelines for critical weights and effective length are advised to use for prior design purposes in combination with the adapted method of NØRGAARD *et al.* [2013] in which a reduction coefficient γ_v, based on x_c, must be taken into account for the vertical load.

Since the range of application for the critical weight guidelines is still small it is recommended to extend this range by varying more parameters in further research, which should make these equations generally better applicable.

Contents

List of symbols

b	Empirical coefficient	[-]
B_a	Armour berm width	[m]
B_c	Base length of the crown wall	[m]
d_{85}	85% - value of grading curve	[m]
d_{15}	15% - value of grading curve	[m]
$d_{n,50}$	Nominal stone diameter	[m]
d	Structure height	[m]
d_a	Thickness of armour layer in front of the crown wall	[m]
d_c	Crown wall height	[m]
d_{ca}	Unprotected height of the crown wall	[m]
$d_{c,prot}$	Protected height of the crown wall	[m]
e_1	Empirical coefficient	[-]
e_2	Empirical coefficient	[-]
F	Force exerted on the crown wall	[N/m]
F_B	Buoyancy induced vertical load	[N/m]
F_G	Nett own weight of the crown wall	[N/m]
$F_{H,max}$	Maximum horizontal force	[N/m]
$F_{H,0.1\%}$	Horizontal force with 0.1% probability of occurrence	[N/m]

F_T	Tensile force	[N/m]
$F_{V,max}$	Maximum vertical force	[N/m]
g	Gravitation acceleration	[m/s^2]
h	Water depth	[m]
h_t	Depth of toe below SWL	[m]
H	Wave height (regular waves)	[m]
$H_{0.1\%}$	Wave height with 0.1% probability of occurrence	[N/m]
H_s	Significant wave height	[m]
L_{0m}	Deep water wave length corresponding to T_m	[m]
L_{0p}	Deep water wave length corresponding to T_p	[m]
M	Moment exerted on crown wall	[Nm/m]
$M_{H,0.1\%}$	Overturning moment with 0.1% probability of occurrence	[Nm/m]
p_m	Stagnation pressure at crown wall face due to wave impact	[N/m^2/m]
P_b	Wave pressure at the base of the crown wall	[N/m^2/m]
p_{s_o}	Dynamic impact pressure based on s_0	[N/m^2/m]
p_u	Uplift wave pressure at crown wall base	[N/m^2/m]
$p_{U,0.1\%}$	Uplift pressure with 0.1% probability of occurrence	[N/m^2/m]
p_r	Reflecting pressure	[N/m^2/m]
R_b	Base freeboard	[m]
R_c	Crown wall crest freeboard	[m]
R_{ca}	Armour crest freeboard	[m]
R_u	Vertical run-up level above SWL	[m]
$R_{u,0.1\%}$	Run-up level above SWL with 0.1% probability of occurrence	[m]
S	Damage number	[-]
s_o	Maximum run-up level at the seaward edge of armour crest	[m]
s_{0p}	Fictitious wave steepness: H_s/L_{0p}	[-]

t_a	Armour layer thickness	[m]
t_f	Filter layer thickness	[m]
T_p	Peak wave period	[s]
T_m	Average wave period	[s]
T	Wave period (regular waves)	[s]
V_1, V_2	Volumes	[m^3/m]
W	Weight of the crown wall	[N/m]
x_c	Length of the base which is covered by water during loading	[m]
x_u	Length of the base which is uncovered by water during loading	[m]
x_G	Distance from turning point to centre of gravity of the crown wall	[m]
x_V	Distance from turning point to point of action of vertical force	[m]
y	Vertical run-up wedge thickness	[m]
y_{eff}	Effective wave pressure impact zone height	[m]
α	Structure slope angle	[°]
γ_v	Reduction factor for uplift pressure/vertical force	[-]
λ	Reduction coefficient for dynamic impact pressure through the armour	[-]
μ_s	Static friction coefficient	[-]
$\mu_{s,wet}$	Static friction coefficient for wet conditions	[-]
$\mu_{s,dry}$	Static friction coefficient for dry conditions	[-]
ρ_w	Density of water	[kg/m^3]
ρ_s	Density of stone or concrete	[kg/m^3]
Δ	Relative density $(\rho_s - \rho_w)/\rho_w$	[-]
ξ	Breaker parameter: $\tan\alpha/\sqrt{H_s/L}$	[-]
ξ_m	Breaker parameter based on $L_0 m$	[-]
ν	Kinematic viscosity	[m^2/s]

1

Introduction

1.1 Background

A formal definition of a breakwater is found in VERHAGEN *et al.* [2012]: "Breakwaters are widely used throughout the world. This type of structure is primarily designed for the protection of vessels harboured within ports and for port facilities from wave action, but sometimes breakwaters are also used to protect beaches from erosion or to protect valuable habitats that are threatened by the destructive forces of the sea." An example of a breakwater and its function is shown in figure 1.1. Waves arrive from the seaside and hit the breakwater which protects the lee side from this wave impact.

Figure 1.1: Nobby's breakwater, Newcastle (R. Foong (2013))

A breakwater often exists of an armour layer, filter layer and a core. These layers exist of different stone sizes whereas geotextile could also be used for the filter

layer. A breakwater is permeable, water can flow from the sea side through the structure to the lee-side.
Since breakwaters are huge structures in which a large amount of stones and types are used it could become really expensive to built them from solely rubble mound.

Therefore, in order to give the breakwater some extra height in a less expensive way, a crown wall could be used. A crown wall is a gravity based L-shaped concrete structure, which is placed on top of a breakwater. An example is shown in figure 1.2.
A crown wall has several functions. First of all, it reduces the amount of overtopping, and secondly, transport in the form of vehicles and pipelines will be enabled due to the created flat surface.

Figure 1.2: Crown wall on top of a breakwater at Dikkowita Port (www.xbloc.com)

1.2 Research motivation

Dutch marine contractor Van Oord was awarded to extend an existing breakwater by more than 1 km with on top of it a crown wall. This breakwater defends Constanţa in which the largest Romanian port of the Black Sea is located.
The breakwater was designed by a local consultant. This design was checked by Van Oord using existing wave load calculation methods in order to determine the expected wave loads on the crown wall. Based on these calculations it was concluded that the crown wall would fail (sliding) when loaded by the given wave conditions.
Therefore, on behalf of Van Oord, physical scaled tests were done by Artelia in Grenoble in which a 1:50 scaled test model was objected to representative wave loads to verify these outcomes. However, against all expectations the crown wall appeared to remain stable, which led to some contradictions.

Due to the different outcomes between the laboratory observations and design calculations it is suspected that the selected method to determine loads on crown wall elements is too conservative, especially when the water level goes down and freeboard R_b (vertical distance between water level and base of crown wall) is introduced, see figure 1.3. Freeboard can also be indicated with respect to the armour crest R_{ca}.

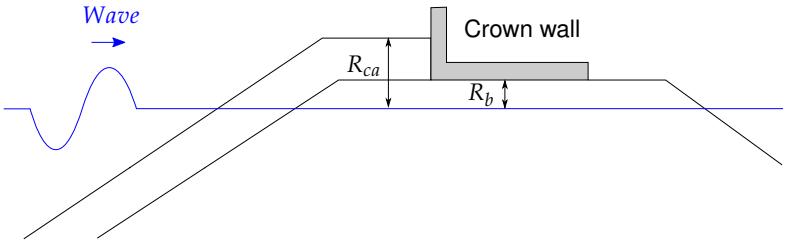

Figure 1.3: A wave approaches a crown wall on top of a rubble mound breakwater. The armour crest freeboard R_{ca} and base freeboard R_b are defined.

Due to a conservative design formula an over-dimensioning takes place which means a structure that is not economical. For a contractor as Van Oord it is desirable to obtain insight in this conservativeness in order to design more economical and thus reduce construction costs.
In this research an analysis is made to find out where this conservativeness comes from. Furthermore, recommendations are given in order to adapt some of the existing design methods. Based on these findings and contradictions the following research question is defined:

'What causes current design methods to be not accurate enough in the design of the crown wall on top of a rubble mound breakwater?'

1.3 Study steps and method

A literature study is carried out to gain more insight in the wave loads on the crown wall. It appears that the following knowledge gaps exist which are associated with the problem:

- Little data is available about the effect of varying freeboard on the stability of the crown wall as function of wave conditions;
- The distribution of the upward pressure against the base slab as a function of freeboard and wave conditions is not sufficiently known;
- Insufficient knowledge about the highly possible phase lag between the horizontal and vertical loads as function of freeboard and wave conditions.

Study steps

Based on these knowledge gaps the following study steps are defined:

1. Investigate the effect and shape of upward pressure distribution on the base as function of freeboard;

2. Define a relationship between vertical loads on the crown wall as function of wave conditions and freeboard;
3. Describe any existing phase difference between the horizontal and vertical loads as function of freeboard;
4. Generate a dataset of critical weights as function of wave conditions and freeboard.
5. Define design guidelines, based on collected data, and describe how current design methods could be improved.

Method

An experimental research is executed in which a physical scaled model is used to investigate the stability of the crown wall as function of hydraulic- and physical parameters. In order to reach the study steps pressures will be measured, uplift stability is tested and lastly a dataset is generated for overall stability.

1.4 Report outline

This section briefly addresses what is treated in the chapters of this report.

Chapter 2: Crown wall on a rubble mound breakwater

In this chapter a background is given of the relevant information of rubble mound breakwaters with on top a crown wall. It gives physical properties of the structure and what the consequences are for the loading and stability of the crown wall.

Chapter 3: Wave load calculation methods

In this chapter the existing wave load calculation methods are given. It appears that one certain method is mostly used in practice since it is the most reliable one. This method, which already has been extended, is treated in more detail.

Chapter 4: Main findings from literature

Main findings from chapters 2 and 3 are summarized and knowledge gaps are defined.

Chapter 5: Methodology

The method of this research is introduced and explained how tests are carried out and what is tested.

Chapter 6: Experimental set-up

The physical scaled model, the set-up and measurement instruments are described in detail.

Chapter 7: Experimental results and analysis

All relevant findings and results are given. These results are analysed, compared to existing theory, whereafter conclusions are drawn. Finally, a proposal is given how existing methods could be improved and design guidelines are presented for critical weights.

Chapter 8: Conclusions and recommendations

Conclusions about the study steps are given and the research question is answered. Finally, recommendations are given for further research into this subject.

2

Crown wall on a rubble mound breakwater

The following sections provide an overview of physical properties of rubble mound breakwaters with a crown wall on top. Furthermore, existing literature about the loading of the structure and stability of the crown wall is presented.

2.1 Rubble mound breakwater

There are many configurations of a crown wall on a rubble mound breakwater, an example is given in figure 2.1. A breakwater consists of rock from a quarry, known as rubble mound, and since there are no water sealing layers included it is a permeable structure in which water can flow freely from the sea- to the lee side.
Different layers can be distinguished which have their own function, stone sizes and gradings.

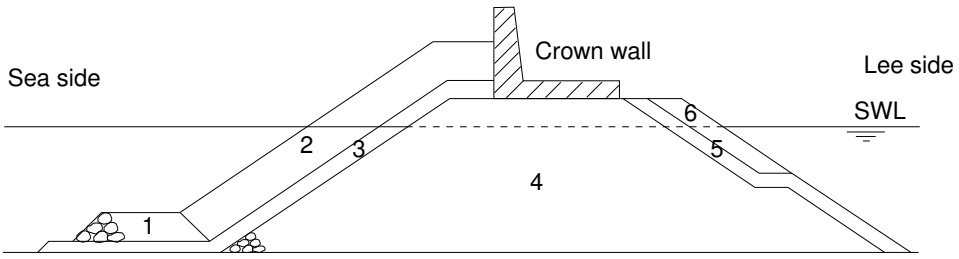

Figure 2.1: Cross section of a breakwater with on top a crown wall

Indication #	Description
1	Toe
2	Armour layer (outer slope)
3	Filter layer (outer slope)
4	Core
5	Filter layer (inner slope)
6	Armour layer (outer slope)

2.1.1 Armour layer

The outer armour layer is subjected to direct wave attack (heavy loads) and protects the whole structure from failure. The inner armour layer prevents the breakwater from failure due to overtopping water.
Different kinds of material are used for armour protection, for example large stone sizes of quarried rock or special designed heavy concrete elements like X-blocks or Core-locs could be used as well, see figure 2.2. In the case of rubble mound, it is generally the heaviest fraction of the quarry yield curve with a narrow grading ($d_{85}/d_{15} < 1.5$) [VERHAGEN *et al.*, 2012].
The armour layer is usually designed according to the Hudson or van der Meer formula. Van der Meer gives the most advanced equation since parameters like permeability, wave steepness and damage level are included. Stability of a rock armour is usually indicated by the stability number $S = H_s/\Delta d_{n50}$.

(a) **(b)**

Figure 2.2: a) Xblocs used as armour layer, (www.xbloc.com) b) Core locs used as armour layer, (www.concretelayer.com)

2.1.2 Toe

According to VERHAGEN *et al.* [2012] wave action is limited from about one wave height below still water level. Heavy armour is not necessary any more, in that case a toe protection is regularly used. An optimization of a toe could lead to a reduction in construction costs.

2.1.3 Core

The core is the foundation of the breakwater and is usually situated directly under the first layer (filter in this case). The core is filled with fine materials (small stone sizes). The crown wall is positioned straight on top of this core.

2.1.4 Filter layer

A filter layer is used to prevent the core material to wash out since this exists of fine material.

2.2 Crown wall

A crown wall is a gravity based L-shaped concrete structure which rests on top of the breakwater. There are several ways in which crown walls can be placed on top of a rubble mound breakwater. According to BURCHARTH [1992] crown walls can be placed from a high, almost unsheltered wall (figure 2.3a) to a sheltered wall with a high berm (figure 2.3d) or in between (figures 2.3 c and d). A wall which protrudes above the berm is more sensitive to wave loads than a sheltered wall, however it is less expensive than placing rubble mound up to the same level as the top of the wall.
The configuration of a crown wall is therefore an economical trade off which should be optimized during design.

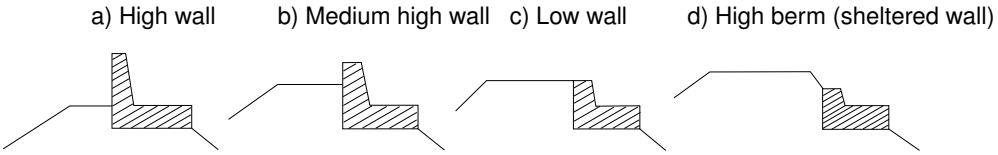

Figure 2.3: Crown wall configurations, [BURCHARTH, 1992]

Sometimes a core penetrating skirt [PEDERSEN, 1996] at the front side of the base slab is used to obtain extra resistance due to passive soil pressure. Besides that, in order to reduce overtopping considerably, a parapet at the top of the wall could be used. This horizontal extension should guide overtopping back into the wave. An example of both types of extensions is given in figure 2.4

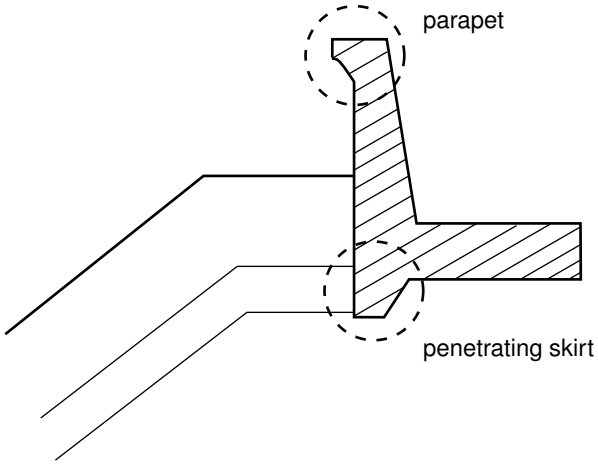

Figure 2.4: Crown wall with a horizontal (parapet) and vertical extension (penetrating skirt) [PEDERSEN, 1996]

2.3 Physical and hydraulic parameters

The design of a coastal structure, such as a crown wall, depends on various parameters in which a distinction can be made between physical (geometrical conditions) and hydraulic parameters (wave conditions).

2.3.1 Physical parameters

In figure 2.5 the physical parameters are defined according to CIRIA *et al.* [2007].

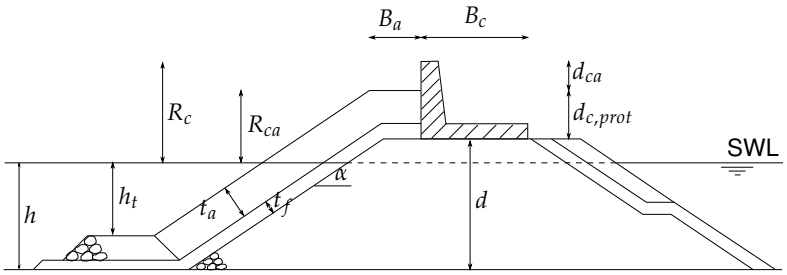

Figure 2.5: Governing parameters related to the structure, breakwater cross-section with on top a crown wall [CIRIA *et al.*, 2007]

- **Armour crest freeboard ($\mathbf{R_{ca}}$)**:

  The vertical distance between the still water level (SWL) and the top of the armour layer.

- **Crest freeboard ($\mathbf{R_c}$)**:

  The vertical distance between SWL and the top of the crown wall.

- **Unprotected crown wall part ($\mathbf{d_{ca}}$)**:

  The vertical distance between the top of the armour layer and top of the crown wall.

- **Structure height (d)**:

  The vertical distance between the sea bed and base slab of the crown wall.

- **Structure width ($\mathbf{B_c}$)**:

  The horizontal distance between the front- and rear end of the crown wall.

- **Armour berm width ($\mathbf{B_a}$)**:

  The width of the top of the armour layer.

- **Armour- and filter layer thickness($\mathbf{t_a}$,$\mathbf{t_f}$)**:

  The thickness of the armour layer (usually $\approx 2d_{n50}$).

- **Angle of the structure slope (α)**:

  Usually the slope of the armour and core are equal. Commonly used are 1/2 or 2/3 slopes.

- **Water depth (h)**:

  The vertical distance from the sea bed to SWL.

- **Depth of toe below SWL (h_t)**:

  The vertical distance from the top of the toe up to SWL.

2.3.2 Hydraulic parameters

Below the hydraulic parameters are described which play an important role in the design of a crown wall.

- **Wave height (H_s,H)**: The wave height is often defined as the spectral wave height H_{m0} or the average of the highest third of the waves $H_{1/3}$ PULLEN *et al.* [2007]. However, PEDERSEN [1996] uses a significant wave height H_s, which is approximately equal to H_{m0}. It is chosen to use H_s and for regular waves H is used.

- **Wave period (T_p, T_m, T)**: Conventional wave periods are the peak period T_p and the average period T_m. For regular waves T will indicate the incident wave period.

- **Wave length (L_{0p}, L_{0m})**: In deep water the wave length is defined as: $\frac{gT^2}{2\pi}$. When the peak wave length is considered T_p must be used whereas T_m is relevant for the mean wave length.

- **Wave steepness (s_{0p})**: Wave steepness is defined as the ratio of wave height to wave length: H_s/L_{0p}. For this study the fictitious steepness in deep water based on the peak period is relevant which is indicated by s_{0p}. Generally a steepness of 0.01 indicates a typical swell wave and a steepness of 0.04 to 0.06 indicates a typical storm wave [PULLEN *et al.*, 2007].

- **Breaker parameter (ξ)**: Indicates whether breaking of a wave will occur on a slope and what kind of breaking/impact can be expected. It is defined as the ratio of slope steepness to wave steepness as follows: $\xi = \frac{tan\alpha}{\sqrt{H/L}}$

2.4 Loading of the crown wall

The loads exerted on a crown wall due to wave action occur in two ways. The primary action takes place on the vertical front face giving rise to large horizontal forces and large overturning moments. Secondly, the wave penetrates into the soil leading to an increase in pore pressures which, if the underside of the wall is placed close to the mean water level, may reach the structure and hence act as a vertical loading on the structure [PEDERSEN, 1996].

In this section literature is presented about the physics and relevant assumptions that are made with respect to the wave loads on a crown wall.

2.4.1 Wave force components

According to PEDERSEN [1996], wave loads on a crown wall can be separated in three wave force components ; a horizontal wave force, an overturning moment and a wall base pressure (figure 2.6). Since water pressure is isotropic, the wall base pressure will cause vertical loads on the crown wall with the same magnitude.
PEDERSEN [1996] did a large amount of tests in which the height of the crown wall was varied. Forces and pressures were measured, also shown in figure 2.6. This record refers to a wave condition with a steepness of $s_{0p} = 0.055$, a significant wave height of $H_s = 0.1760$ m and a peak wave period of $T_p = 1.60$ s.

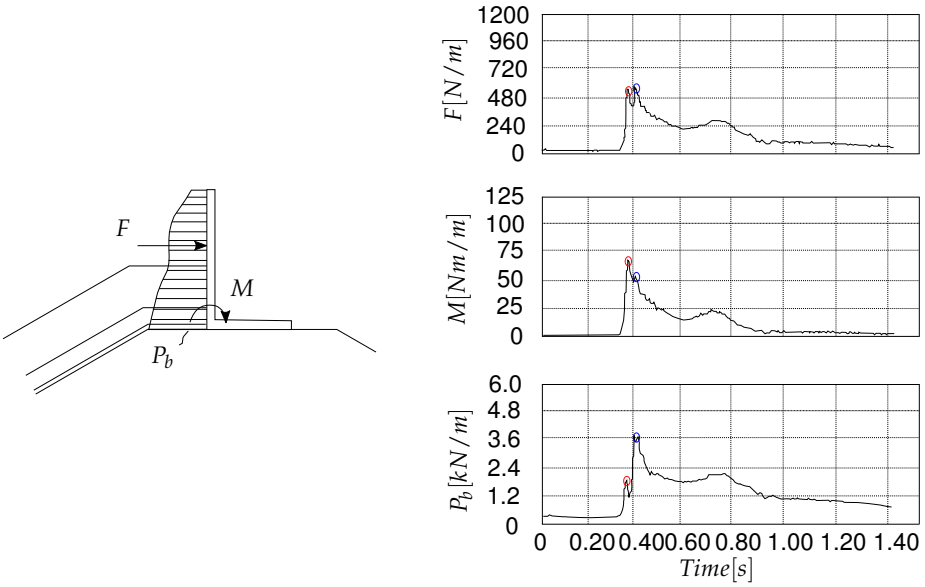

Figure 2.6: Wave forces component definition and recordings, [PEDERSEN, 1996]

In the top graph it can be seen that the force signal is double peaked (in red and blue) with a small amount of time in between them (app. 0.03 sec) which is only expected in the cases of high crown walls.
The magnitude of the horizontal force is nearly identical for the two peaks whereas the overturning moment has a clear maximum at the first peak (red circles) and the base pressure reaches its maximum around the second peak (blue circles).

Wave attack progression

From the graphs in figure 2.6, PEDERSEN [1996] states that wave attack progresses in the following way:

- A solid water impact in the form of a water hammer impinges on the upper unprotected part of the wall. This impact causes a large overturning

moment and a large horizontal force impact whereas the base pressure is only slightly affected (at location of red circle) which indicates a certain lag between the initial horizontal- and vertical loads.

- The water hammer is reflected from the wall and al three force components decrease (between red and blue circle).
- The still progressing wave now fully covers the wall resulting in large magnitudes of all the force components. The horizontal force and base pressure have their maximum values at this stage whereas the overturning moment is somewhat smaller than before (at location of blue circle).

2.4.2 Horizontal pressure distribution

The horizontal pressure distribution against the wall of a structure on top of a rubble mound breakwater is rather complex. The crown wall is (optional) partly protected by an armour layer and since this layer is not uniform due to randomly placed stones, the pressure distribution will not be equal along the length of the crown wall.
Therefore the horizontal pressure is empirically determined in which some assumptions are made.

From results of an experimental study by MARTIN [1995], it is concluded that when a wave hits a vertical wall after breaking in the armour slope, the first peak is generated due to stagnation of a dynamic impact, while the second peak occurs after the instant of maximum run-up and is related to the water mass down-rushing the wall.
In figure 2.7 this first peak, due to dynamic pressures, is indicated by 'A'. Because of the armour, which is presented by the dashed line, two regions can be distinguished; an upper part (above armour layer) and a lower part (protected by the armour layer). In both regions, the pressure is more or less constant but higher in the upper region since there is no armour layer protection.
The second peak, indicated by B, is the reflecting pressure and increases downwards, since it is more or less quasi-static. It can be seen that the presence of an armour layer is less of an influence.

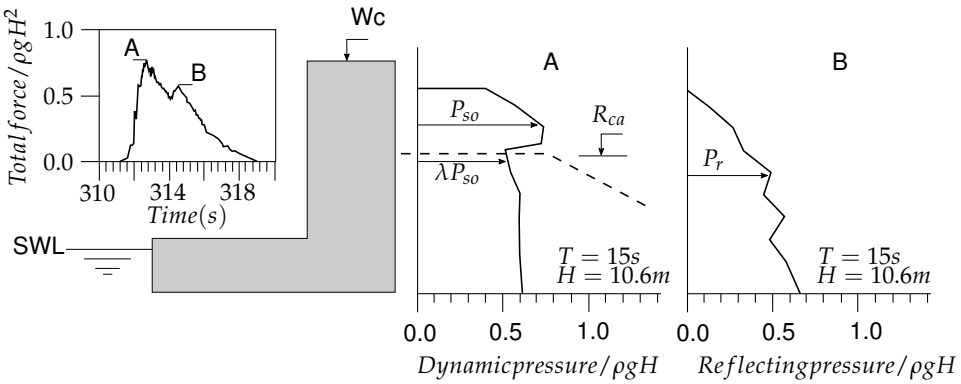

Figure 2.7: Experimental dynamic and reflecting pressure distributions for broken waves MARTIN *et al.* [1999]

PEDERSEN [1996] did several tests in which the height of the crown wall was varied. Pressures were measured from which an assumption for the horizontal pressure distribution was derived. In figure 2.8 a measurement of pressures against the crown wall is shown for a comparable crown wall configuration as in MARTIN *et al.* [1999], figure 2.7.
Two time steps can be seen; $T = 0s$ and $T = 0.0273s$.
Although PEDERSEN [1996] did not distinguish a dynamic and reflecting part it seems that the pressure recording at $T = 0s$ corresponds more or less with the dynamic pressure distribution (part A) and at $T = 0.0273s$ it follows more or less the measured reflecting pressure (part B) in figure 2.7.

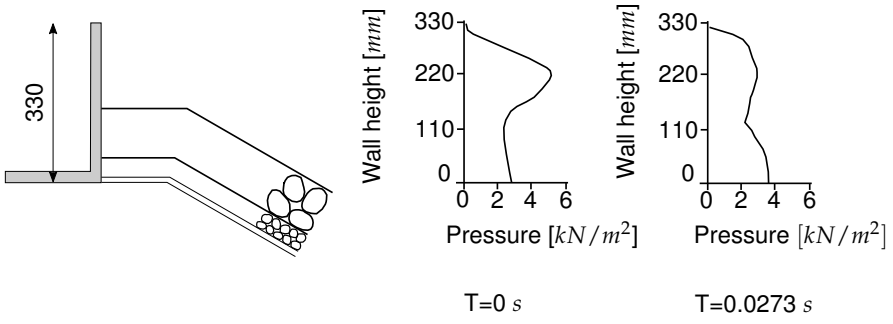

Figure 2.8: Pressure distribution on a crown wall during maximum wave force, from PEDERSEN [1996]

Effect of wave-steepness on pressure distribution

Breaking of a wave depends on the steepness of the wave; the steeper a wave gets the more likely it will break on the slope of a breakwater which results in a dynamic impact, which is a high peak pressure with a short duration. Due to breaking in front of the crown wall a lot of wave energy is already dissipated before hitting the structure [VERHAGEN *et al.*, 2012].

In the case of a low steepness a wave could reach the wall as a standing wave with a quasi-static impact [MARTIN *et al.*, 1999].
LOSADA *et al.* [1995] gives an indication of the time evolution of pressure distribution on a vertical wall under increasing wave steepness, which can be seen in figure 2.9.

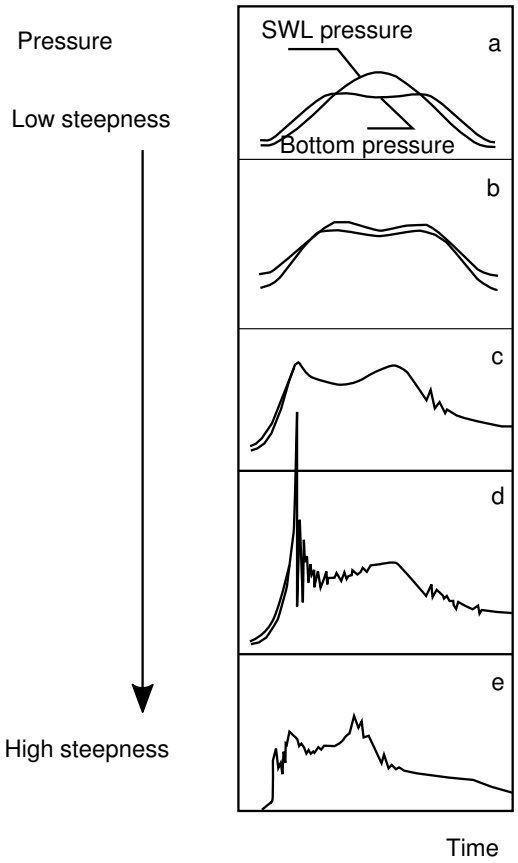

Figure 2.9: Time evolution of wave pressure distribution on a vertical wall under increasing wave steepness, [LOSADA *et al.*, 1995]

MARTIN *et al.* [1999] analysed this pressure distribution and described it as follows:
For waves with a slight steepness reaching the wall, the pressure-time series induced by a standing wave show a sinusoidal shape. If the wave steepness gets further increased, the peak pressure at the bottom of the wall fluctuates with twice the wave frequency, which can be seen in figure 2.9 a. As the wave steepness is further increased, the fluctuation expands up to the water surface. The double peak induced by the standing wave system is symmetric, figure 2.9 b.
Further increasing of the wave steepness, being close to breaking conditions, the double peak of the pressure- time curve becomes asymmetric with the former being shorter and higher, figure 2.9 c. The asymmetry of the double peak indi-

cates that a transition from a standing to a breaking wave system takes place [OUMERACI *et al.*, 1993].
When an incident wave breaks on the wall, the first peak may increase extraordinarily and may even split into two peaks with a very short duration which is shown in figure 2.9 d. This peak is also known as shock pressure according to BAGNOLD [1939]. The peak pressure profile consists of a dynamic and quasi-static component in which the dynamic peak is nearly always higher compared to the quasi static part. This pressure profile has the shape of a 'chuch roof' RAMACHANDRAN *et al.* [2012] and CHEN *et al.* [2014].
A wave can also break before it hits a structure as is shown in figure 2.9 e. The double peak pattern of the time pressure distribution is still apparent. Their relative magnitude and duration depend on the distance between the breaking point and the hit wall.

2.4.3 Upward pressure distribution

Little knowledge exists with respect to the upward pressure distribution against the base of the crown wall on top of a permeable structure like a rubble mound breakwater.
This is due to the difficulty of measuring upward pressures in small scale flume tests because of strong scale effects related to the flow inside the porous mound PEDERSEN [1996].
In general a linear variation of wave pressure under the crown wall is considered by IRIBARREN AND NOGALES [1964] JUUL JENSEN [1984], PEDERSEN [1996] and MARTIN *et al.* [1999]. An exception is found by LOSADA *et al.* [1993] who obtained a parabolic pressure distribution against the base of the crown wall resting on porous media. However, these findings do not differ significantly from a linear trend.
MARTIN *et al.* [1999] gives the best physical insight with respect to loads around the crown wall according to CIRIA *et al.* [2007] and therefore, its assumed upward pressure distribution is given in figure 2.10. The upward pressure at the front of the wall equals the horizontal pressure value at the bottom of the wall from which a linear decrease to zero occurs.

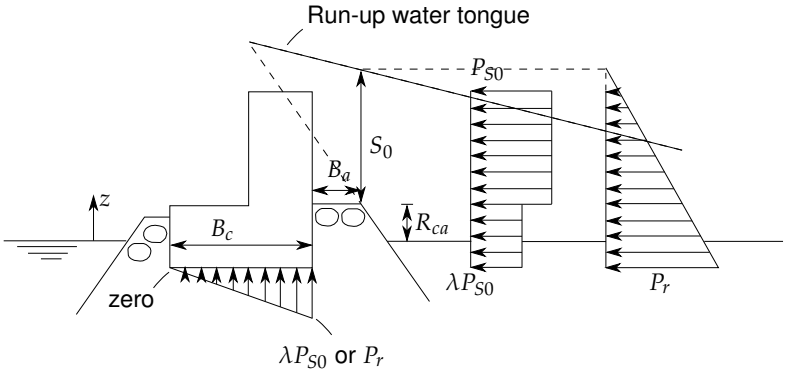

Figure 2.10: Total pressure distribution according to MARTIN *et al.* [1999]

2.5 Stability of a crown wall

According to PEDERSEN [1996] from a safety point of view the stability of the crown wall is essential since a failure of this structure might lead to a total breakdown of the whole rubble mound breakwater.

2.5.1 Failure modes

According to CIRIA *et al.* [2007]: failure modes for crown walls can be grouped into those depending on the strength of the superstructure (such as breakage) and those depending on the interaction with the underlying structure (such as sliding and overturning).
Within these groups four types of failure can be distinguished, which are shown in figure 2.11.
Cracking and geo-technical failure, which are strength properties of the crown wall or breakwater, could occur. If wave loads get too high sliding and overturning/tilting could lead to failure modes which are relevant in this research.

According to PEDERSEN [1996] sliding is the most common reason for failure of crown walls and is therefore the only considered stability criteria in this study.

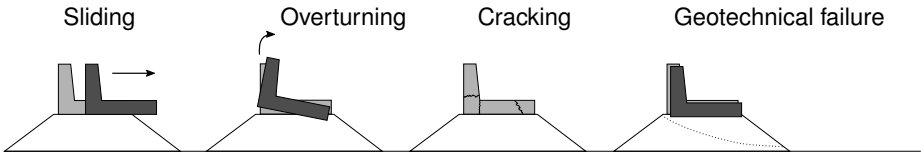

Figure 2.11: Crown wall failure modes, [PEDERSEN, 1996]

2.5.2 Stability criteria

In figure 2.12 a schematic view is given of a crown wall which is loaded in horizontal and vertical direction. The horizontal and vertical pressure distributions are simplified as concentrated forces. The stability criteria for sliding is presented.
The crown wall is a gravity based structure. Stability is obtained when the resistance against sliding is larger than the horizontal force exerted on the element.

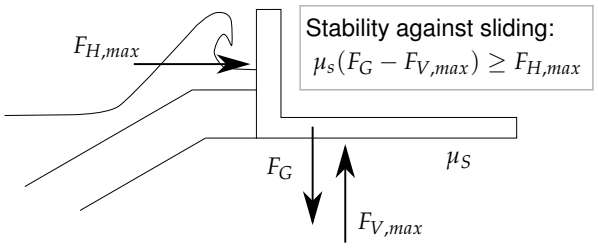

Figure 2.12: A simplification of wave loads on a crown wall

F_G	=	(buoyancy-reduced) weight of the crown wall element, $= (M_{cw} - V_{cw}\rho_w)g$, where M_{cw} and V_{cw} are the mass and the volume of the crown wall [N/m];
$F_{V,max}$	=	wave-induced uplift force [N/m];
$F_{H,max}$	=	wave-induced horizontal force [N/m];
μ_s	=	(static) friction coefficient [-].

3

Wave load calculation methods

In order to design a crown wall on top of a rubble mound breakwater wave loads must be known to determine whether it should be stable or not. Several wave load calculation methods exist which convert wave conditions into wave loads as function of physical properties of the total structure.
In this chapter a comparison of existing methods is given from which the most commonly used methods are described in more detail.

3.1 Comparison of methods

NEGRO VALDECANTOS *et al.* [2013] did a comparative analysis of currently available methods for calculating loads on structures in sloping breakwaters. The aim of this study was to analyse and compare existing wave wall calculation methods, determining their ranges of application and detecting their uncertainties.
The analysed available methods are given in table 3.1.

Table 3.1: Available wave load calculation methods according to NEGRO VALDECANTOS *et al.* [2013]

Method
IRIBARREN AND NOGALES [1964]
GÜNBAK AND GÖKCE [1984]
BRADBURY AND ALLSOP [1988]
PEDERSEN [1996]
MARTIN *et al.* [1999]
BERENGUER AND BAONZA [2006]

Some of the methods indicate their range of validity while others do not and are therefore assumed to be applicable in any case. However, it is recommended to know the conditions under which the considered formulations were obtained before applying them to a case far from the original parameters. It is advisable to use more than one method to determine results coming closer to reality. Lastly the existing calculation methods should be used for prior sizing. To come to a final design additionally tests on a physical model are recommended.

It is stated by NEGRO VALDECANTOS *et al.* [2013] (and confirmed by BRAÑA AND GUILLÉN [2005]) that MARTIN *et al.* [1999] gives the best physical insight since it separately analyses the dynamic and quasi-static forces on the structure, whereas PEDERSEN [1996] is the most reliable method even outside the range of application. For that reason the method of PEDERSEN [1996] will be investigated within this research. Additionally the method of PEDERSEN [1996] is extended by NØRGAARD *et al.* [2013] which will be discussed either.

3.2 Pedersen (1996)

PEDERSEN [1996] assumes that high enough waves lead to an impact pressure, p_m, based on a hypothetical run-up wedge. Pressure on the wall occurs since an amount of water with a certain velocity collapses (stagnation) perpendicularly against the wall. In figure 3.1 this process is depicted and it includes the assumed pressure distribution over the vertical wall and horizontal base slab of the structure.

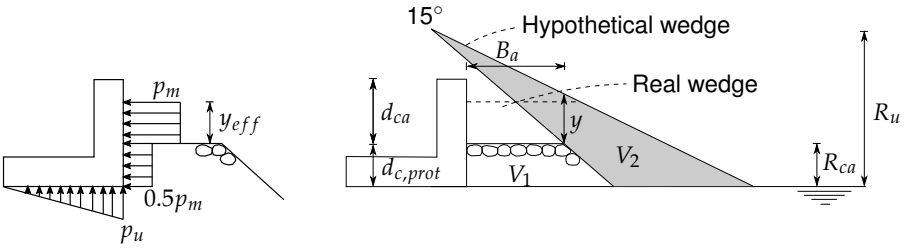

Figure 3.1: Pressure distribution according to PEDERSEN [1996]

Based on this, the pressure due to horizontal wave impact is defined as follows:

$$p_m = g\rho_w(R_{u,0.1\%} - R_{ca})$$

R_{ca} is the vertical distance from SWL up to the armour crest. $R_{u,0.1\%}$ represents the 1 in 1000 times run-up level according to VAN DER MEER AND STAM [1992]. The corresponding equations, which depend on the breaker parameter, ξ_m are given below:

For:

$\xi_m \leq 1.5$

$$\frac{R_{u,0.1\%}}{H_s} = 1.12 \cdot \xi_m$$

$\xi_m > 1.5$

$$\frac{R_{u,0.1\%}}{H_s} = 1.34 \cdot \xi_m^{0.55}$$

With: $\xi_m = tan\alpha / \sqrt{H_s / L_{0m}}$

The amount of run-up which is relevant for the structure is indicated by the real wedge with a thickness y and is calculated by the following expression:

$$y = \frac{R_{u,0.1\%} - R_{ca}}{sin\alpha} \frac{sin15^\circ}{cos(\alpha - 15^\circ)}$$

In this equation α is the slope angle of the armour layer.

The effective height of the impact zone, y_{eff}, is given by:

$$y_{eff} = min[\frac{y}{2}; d_{ca}; 0]$$

The total horizontal force which occurs 1 in 1000 times is calculated with the following equation:

$$F_{H,0.1\%} = 0.21\sqrt{\frac{L_{0m}}{B_a}}(1.6 p_m y_{eff} + V\frac{p_m}{2} d_{c,prot})$$

The overturning moment corresponding to the maximum load is calculated by:

$$M_{H,0.1\%} = aF_{H,0.1\%} = 0.55(d_{c,prot} + y_{eff})F_{H,0.1\%}$$

The maximum vertical load could be determined according to the uplift pressure, $p_{U,0.1\%}$ which occurs 1 in 1000 times. The uplift pressure is calculated as follows:

$$p_{U,0.1\%} = 1.0 V p_m$$

It is assumed that the uplift pressure maintains the value of the horizontal pressure at the bottom of the crown wall. It will decrease triangular to zero at the rear end of the base slab.

In table 3.2 the relevant parameters, used by PEDERSEN [1996], are shown.

Table 3.2: Parameters used by PEDERSEN [1996]

Parameter	Description	Dimension
p_m	Horizontal wave impact pressure component	$N/m^2/m$
R_{ca}	Vertical distance between SWL and crest of armour	m
$R_{u,0.1\%}$	0.1 % Run-up level	m
y	Wedge thickness (minimum value=0)	m
y_{eff}	Effective height of the impact zone	m
d_{ca}	Unprotected height of the crown wall	m
L_{0m}	Deep water wave length corresponding to mean period	m
B_a	Berm width of the armour layer in front of the crown wall	m
$d_{c,prot}$	Protected (by armour) height of the crown wall	m
V	$\text{Min}\{V_2/V_1, 1\}$, corresponding to figure 3.1	m^2
$F_{H,0.1\%}$	Horizontal wave force with 0.1% probability of occurrence	N/m
$M_{H,0.1\%}$	Overturning moment with 0.1% probability of occurrence	Nm/m
$p_{U,0.1\%}$	Uplift pressure with 0.1% probability of occurrence	$N/m^2/m$

3.2.1 Range of application

Table 3.3 indicates the validity of the method, by giving parameter ranges for which tests were done by PEDERSEN [1996].

Table 3.3: Parameter ranges for method by PEDERSEN [1996]

Parameter	Description	Range
ξ_m	Breaker parameter using T_m	1.1-4.2
H_s/R_{ca}	Relative wave height	0.5-1.5
R_c/R_{ca}	Relative run-up level	1-2.6
R_{ca}/B_a	Relative berm width	0.3-1
$cot\alpha$	Front side slope	1.5-3.5

3.3 Extension by Nørgaard et al. (2013)

According to NØRGAARD *et al.* [2013], the semi-empirical formulae of PEDERSEN [1996] are based on model tests with deep to intermediate water. By doing tests with shallow water conditions NØRGAARD *et al.* [2013] proved that Pedersen overpredict the loads in shallow water conditions. Therefore a modification/extension of the formulae to cover loads in both deep and shallow water conditions has been established. In these sections the modifications are treated separately.

3.3.1 Modification 1

Firstly, a modification with respect to the run-up is made in order to include shallow water wave conditions. Instead of using H_s which is done by VAN DER MEER [1988], $H_{0.1\%}$ is used which results in the following equations for the maximum run-up:

For:

$\xi_m \leq 1.5$

$$R_{u,0.1\%} = 0.603 \cdot H_{0.1\%}\xi_m$$

$\xi_m > 1.5$

$$R_{u,0.1\%} = 0.722 \cdot H_{0.1\%}\xi_m^{0.55}$$

3.3.2 Modification 2

Secondly, the empirical scale factor b which is used by PEDERSEN [1996] to calculate the horizontal force exerted on the unprotected part of the crown wall, is adjusted from 1.6 to 1 by Norgaard.
As a result, the total horizontal force is be defined as:

$$F_{H,0.1\%,mod} = 0.21 \cdot \sqrt{\frac{L_{m0}}{B}} \cdot (p_m \cdot y_{eff} + \frac{p_m}{2} \cdot V \cdot d_{c,prot})$$

3.3.3 Modification 3

Finally, a modification is made with respect to the overturning moment in which coefficients e_1 and e_2 are introduced to bring the attack points of the loads into account for varying protection height of the structure. As a result, the modified overturning moment is defined as:

$$M_{H,0.1\%,mod} = (h_{prot} + \frac{1}{2} \cdot y_{eff} \cdot e_2) \cdot F_{Hu,0.1\%} + \frac{1}{2} \cdot h_{prot} \cdot F_{Hl,0.1\%} \cdot e_1$$

with:

$$e_1 = 0.95$$

$$e_2 = 0.40$$

$$F_{Hu,0.1\%} = 0.21 \cdot \sqrt{\frac{L_{m0}}{B}} \cdot p_m \cdot y_{eff}$$

$$F_{Hl,0.1\%} = \frac{1}{2} \cdot 0.21 \sqrt{\frac{L_{m0}}{B}} \cdot p_m \cdot V \cdot d_{c,prot}$$

3.3.4 Range of application

The modifications of NØRGAARD *et al.* [2013] lead to an extension of the range of application for the method of PEDERSEN [1996]. The range depends on d_{ca}, which is the unprotected part of the crown wall (figure 3.1), and is shown in table 3.4.

Table 3.4: Parameter ranges for method by PEDERSEN [1996] extended by NØRGAARD *et al.* [2013]

Parameter	Description	Ranges $d_{ca} = 0$	Ranges $d_{ca} > 0$
ξ_m	Breaker parameter using T_m	2.3-4.9	3.31-4.64
H_s / R_{ca}	Relative wave height	0.5-1.63	0.52-1.14
R_c / R_{ca}	Relative run-up level	0.78-1	1-1.7
R_{ca} / B_a	Relative berm width	0.58-1.21	0.58-1.21
H_{m0} / h	Relative wave height	0.19-0.55	0.19-0.55
H_{m0} / L_{m0}	Relative wave length	0.018-0.073	0.02-0.041

4

Main findings from literature

The interaction between horizontal and vertical loading of the crown wall is a complex process. Loads on the structure depend, amongst other things, on wave height, wave period and geometrical properties of the breakwater and crown wall.
Several wave load calculation methods can be used to calculate loads on the crown wall in order to make a proper design.
However, due to results of physical scaled model testing in Grenoble it has been observed that current design methods seem to be conservative in predicting whether the crown wall is stable or not. This conservativeness is highly due to the lack of existing knowledge about the effect of freeboard. Until now, for stability calculations it is assumed that the maximum horizontal and vertical loads occur simultaneously without phase lag. Besides, the upward pressure should only reach zero at the rear end of the base of the crown wall.
Though, for decreasing water level and so increasing freeboard, it could be expected that there occurs a certain phase lag between horizontal and vertical loads whereas upward pressure could be less effective than assumed, and so the point at which vertical pressure becomes zero could shift to the front instead of remain fixed at the rear end of the base slab independent of freeboard.

This leads to the following knowledge gaps:

- Little data is available about the effect of varying freeboard on the stability of the crown wall as function of wave conditions;
- The distribution of the upward pressure against the base slab as a function of freeboard and wave conditions is not sufficiently known;
- Insufficient knowledge about the highly possible phase lag between the horizontal and vertical loads as function of freeboard and wave conditions.

5

Methodology

5.1 Study area

Until now, the design of a crown wall on top of a rubble mound breakwater tends to be too conservative. In order to close the knowledge gaps which are defined in chapter 4 the following study steps are defined:

Study steps

1. Obtain data about the effect and shape of upward pressure distribution on the base of the crown wall as function of freeboard;
2. Define a relationship between vertical loads on the crown wall as function of wave conditions and freeboard;
3. Describe any existing phase difference between the horizontal and vertical loads as function of freeboard;
4. Generate a dataset of critical weights as function of wave conditions and freeboard;
5. Define design guidelines, based on collected data, and describe how current design methods could be improved.

5.2 Experimental research

In order to reach the study steps, an experimental research is carried out in which a physical scaled model (1:30) is used. A model of a breakwater is built with on top three crown wall elements which are subjected to wave loads.

5.2.1 Parameters

Judging from the study steps; wave conditions, freeboard and weight of the crown wall are the main parameters on which is focussed in this research and will be varied during testing.
The parameters which are of influence on the stability of the crown wall, and their range are shown in figure 5.1 and table 5.1.
The total structure has a height of 0.72 m and a length of 2.10 m.

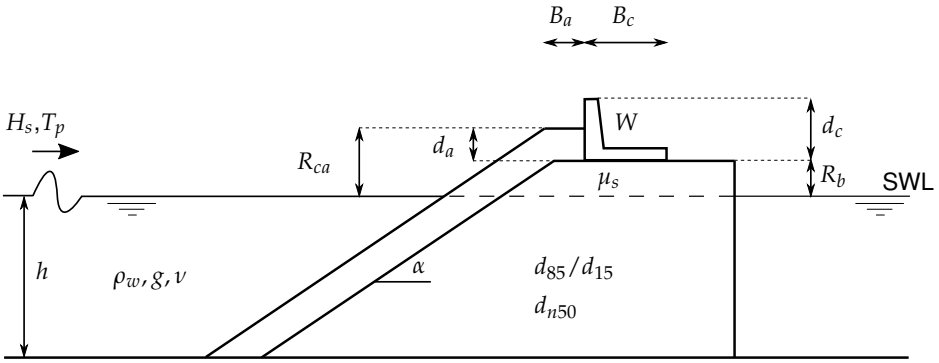

Figure 5.1: Test parameters

Table 5.1: Parameter range

Symbol	Description	Constant (C)/ Variable (V)	Range	Unit
H_s	Significant wave height	V	0.09-0.16	m
T_p	Peak period	V	1.22-3.18	s
h	Water depth	V	0.56-0.65	m
R_b	Base freeboard	V	0-0.09	m
R_{ca}	Armour crest freeboard	V	0.08-0.17	m
α	Angle of structure slope	C	26.7	$^\circ$
B_a	Armour berm width	C	0.15	m
B_c	Structure width	C	0.3	m
d_c	Crown wall height	C	0.15	m
d_a	Armour layer thickness	C	0.08	m
d_{50}	Nominal grain diameter core	C	0.0145	m
d_{50}	Nominal grain diameter armour	C	0.0365	m
$(d_{85}/d_{15})_{core}$	Type of grading core	C	1.39	-
$(d_{85}/d_{15})_{armour}$	Type of grading armour	C	1.45	-
W	Weight of the crown wall	V	30 - 700	N/m
μ_s	Static friction coefficient	V	0.72-0.77	-
ρ_w	Density of water	C	1000	kg/m^3
g	gravitation acceleration	C	9.81	m/s^2
ν	Kinematic viscosity	C	10^{-6}	m^2/s

5.2.2 Dimensionless parameters

According to the 'Buckingham pi theorem' a dimensional analysis must be carried out in order to describe the investigated problem correctly. According to the parameters in table 5.1 not all parameters are directly related to the stability of the crown wall, other parameters could be derived from another parameter which means that these are directly related to each other. As a result the following relationship of dimensionless weight as function of dimensionless parameters is defined:

$$\frac{W}{\mu_s \rho_w g B_c d_c} = f\left(\frac{H_s}{R_{ca}}, \frac{H_s}{\frac{gT_p^2}{2\pi}}, \frac{B_a}{d_a}, \frac{B_c}{d_a}, \frac{d_c}{d_a}, \frac{d_{50,c}}{d_{50,a}}, (d_{85}/d_{15})_{core}, (d_{85}/d_{15})_{armour}, cot\alpha\right)$$

Within this research relationships are obtained for critical weights as function of wave height and freeboard for two different fictitious wave steepness s_{0p}. The remaining parameters are properties of the model and function as a range of application for these relations.

5.3 Test conditions

Different test conditions are used in which wave height, wave period and freeboard are varied. Two types of waves are used, namely, waves with a low steepness ($s_{0p} = 0.01$) and with a high steepness ($s_{0p} = 0.04$). The low steepness waves are referred to as 'swell waves' whereas the high steepness waves are indicated as 'storm waves'.
In total 35 different test conditions are used as given in Appendix A.

5.4 Test subjects

Within the experiments research is done to overall stability and vertical stability, additionally horizontal and upward pressures are measured against the base and wall of the crown wall. In this section these subjects are described in detail.

5.4.1 Overall stability

In testing the overall stability, the crown wall is loaded in both horizontal ($F_{H,max}$) and vertical direction ($F_{V,max}$) and is assumed to be overall stable when the resistance against sliding is larger than the exerted effective horizontal loading. Resistance against sliding depends on the static friction coefficient μ_s and nett own weight of the structure $F_G = W - F_{V,max}$ (Buoyancy excluded). A distinction can be made between wet and dry conditions for friction, in this research the wet friction coefficient $\mu_{s,wet}$ is relevant.
A crown wall fails if it slides over the core of the breakwater with a minimal displacement of $\Delta s \approx 0.2 - 0.3$ mm, according to figure 5.2.
After a test run the element with a certain weight remained stable or has failed. An iterative process takes place in which the weight of the crown wall will be adapted until failure or stability occurs. The range width between stable- and failure weights of the crown wall will be at most 5%. The critical weight, which is in between the smallest stable mass and largest failure mass, deviates at a maximum 2.5 % from a stable- and failure situation.

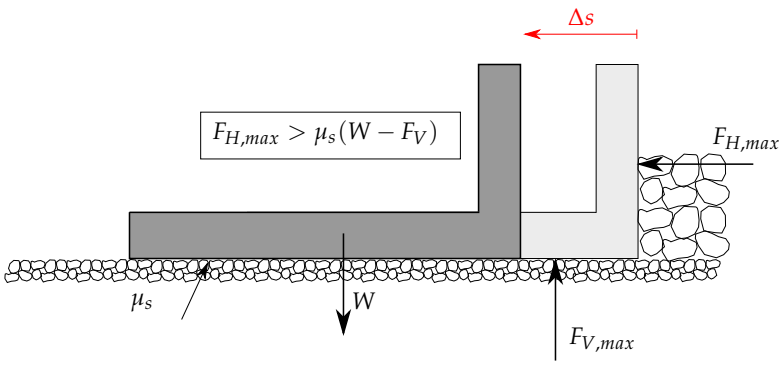

Figure 5.2: Sliding failure mode

5.4.2 Vertical stability

In testing vertical stability, the crown wall is loaded in vertical direction whereas horizontal loads are obstructed to hit the crown wall by a steel plate in front of the structure, see figure 5.3.
The element is connected to the breakwater by a hinge. Vertical displacement occurs if overturning takes place, so no longer moment equilibrium around point O exists. A threshold of $\Delta s \approx 0.1$ mm is defined. By varying the weight of the crown wall iteratively prior to each test run, failure and stable weights are found per test condition. The range width between the smallest stable and largest failure weights of the crown wall will be at most 5%. As a result, the critical mass deviates at a maximum 2.5 % from a stable- and failure situation. From the data of critical masses, estimates of vertical loads are derived based on: $F_{V,max} = W x_G / x_V$.

Remarks and assumptions

A small gap between the steel plate and wall of the element exists to enable the crown to move freely upward without be obstructed by the plate. This could however, result in an upward pressure loss through the gap. To prevent the pressure to escape through this gap, a thin elastic foil is glued to the steel plate and placed under the base of the crown wall.
Additionally there are some assumptions made which are important to notice:

- The hinge does not exert a reaction force in the form of a moment;
- The foil which blocks a possible pressure loss exerts a negligible reaction force on the crown wall;
- Centre of gravity of the crown wall is constant for every test run, so x_G does not change (in fact $x_G = 0.177 \pm 0.001$ m);
- The point of action for the vertical force, based on the upward pressure profile, depends on the results and findings of pressure records and video analysis (treated in chapter 7);
- No extra buoyancy term is taken into account;

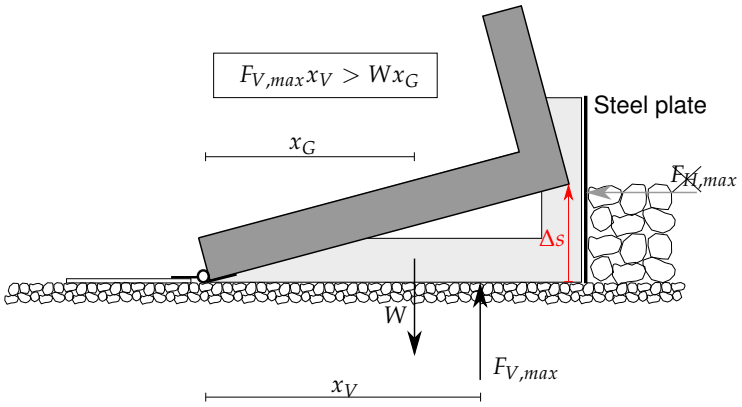

Figure 5.3: Overturning failure mode

5.4.3 Pressure measurements

At 9 locations in the element pressures are measured, see figure 5.4. The location of the pressure sensors are given in table 5.2. Technical properties of the pressure sensors and the processing of the data is described in chapters 6 and 7.

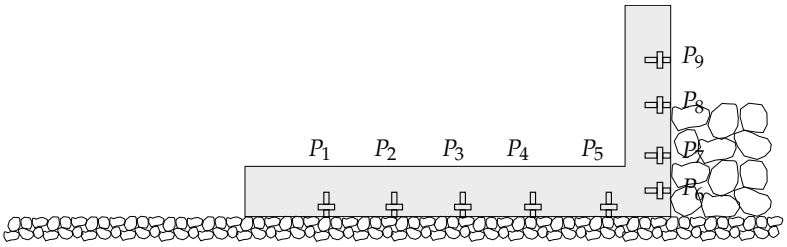

Figure 5.4: Pressure sensors in crown wall

Table 5.2: Location of pressure sensors

Sensor	Location from front [m]	Location from bottom [m]
P_1	0.241	0
P_2	0.191	0
P_3	0.141	0
P_4	0.091	0
P_5	0.041	0
P_6	0	0.020
P_7	0	0.049
P_8	0	0.080
P_9	0	0.119

5.5 Test plan

Regular waves are used to calibrate the system. Irregular waves are used to obtain data with respect to analysing stability in detail. Each test run exists of at least 1000 irregular waves.

The experiments are divided in two parts, test series A and B. In test series A pressures, vertical stability and simultaneously the overall stability are investigated for the test conditions in table A.01 in Appendix A.
In test series B the overall stability is examined for test conditions shown in table A.01 in Appendix A. Corresponding test conditions for both test series are shown in Appendix A.
From the overall stability critical weights can be obtained at which the crown wall is on the boundary between stability and failure with respect to a sliding failure mechanism.

The breakwater is divided into three sections over width, namely: section A, B and C. This makes it possible to use 3 crown wall elements simultaneously. Therefore, more test configurations can be tested simultaneously (test series A) and a larger dataset of critical masses is obtained (test series B). In table 5.3 a summary is given of what is tested per section and the treated study goals per test series.

Table 5.3: Test plan for the crown wall per section of the breakwater

Section	Test series A	Test series B
A	Overall stability	Overall stability
B	Vertical stability	Overall stability
C	Pressure measurements	Overall stability
Treated study goals:	1,2,3	4

6

Experimental set-up

In this chapter the experimental set-up is given. The execution of the rubble mound breakwater is described and materials which were used to build this structure.
Furthermore, measurement equipment is described with their ranges and how these to be used.

6.1 Experimental set-up

The tests are performed in the 2-D wave flume in the Waterlab of Civil Engineering & Geosciences at the TU Delft.
This flume has an effective length of 42 m, a width of 0.80 m and a height of 1 m. The structure is located at 28 m from the wave generator, a sketch of the set-up is depicted in figure 6.1. In figure 6.2 and overview of the wave flume is shown whereas figure 6.3 shows the height and width of the flume.

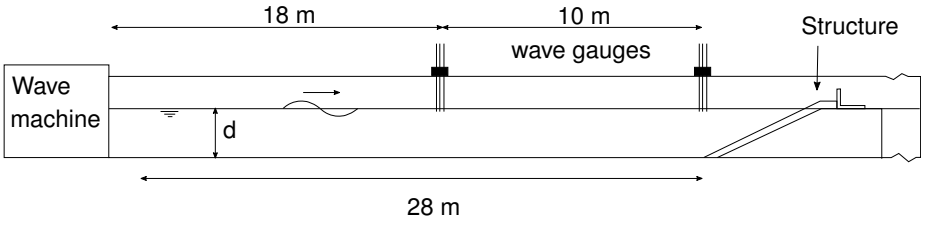

Figure 6.1: Averaged cross sections of the structure based on 12 slices

The piston type wave generator is electro-mechanically driven and is able to produce several kind of waves. Input variables are water depth, significant wave height and a peak wave period.
The flume is equipped with an automatic reflection compensation to reduce the effect of reflected waves on the wave paddle. As a result, the incoming signal at the structure is the desired signal at all times.

Figure 6.2: Overview of the wave flume

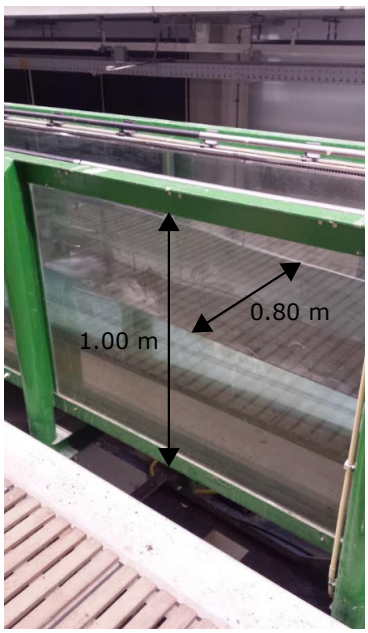

Figure 6.3: Width and height of the flume

6.2 Description of the scaled model

The scaled model represents a rubble mound breakwater with a crown wall on top, a coastal defence structure as used in Constanţa Romania. A sketch of a cross section of this structure is given in figure 6.4. This breakwater is used in determining the main dimensions of the model breakwater.

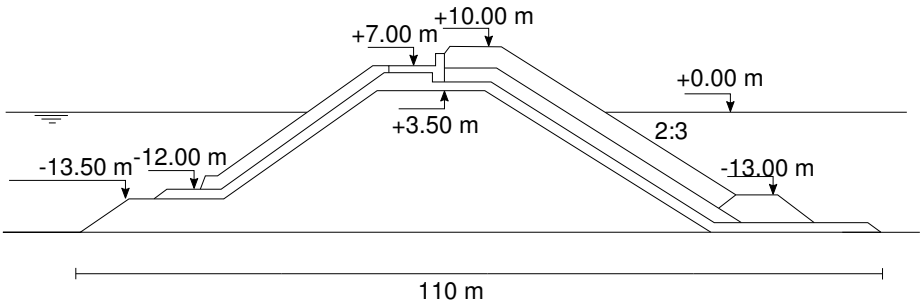

Figure 6.4: A cross-section of the breakwater of Constanţa, Romania

6.2.1 Breakwater

The breakwater is made out of basalt rubble mound which has a density of 3000 kg/m^3. The stones are glued together using elastocoast which is a sustainable two component-glue designed for strengthening of revetments (produced by

BASF), which results in tight connections between the contact areas of the stones, hardly filling the pores with glue. As a result, the structure will not damage and remains permeable during tests.
As can be seen in figure 6.4 the breakwater exists of several kinds of layers, namely: a core and a under-, filter- and armour-layer. Since there is no danger that core material is washed out, the scaled structure is made up of a core and armour in which other layers are excluded, this means a structure with a permeability coefficient of P=0.5 according to VERHAGEN *et al.* [2012]. Furthermore, it is assumed that the inner slope does not have an effect on the stability of a crown wall and is therefore excluded either.

Execution

From a practical point of view the core is separated into a centre-part and a slope. On top of the slope the armour layer is placed in situ.

The centre-part and slope are constructed by mixing stones and elastocoast (2% of total stone-volume) in a concrete-mixer and placing them in a mold. The centre-part is constructed upside down so that the top is perfectly flat. Hoisting frames are welded and placed in the mold to ensure the structure remains intact when using the crane for placement in the wave flume. Pictures of the execution are shown in Appendix B.
The slope is built on top of a steel plate to give the structure more strength during hoisting.
The armour layer is placed on top of the slope and is constructed in situ in the flume in which elastocoast is used as well to ensure the armour to remain unchanged during testing.
Figure 6.5 shows the core and armour in the wave flume.

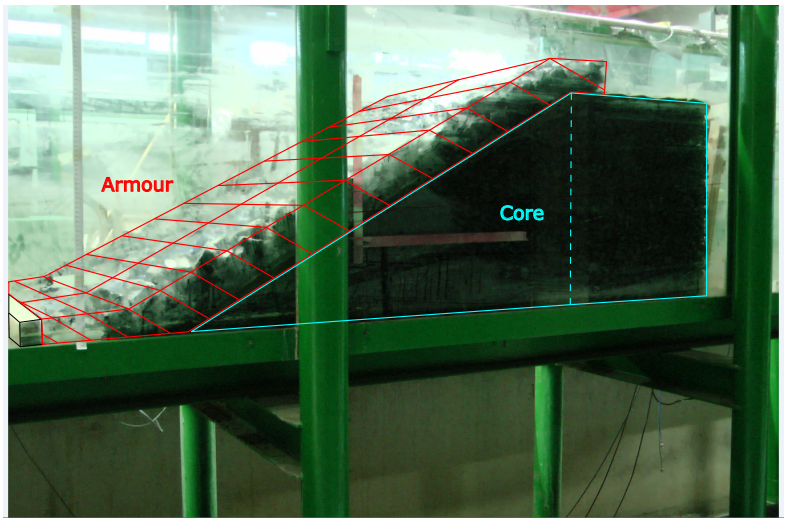

Figure 6.5: Breakwater in the wave flume. In red: armour layer, in blue: core (dashed line indicates the centre part and the slope)

6.2.2 Crown wall

The crown wall is simplified as a L-shaped structure (without a penetrating skirt) which is shown in figure 6.6 and figure 6.7. It has a length of 0.30 m, a height of 0.15 m and a width of 0.26 m. Furthermore, standing cuffs of 0.05 m are used to prevent inflowing water from both sides. The elements are made of tricoya, which is a wood species especially made for outdoor applications and will therefore hardly deform (in comparison to other wood species) when it comes in contact with water. In practice, crown walls are concrete structures, however, this would restrict the range of wave heights in which failure of the crown wall could be found, since concrete scaled elements would be too heavy to fail for smaller wave heights.
Tests were done with the material by placing a specimen in water for 1 day. It is observed that length and thickness increases at a maximum of 0.5%. However, the mass could increase by 5%.
During the test series a crown wall element will not be in contact with water for a long period of time. These deformation values should not occur and as a result the material is assumed to be suitable for these tests although mass of the elements should be checked regularly.
In between test-runs the mass of an element is varied by steel plates with sizes (255 x 240 mm and 240 x 100 mm) such that the centre of gravity remains at the same location, which is located at 0.177 ± 0.001 m from the rear end of the crown wall.

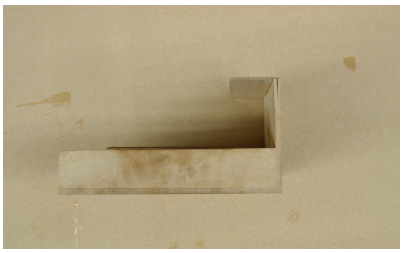

Figure 6.6: Side view: L-shaped crown wall

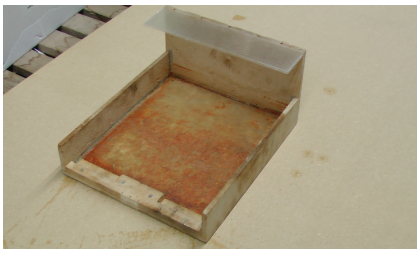

Figure 6.7: 3D view: Scaled crown wall

6.2.3 Pressure box

A fixated crest element with the same dimensions as the crown wall and instrumented with pressure sensors is used to measure pressures during a test run (figure 6.8). In order to ensure that electronics could not come in contact with water the crown wall is converted into a water-impermeable 'pressure box'. During calibration runs high noise levels were found highly due to resonance of membranes in the sensors. Tubes are attached to the sensors and filled with water to mute the vibrations of the membrane. Furthermore the box is filled with sand to impede the propagation of (highly possible) sound waves. The tubes are connected to a reservoir which is filled with water to ensure a constant reference pressure for each sensor. As a consequence, the natural frequency of the membranes will decrease. The implementation of sensors in the crown wall is shown in figure 6.8. Figure 6.9 shows the pressure box as used during testing.

Detailed information about the sensors is given in paragraph 6.4.4, whereas the exact placement of the sensors can be seen in Appendix D.

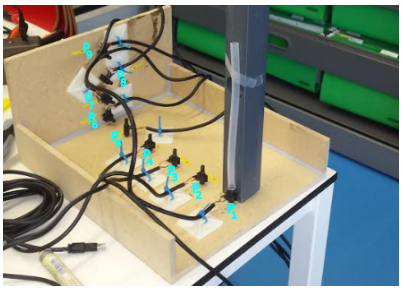

Figure 6.8: Pressure sensors, P_1 to P_9, inplemented in crown wall

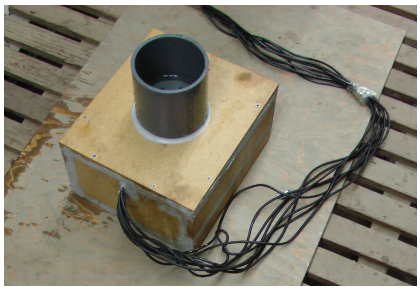

Figure 6.9: Water-impermeable pressure box with reservoir on top

Filtered vs. unfiltered data

Initially a measuring sample rate of 10 kHz was used. However, many peaks were observed which is likely due to air entrainment. Therefore, data is filtered using a 5^{th}- order Butherworth filter with a lowpass rate of 10 Hz.
In figures 6.10 and 6.11 an unfiltered and filtered pressure record is given for sensors P_1 and P_5 during test condition B_{swell3}. It is observed that high peaks are flattened substantially, especially for P_1 in which the peak is filtered out for 40 - 50%. However for P_5, maximum peaks are only reduced by 20 - 30%.
More important is the fact that the shape of the filtered pressures follows the unfiltered pressures quite nicely for both sensors P_1 and P_5. This could be explained as follows, pressure sensors P_1 and P_5 are located in the base slab and measure upward pressures. Since the water movement is inhibited by the porous core dynamic loading will hardly occur. Upward pressure is more or less quasi static of nature and therefore the filtered pressure data is assumed to be reliable.
In figure 6.12 a pressure record for P_6 can be seen, which is located in the wall of the element but fully protected by the armour layer. Due to this protection, dynamic water movements are inhibited as well and therefore the loading pattern will be more or less quasi static which is confirmed by the profile since the filtered data follows the unfiltered data decently with the exception of one pressure peak that is almost filtered out completely.
Sensor P_8 is just at the unprotected side of the armour and therefore subjected to dynamic loads. As expected problems arise which can be seen in figure 6.13 where the filtered profile differs substantially from the unfiltered data since many pressure peaks are filtered out.

Based on the comparison between unfiltered and filtered data it could be concluded that the pressure data is without doubt useful in order to make a qualitative analysis. However, care must be taken when considering a quantitative analysis. The sensors in the wall, especially P_8 and P_9 which are unprotected, are exposed to short-duration dynamic impact which is difficult to distinguish, therefore unreliable results can be expected. Whereas upward peak pressures could be actually 20-50% larger than measured after filtering.

Loads which are more or less quasi-static could be measured whereas consequence dynamic loads with large fluctuations will not be measured correctly.

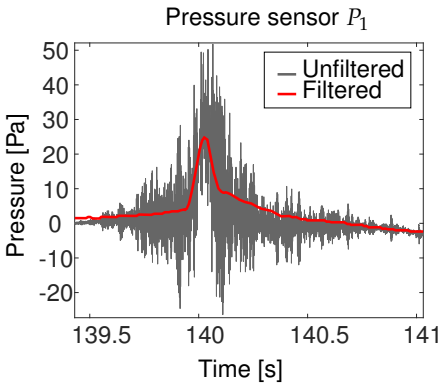

Figure 6.10: Unfiltered and filtered data for sensor 1

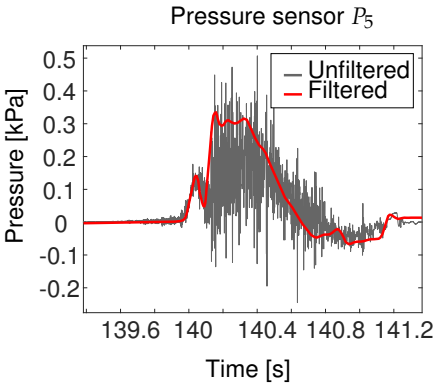

Figure 6.11: Unfiltered and filtered data for sensor 5

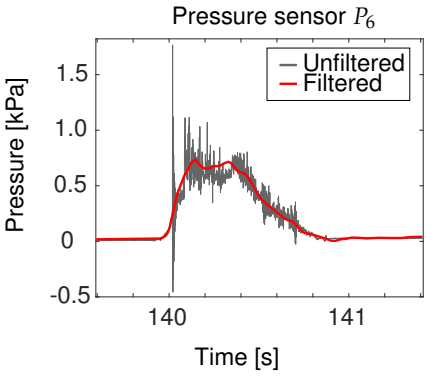

Figure 6.12: Unfiltered and filtered data for sensor 6

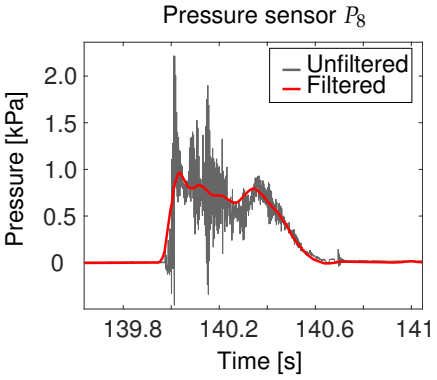

Figure 6.13: Unfiltered and filtered data for sensor 8

Base level shifts

It is observed that for most of the time pressure records, signals do not return to 0 after a load has been occurred, which can be seen in figures 6.14 to 6.17. Especially for sensors P_6 to P_9 this problem occurs which is possibly due to air entrainment. The sensors in the base slab are less vulnerable to air entrainment which can be seen in the pressure record.

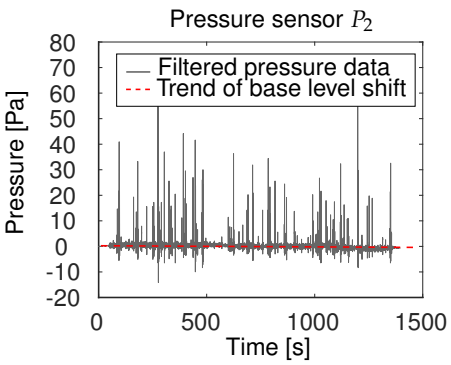

Figure 6.14: Unfiltered and filtered data for sensor 1

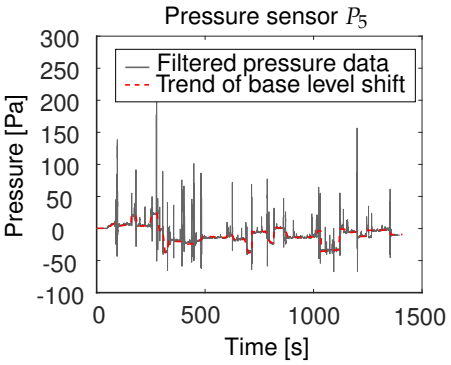

Figure 6.15: Unfiltered and filtered data for sensor 5

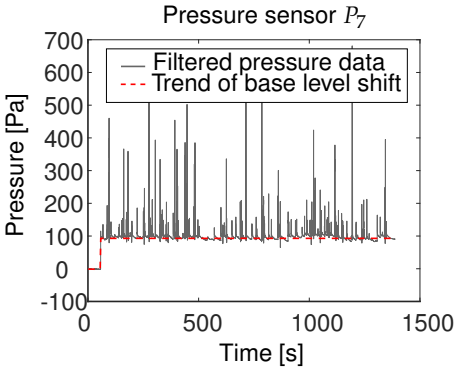

Figure 6.16: Unfiltered and filtered data for sensor 6

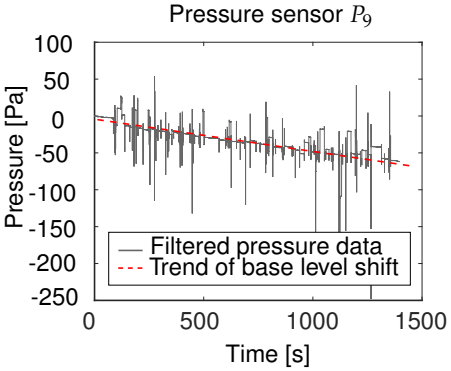

Figure 6.17: Unfiltered and filtered data for sensor 8

Correction base level shifts

Base level shifts, even small ones, should be corrected to know the pressure at a certain time step. An example is shown in figure 6.18. The pressure signals between 87.6 s - 88.2 s are investigated. Prior to the load from 87.8 s a base level shift has occurred with respect to the initial base level at 0 s.
To obtain actual pressures within this interval the pressure prior to a load is considered at T_f. At T_0 the wave did not reach the structure yet and therefore no load is applied which means that the pressure is absolutely zero.
Actual pressures are calculated by:

$$P_{actual}(T) = P(T) - P(T_f) - P(T_0)$$

In which $P(T)$ is the pressure at a time step within the considered pressure envelope.

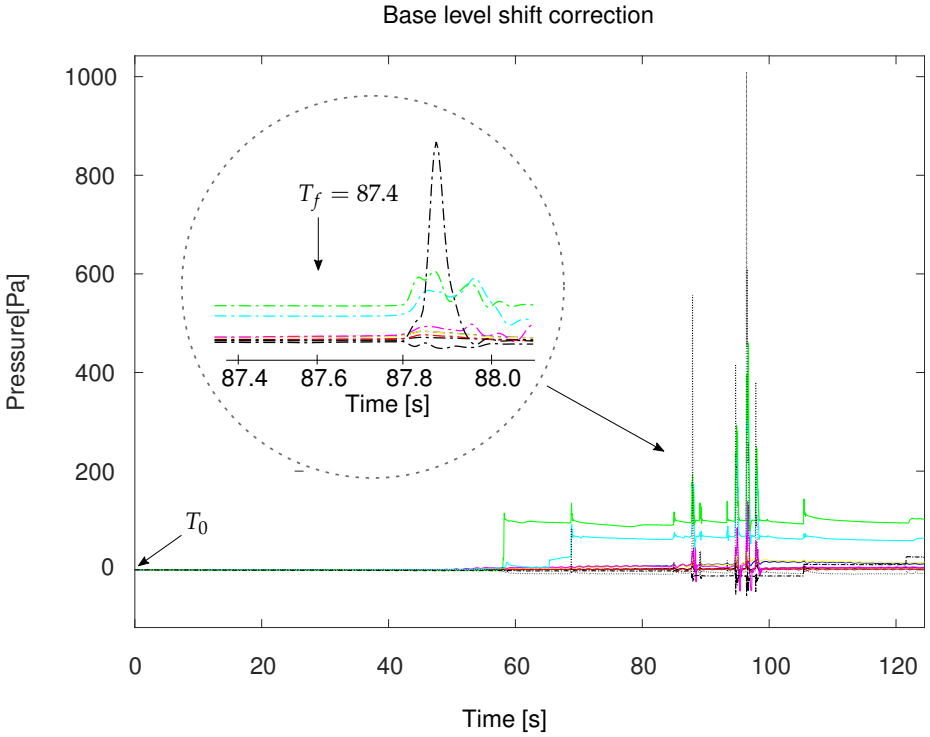

Figure 6.18: Correction base level shift

6.2.4 Frame

On top of the breakwater a frame separates three crown wall elements (figures 6.19 & 6.21). The frame exists of two steel plates (thickness 3 mm) which fit into two slits on top of the core which is shown in figure 6.20. Bolts make it possible to attach plates which drain overtopping water.
As a result, three sections occur indicated by A, B and C. Therefore the structure and flow pattern of waves could be divided into three strips indicated in red, white and blue in figure 6.22.

Figure 6.19: 3D view: Frame

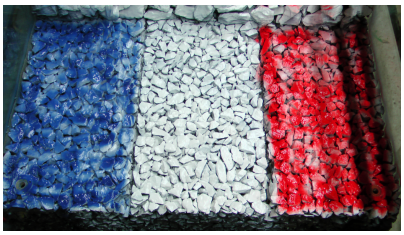

Figure 6.20: Slits in the core

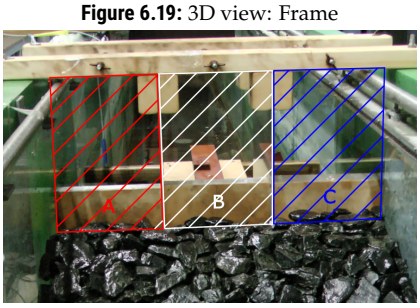

Figure 6.21: Frame on top of the structure separates section A, B and C

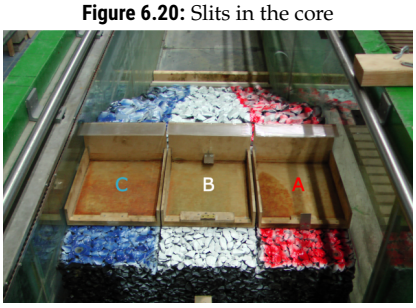

Figure 6.22: Structure divided in three strips

6.2.5 Obstruction element

Vertical loads are derived based on upward displacement. This is done by connecting the crown wall to a hinge which is fixed to the breakwater, see figure 6.25. To ensure that vertical displacements only depend on upward pressure the horizontal loading must be obstructed. This is done by making use of a steel element which is attached to the middle section of the frame, see figure 6.24. This element is a U-profile which fits around the steel plates of the frame. Due to its stiffness horizontal forces are transferred to the frame but not to the crown wall. Since the crown must be able to displace freely when failure occurs, a small gap between the wall and steel plate exists which could lead to vertical pressure loss. To prevent pressure loss, a transparent thin film is glued to the steel profile and folded in such a way that it sticks to the base slab due to capillary action, see figure 6.23.

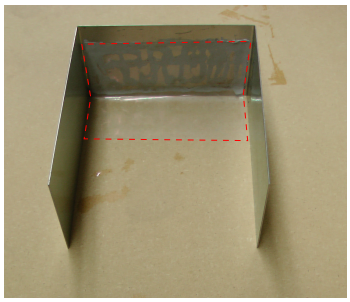

Figure 6.23: Thin film glued to plate and folded under base to avoid pressure loss

Figure 6.24: In the middle: U-profile to obstruct horizontal loads

Figure 6.25: Crown wall connected to a hinge

6.2.6 Overtopping plate

The mass of the crown wall must remain more or less constant during a test run. Overtopping plates (tricoya) prevent storage of overtopping water in the elements. Figure 6.26 shows three plates attached to the frame. The function of

such a plate is shown in figure 6.27; overtopping water is partly drained due to the plate (red arrow) and reflected (green arrow).

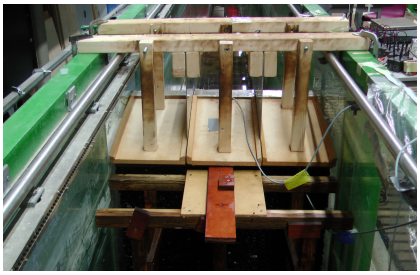

Figure 6.26: Back view: Overtopping plates fixed to the frame

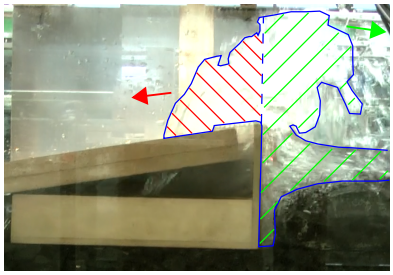

Figure 6.27: Overtopping water partly drained and partly reflected

6.2.7 Armour plate

During the first number of tests it has been noticed that there is a difference in the amount of water which flows into the various sections. To investigate whether these differences are due deviations in geometry of the breakwater a plate is placed on top of the armour, see figure 6.28. The plate has a width of 0.795 m and a length of 1.70 m (armour sizes). To ensure that the conditions are equal for each section the plate is levelled using a plumb rule, see figure 6.29.

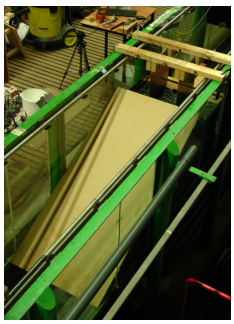

Figure 6.28: Plate placed on top of the armour layer

Figure 6.29: Plate levelled using a plumb rule

6.3 Scaling

According to CIRIA *et al.* [2007] the scale factor, n, of a parameter X is defined as the ratio of its value in reality (prototype) and in the model: $n_X = X_p / X_m$. Relevant scaling laws are Froude scaling and Reynolds scaling. It appears that these laws are in conflict with each other, especially for flow through the porous medium this could lead to scale effects.

6.3.1 Geometric scale

Geometrical similarity is based on the prototype and limitations and properties of the flume and wave machine. A boundary for dimensioning the model is the occurrence of the highest expected wave occurs in combination with the biggest water depth, which should not over top the wave flume.
As a result, the physical model is geometrically scaled by approximately a factor $n_L = 30$ (1:30 model).

6.3.2 Froude scaling law

Froude describes the relation between inertial and gravitational forces in the fluid and is especially suitable when the considered process is dominated by wave action and when the stability of a structure is investigated. The Froude-number is defined as follows:

$$Fr = \frac{U}{\sqrt{gd}}$$

When the process is correctly scaled according to Froude, the Froude number in the prototype and model are equal. From geometric scaling it follows that the

length scale of the prototype over the length scale of the model is defined as: $L_p/L_m = n_L$. From this, the time scale can be determined by: $T_p/T_m = \sqrt{n_L}$, whereas forces should be scaled by: $F_p/F_m = n_L^3$.

6.3.3 Reynolds scaling

The Reynolds number, $Re = \frac{Ud}{v}$, represents the ratio between inertial and viscous forces. It gives an indication of the amount of turbulence in the model. Typical values for the transition between laminar and turbulent flow are Re = 1000-2000. Reynolds scaling and Froude scaling are in contradiction to each other.
Where the Froude scaling is correct in scaling waves, it causes incorrectly scaling of viscosity, elasticity and surface tension. The linear geometric scaling of material diameters, stones in the core, which follows from Froude scaling may lead to much too large viscous forces corresponding to too small Reynolds numbers, especially in the core of small scale models. The related increase in flow resistance reduces the flow in and out of the core, which causes relatively larger up-rush and down-rush velocities. As a result run-up levels will be too high and armour stability too low.

6.3.4 Scaling of porous media by BURCHARTH *et al.* [1999]

In order to deal with the scaling problems described above, the scaling method of BURCHARTH *et al.* [1999] is used. The method proposes that the diameter of the core material in the model is chosen in such a way that the Froude law holds for a characteristic pore velocity. The characteristic pore velocity is chosen as the average of a most critical area in the core with respect to a porous flow and can be calculated using the Forchheimer equation.
In the paper of BURCHARTH *et al.* [1999] the breakwater of Zeebrugge is used as prototype which is used in this study as well in order to make an estimate of a sufficient nominal stone diameter for the core.

Nominal stone diameter in the core

Based on a random sample of 500 stones the nominal diameter of the core equals $d_{n50_{core}}$ = 14.53 mm, with a narrow grading type of $(d_{85}/d_{15})_{core}$ = 1.39. The grading curve for stones in the core is shown in Appendix C.

Nominal stone diameter in the armour

Based on a random sample of 500 stones the nominal diameter of the armour equals $d_{n50_{armour}}$ = 36.51 mm, with a narrow grading type of $(d_{85}/d_{15})_{core}$ = 1.45. The grading curve for stones in the armour layer is shown in Appendix C.

Wave height scaling

In practice the armour layer stone size is determined by the method of VAN DER MEER [1988] to obtain stability based on a significant wave height.

Since $d_{n50_{armour}}$ is yet determined, representative wave heights could be calculated based on plunging and surging breaker types.
VAN DER MEER [1988] defined equations for plunging and surging breakers in which a distinction is made in the form of a transition-value for the breaker parameter $\xi_0 m$. Based on these equations armour stability is obtained using design wave heights.
Within these calculations the assumptions are made for relevant parameters.

The relative density, $\Delta = \frac{\rho_s - \rho_w}{\rho_w}$, for basalt ($\rho_s = 2600 \text{kg/m}^3$) is equal to 2. The notional permeability is for a core/armour breakwater equal to 0.5 according to VAN DER MEER [1988]. The slope of the structure is equal to 1:2 ($\alpha = 27^\circ$). Based on an example given in VERHAGEN *et al.* [2012] a stability number S=2 is assumed under influence of N=3000 waves. Two breaker types are tested, a plunging- ($\xi_{0m} = 2$) and a surging breaker ($\xi_{0m} = 4$).

As a result, the breaker parameter at which the transition between plunging and surging takes place equals 3.6. The significant wave height which corresponds with the scaled model for a plunging breaker in these conditions equals $H_s \approx 0.145$ m. For a surging breaker type the representative wave height is $H_s \approx 0.115$ m.

NOTE: When wave conditions are tested with a smaller significant wave height than above, actually the armour is designed too heavy. Otherwise, when stones are not glued together stability of the armour, and constant near-structure flow during consecutive tests, could not be guaranteed in case of larger wave heights.

6.4 Measurement instruments

In this paragraph measurement instruments are described which are used to obtain data. This data is processed using DASYLab which is a software program for data acquisition control and analysis. Output is expressed in voltage [V] in which the output-range goes from -10V to 10V. Voltage is translated into relevant units using MATLAB.
All instruments are calibrated, results are shown in Appendix E. Technical properties of the instruments are given in Appendix F.

6.4.1 Wave gauges

Wave gauges measure wave heights based on conductivity. In order to determine incoming regular waves two wave gauges are necessary which have a spacing of approximately 1/4 of the average wave length. In the case of irregular waves a wave spectrum over a certain spectral bandwidth must be obtained for which 3 wave gauges are required which have a spacing of 0.40 m and 0.30 m (figure 6.30).
Two sets of three gauges are used to analyse the wave characteristics at two different locations. One set is located in the middle of the flume at 18 m from the wave machine, whereas the second set of gauges is positioned at the toe of the breakwater.
The wave gauges measure with a frequency of 100 Hz and are able to produce

an incoming and reflected wave spectrum which is based on the method of MANSARD AND FUNKE [1980].

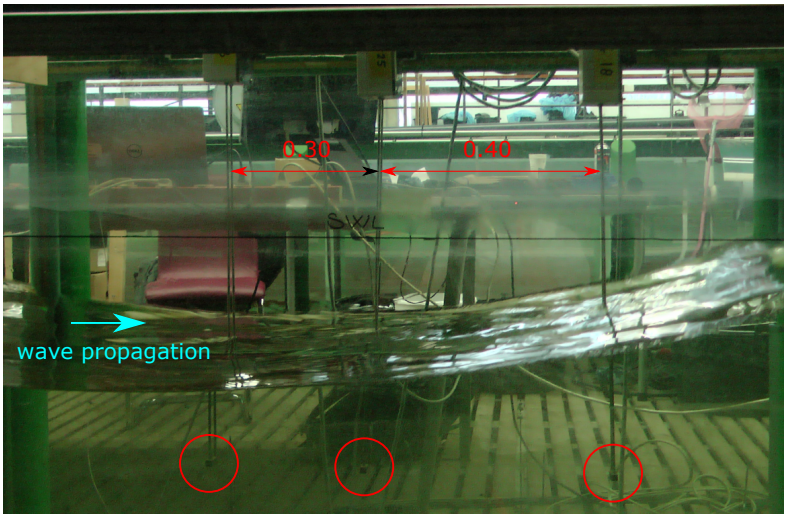

Figure 6.30: Wave gauges: Spacing of 0.30 m and 0.40 m. Cubes, indicated by red circles, measuring conductivity

6.4.2 Video camera

A 10.6 mega-pixel Panasonic HDC-HS200 video camera with a frame rate of 25 frames per second (FPS) is used for videos and images. Mainly the processes around the crown wall are recorded from a side view. To synchronize videos to displacement- and pressure data a LED-light is used which lights up when data processing starts. It must be noted that there is a 0.5 sec lag between the pulse and lighting up of the LED.

6.4.3 Magnetic rangefinders

Magnetic rangefinders (figures 6.31 & 6.32) are used to measure displacements of the crown wall elements. Because of magnetic properties water does not have an influence on the measurements. In fact displacements up to 17 mm could be measured, however given the output boundaries of DASYLab (-10V to 10V) only displacements between 0 mm and 12 mm with an accuracy of 0.1 mm could be measured. The range finders sample with a frequency of 100 Hz.

6.4.4 Pressure sensors

The pressure sensors, as in figure 6.33, can measure pressures up to 0.5 PSI (0.35 m static water pressure). The sensor measures pressures on both sides of a membrane from which a resultant pressure, $P_R = P_2 - P_1$, is obtained.
The sensors sample with a frequency rate of 10000 Hz (10 kHz). Although measures have been taken to mute noise (see paragraph 6.2.3) still large peaks are established during calibration tests which do not represent a realistic pressure

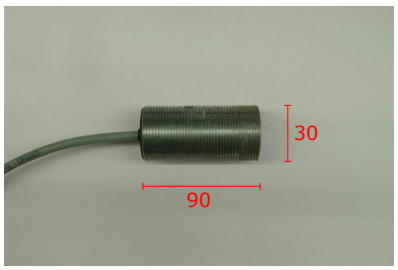

Figure 6.31: Top view: Magnetic range finder, sizes in [mm]

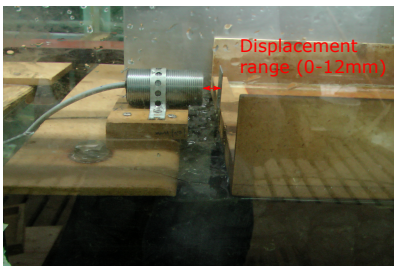

Figure 6.32: Side view: Range of measured displacements

in those specific conditions.
A lowpass 5^{th}- order Butterworth filter is used to get rid of these peaks at a maximum passing rate of 10 Hz. This means that pressure fluctuations which fluctuate with a frequency above 10 Hz are flattened within the pressure records. This lowpass rate is quite low since real peaks could be higher, however it should be possible to obtain a good estimate of the pressure profile.

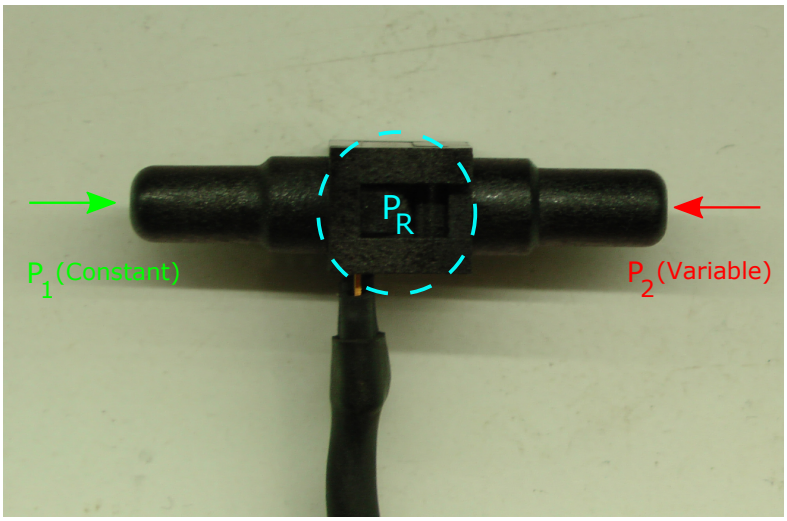

Figure 6.33: Pressure sensor 0.5 PSI

6.4.5 Load cell

A load cell is used to determine the static friction coefficient between crown wall and top of the breakwater. It concerns a load cell with a maximum loading capacity of 15 kg (150 N). The load cell is attached to a carriage (figure 6.34) which moves on the wave flume to ensure a consequent tensile force on the crown (loading under a straight angle).

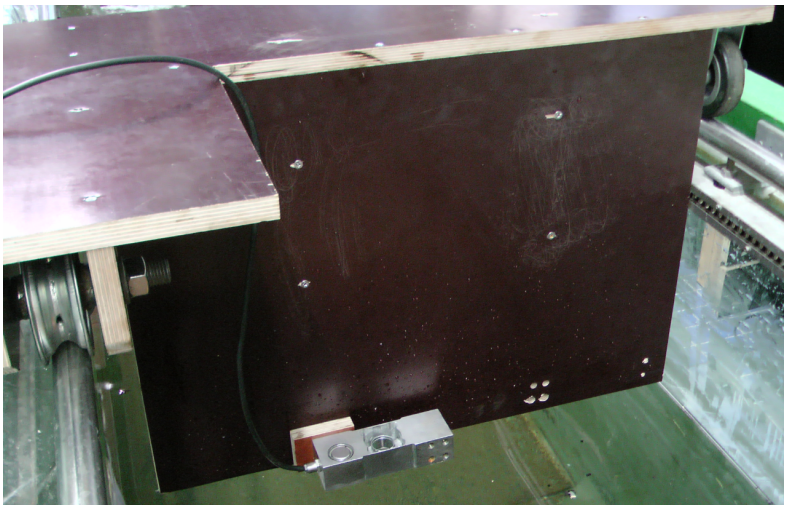

Figure 6.34: Load cell attached to measurement carriage

The determination of the friction coefficient is carried out according to figure 6.35. During a friction-measurement the tensile force is obtained at which the crown wall starts to slide. When this tensile force is divided by the weight of the crown wall the static friction coefficient is derived. The sample rate is 100 Hz.

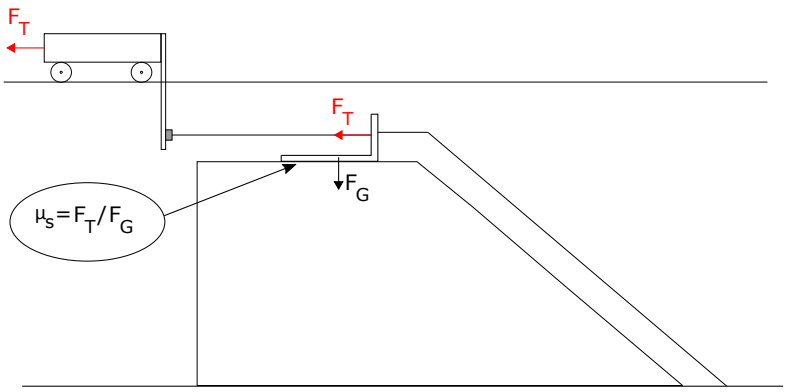

Figure 6.35: Method for determining the static friction coefficient

6.4.6 Laser scanner

A laser scanner is used to measure the contours of the core and armour layer. This is shown in figure 6.37. At every displacement of 0.5 mm a measurement point/pulse is registered. Tests have shown that basalt stones should be lightly coloured due to laser light absorption by dark surfaces which disturb the measurements.
For each section (A,B and C) 12 slices will be measured dived over the width. These contour measurements are used for a statistical analysis of geometry of the breakwater and whether differences provide deviating conditions around the crown wall.

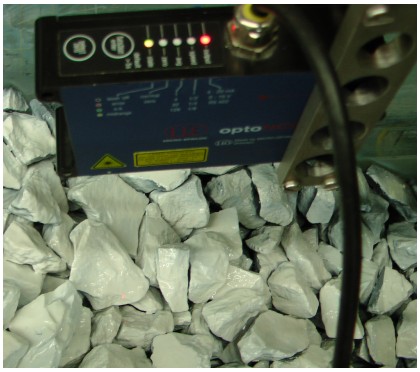

Figure 6.36: optoNCDT laser equipment

Figure 6.37: Laser measuring the contours of the armour and core

7

Experimental results and analysis

7.1 Introduction

In this study, the main objective is to explore relationships between stability of a crown wall under influence of varying wave conditions. In this chapter the main focus is on the following topics:

- Stability of the crown wall as a function of wave height, wave period and freeboard;
- Vertical load on the crown wall as function of wave height, wave period and freeboard;
- Horizontal and vertical pressures envelop against the wall and base of the crown wall as function of wave height, wave period and freeboard.

During the experimental study a number of hydraulic parameters are varied whereas geometrical properties remained unchanged. Further details are described in chapter 4.

In section 7.2 general findings are described which are of importance for further analysis of the results. The results are given in section 7.3, whereas an analysis of these results is given in section 7.4.

7.2 General findings

In this section general findings, which are of importance for further analysis of test results, are described.

7.2.1 Friction coefficient

Static friction coefficients are obtained in both dry and wet conditions for the three different sections, see table 7.1. A 95% confidence interval is given for an average friction coefficient based on a large number of samples (80) to ensure a precise interval. For section A the highest friction coefficient is found whereas section B has the lowest friction value. It is observed that friction values in wet conditions tend to be higher than in dry conditions. This is most likely due to a sticky/suction effect between the crown wall and core since the structure

is permeable. Secondly, the crown wall elements are fabricated from a softer material (wood) than concrete which is used in practice. It is expected that the rubble mound presses more easily into the wood which increases the friction coefficient as well.
According to CIRIA *et al.* [2007], the friction to be used between a concrete element and rubble mound breakwater is approximately 0.5. However, from an analysis of the damage and repair of Antalya harbour breakwater in BRUUN [2013], friction values of 0.7 were measured.
In comparison to these values it is concluded that the friction coefficient in this study is somewhat high which is highly due to the soft wood in comparison to concrete. The friction will be taken into account so that stability is compensated for the higher friction. For the stability analysis the wet friction coefficients are used since failure occurred in wet conditions for each test condition.

Table 7.1: Static friction values

Section	$\mu_{s,dry}$ [-]	$\mu_{s,wet}$ [-]
A	0.70±0.01	0.77±0.01
B	0.67±0.01	0.72±0.01
C	0.69±0.01	0.74±0.01

7.2.2 Geometry differences

It is observed that different amounts of overtopping water flow into the three sections, especially for storm waves these differences are relatively large. In figure 7.1(a) this phenomenon is depicted in which the water of an overtopping wave is coloured red.
It can be seen that the largest amount of water enters section B followed by C and then A (also observed for regular waves).
The same tests have been carried out using a smooth slope (armour was covered by a plate) to ensure an equal geometry over width, see figure 7.1(b).
It can be seen that the front line of the entered water is more or less levelled for all three sections. Therefore, it can be concluded that geometry deviations of the armour layer are responsible for differences in the amount of water entering the sections.

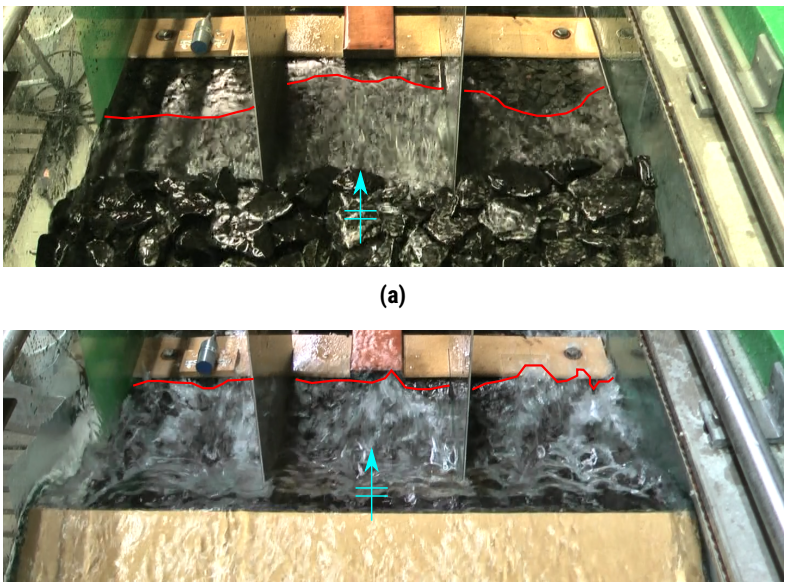

(a)

(b)

Figure 7.1: Overtopping water impact the structure. a) Differences in amount of water due to armour layer deviations. b) Differences disappear for a smooth slope.

From laser measurements average cross sections (95% confidence interval) of the structure per section are obtained based on a sample of 12 measurement strips. These are plotted together in figure 7.2.
It can be seen that cross section A has the highest level whereas cross section B tends to have the lowest structure height at most locations.
Since deep water conditions are assumed, inflow differences should especially occur as a result of geometry deviations around the still water level (SWL), which is shown in figure 7.3. In the lower part of the SWL range the armour of sections A and C is significantly higher than for B (order of magnitude: 1 - 3 cm). Above SWL range the contours of section B and C are more or less equal whereas section A is on average 2 - 3 cm higher. In the last 3 cm of the armour berm, a peak is observed for section C.

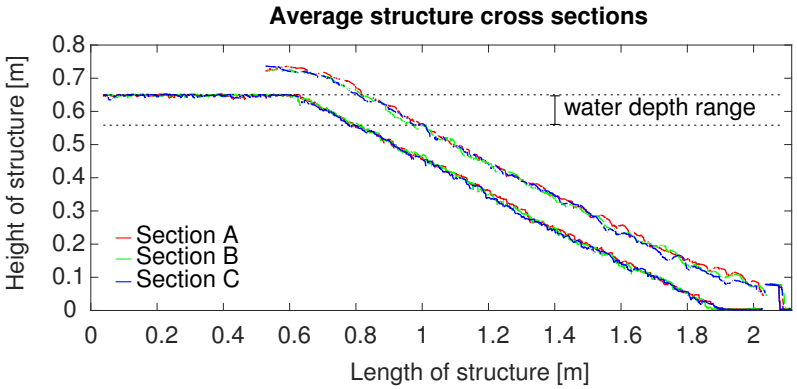

Figure 7.2: Averaged cross sections of the structure based on 12 slices

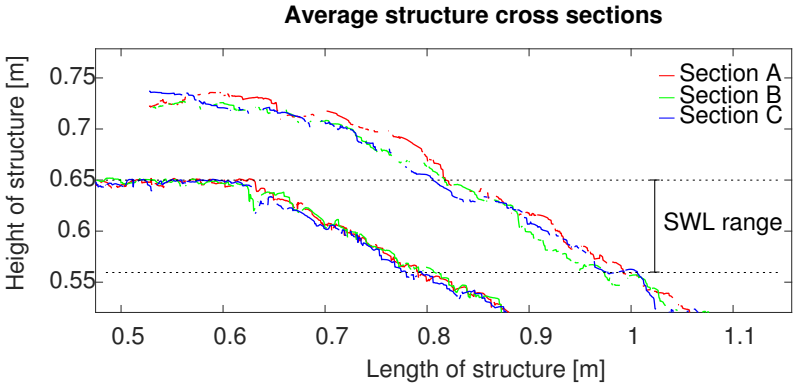

Figure 7.3: Average cross sections, zooming around SWL

Except from average cross sections, additionally standard deviations are calculated at every measurement point. From these standard deviations upper and lower boundaries are defined (based on a 95% confidence interval for 3400 samples) for each cross section. In table 7.2 the average standard deviation for the armour layer per section is given. The standard deviations are more or less equal to 30% of $d_{n50,a}$. Besides, standard deviations are equal for each section, this indicates that differences in results between sections are not dependent on the roughness of the breakwater.

Table 7.2: Average standard deviation of armour layer

Section	σ [m]	Fraction of $d_{n50,a}$
A	0.012	0.33 $d_{n50,a}$
B	0.012	0.33 $d_{n50,a}$
C	0.012	0.33 $d_{n50,a}$

7.2.3 Wave impact

During testing it is observed that the crest of a steeper wave ($s_{op} = 0.04$) curls over when 'feeling' the geometry of the armour. An air pocket is enclosed and wave energy is dissipated (figure 7.4) in the form of a plunging/collapsing breaker type [VERHAGEN *et al.*, 2012].
In the case of swell waves ($s_{op} = 0.01$) it is observed that waves surge up and down the slope of the breakwater with minor air entrainment (figure 7.5). This wave could be indicated by a surging breaker [VERHAGEN *et al.*, 2012]. This surging pattern leads to less energy dissipation before hitting the structure in comparison to plunging/collapsing breakers. Therefore, a swell wave exerts a higher load on the crown wall than a storm wave for same wave height and freeboard.

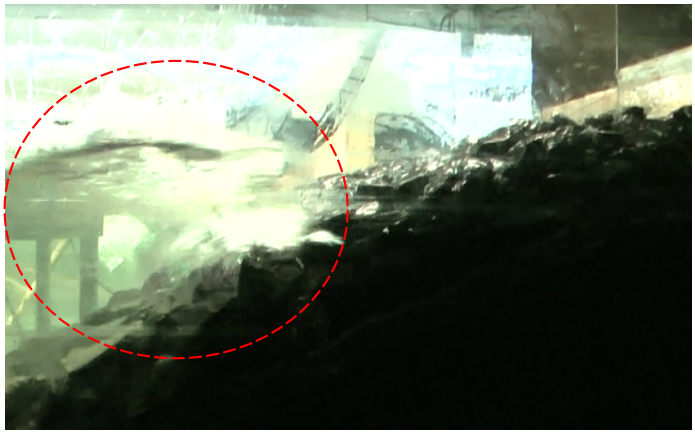

Figure 7.4: Plunging/collapsing breaker type, substantial energy dissipation

Figure 7.5: Surging breaker type, less energy dissipation

7.3 Experimental results

In this section, results of the main test subjects of this research are presented. Below a flowchart is shown in which per section the treated subjects and corresponding results can be seen.

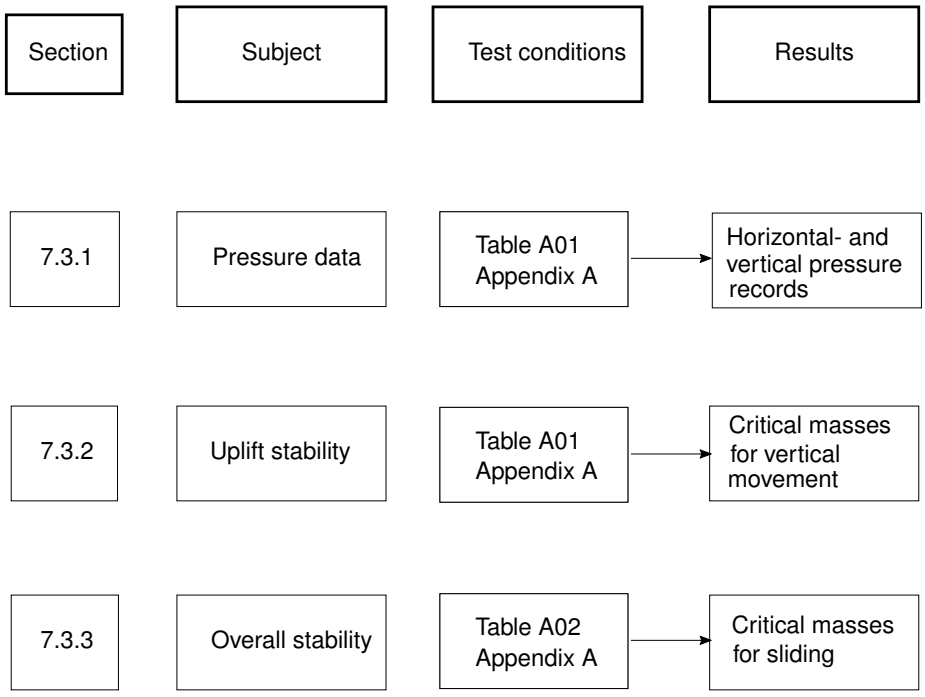

7.3.1 Pressure data

Pressure data is obtained for the test conditions in table A.02 of Appendix A. Four sensors in the wall were used to measure horizontal pressures and upward pressures were measured by five sensors in the base, see Appendix D for exact locations.
Since the signals are filtered quite heavily a qualitative analysis can be made but a quantitative analysis is omitted.

7.3.2 Uplift stability

Critical masses are obtained with respect to vertical stability of the element for test conditions given in table A.02 Appendix A. Results are shown in figure 7.6 in which these masses are plotted as function of dimensionless wave height. It could be stated that a relatively large wave period in combination with large ratio H_s/R_{ca} lead to the biggest critical mass whereas a small ratio of H_s/R_{ca} and short wave period lead to smaller masses.
Since these masses are measured in only one section errors bars are not presented.

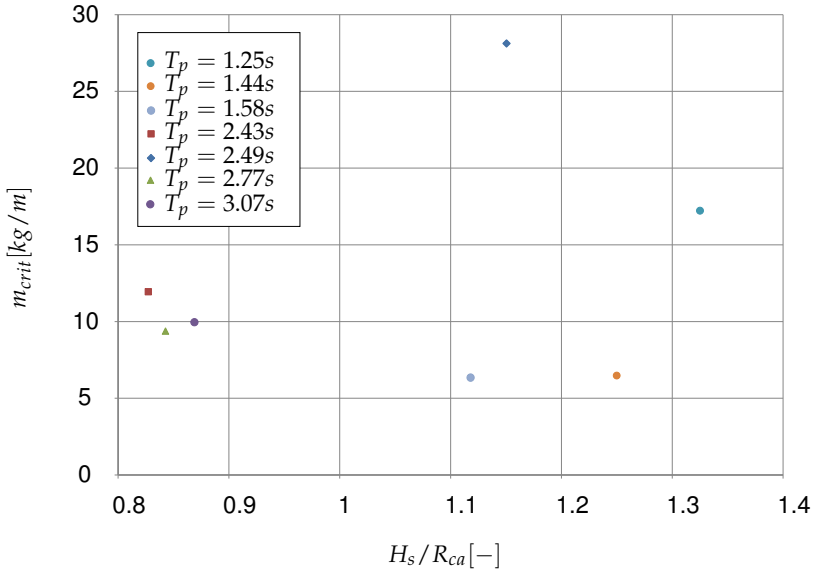

Figure 7.6: Base level shift after loading

7.3.3 Overall stability

Critical masses of the crown wall are found for the test conditions given in table A.01 Appendix A. The masses are divided by the static friction corresponding to the measured section and by the width of the crown wall. This results in a mass per meter width in which the effect of friction is taken into account.
The data points represent the average critical masses of sections A,B and C and are displayed with an error bar which indicate the minimal and maximal measured values.

From the data plots, without performing a physical analysis, it could be summarised that:

- An increase in wave height leads to an increase in critical mass;
- An increase in freeboard leads to a decrease in critical mass;
- An increase in wave period leads to an increase in critical mass.

Influence of wave height

As representative wave height the incident significant wave height measured just in front of the breakwater (at the toe) is used.
Figure 7.7 and figure 7.8 show the effect of a changing wave height on the stability of the crown wall. In general for both wave steepness an increasing wave height leads to an increase in critical mass (higher loads).

Influence of freeboard

In figure 7.9 results are shown in which the influence of armour crest freeboard variation on the crown wall- stability can be seen. The wave height is presented as dimensionless wave height H_s / R_{ca} which represents the ratio between significant wave height and armour crest freeboard.
Clearly, an increase of this ratio leads to an increasing load and therefore higher critical mass.

Influence of wave period

From figure 7.9 the influence of wave period on the stability of the crown wall can also be observed. It is clear that larger periods lead to higher loads and critical masses for a constant H_s / R_{ca}.
In general swell waves (purple and green lines) exert bigger total loads than storm waves (red and blue lines). This is in accordance to the findings in section 7.2.3.

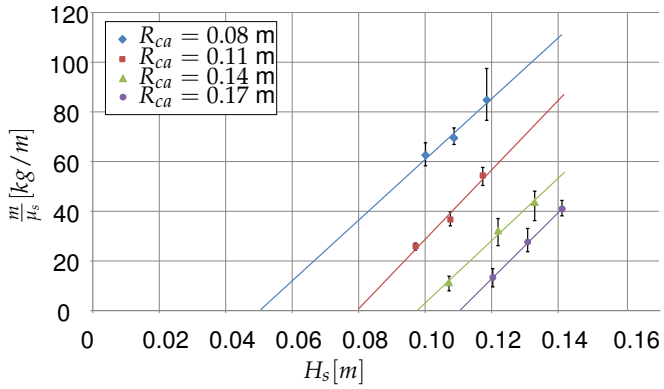

Figure 7.7: Influence of wave height on critical mass for s_{0p}=0.01

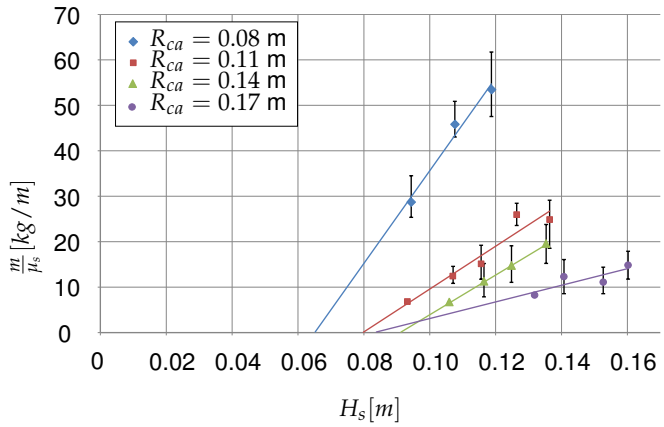

Figure 7.8: Influence of wave height on critical mass for s_{0p}=0.04

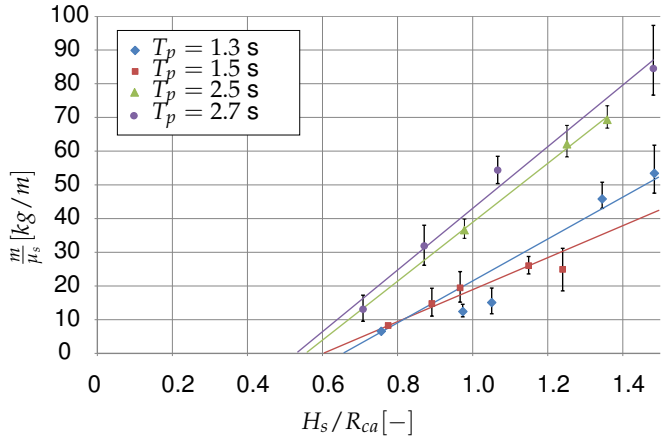

Figure 7.9: Influence of armour crest freeboard on critical mass for 4 wave periods

7.4 Experimental data analysis

Below a flowchart is shown in which per section the treated analysis and corresponding findings can be seen.

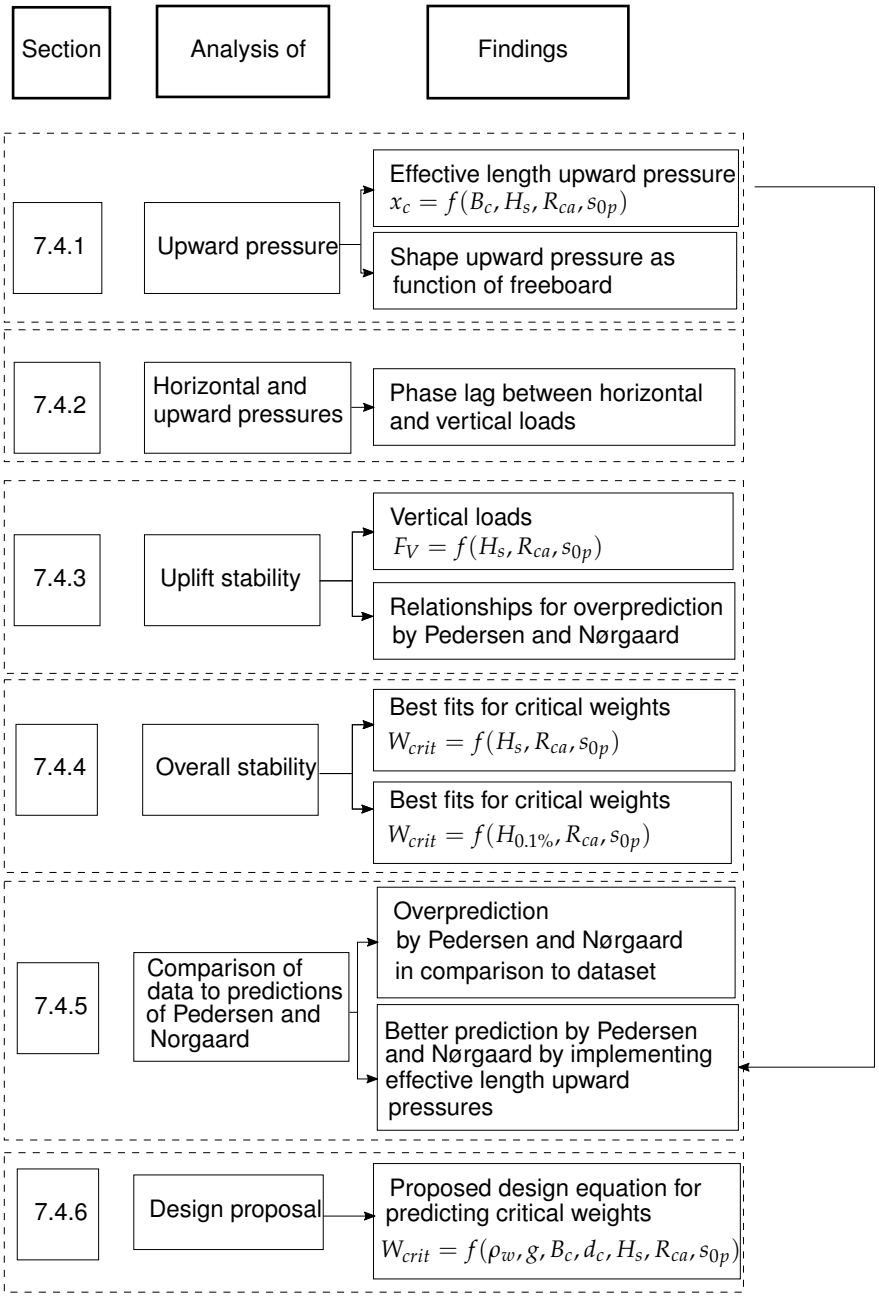

7.4.1 Upward pressure

Below, the analysis of the upward pressure is described which is divided in two parts. In the first section the part of the base slab which will be covered by water for certain wave conditions is investigated. In the second section an analysis is done with respect to the shape of the upward pressure profile. Finally a conclusion is drawn in which a comparison is made between the analysed data and existing knowledge.

Covered part of base

From video images it follows that the part of the base which comes in contact with water depends on freeboard. In figure 7.10 a picture taken from a video record around failure of the crown wall is shown. Also the corresponding pressure profile can be seen for 4 time steps within the failure interval.
From visual analysis it is observed that approximately a maximum of 70% of the base comes in contact with water at the moment of failure, the boundary between contact/no contact is indicated by a red arrow. This location corresponds quite nicely with the profile where pressure is more or less reduced to 0 at the same location. The covered length is indicated by x_c, the uncovered length is indicated by x_u.

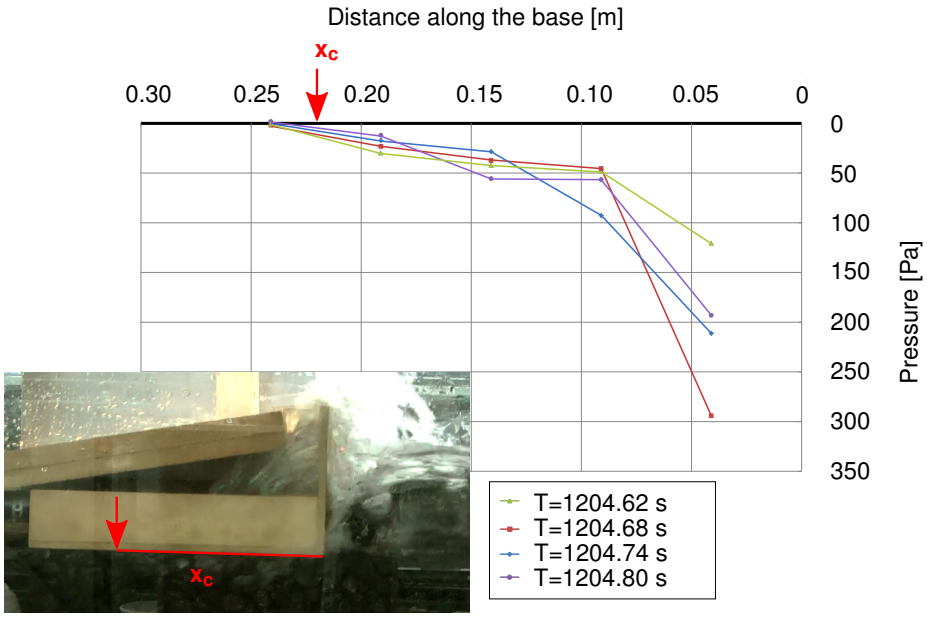

Figure 7.10: Maximum vertical pressures at three time steps for pressure record of test condition: A_{swell1}

The video analysis has been done for the test conditions in both tables in Appendix A whereas the check by pressure records is only done for conditions in table A.01.
The wet part of the base slab x_c/B_c is presented as function of dimensionless

wave height H_s/R_{ca} for swell- and storm waves which is shown in figure 7.11. A linear relationship is found for the wet part of the base as function of dimensionless wave height for both wave types. The determination coefficient R^2 for the fit of points is smaller for $s_{0p} = 0.01$ than for $s_{0p} = 0.04$. This seemed to be caused by the outlier left of the fit around 80% wet part. These values of $R^2 = 0.76$ and $R^2 = 0.88$ indicate a moderate to decent fit.

It can be seen that small values of H_s/R_{ca} (0.65-0.75) lead to an almost negligible effect of upward pressure against the crown wall. When the dimensionless wave height reaches approximately 1.05 or higher for swell waves the base slab comes completely in contact with water and so pressure exerts a load over the entire length of the base. For storm waves the threshold lies at a dimensionless wave height of approximately 1.35 or larger.

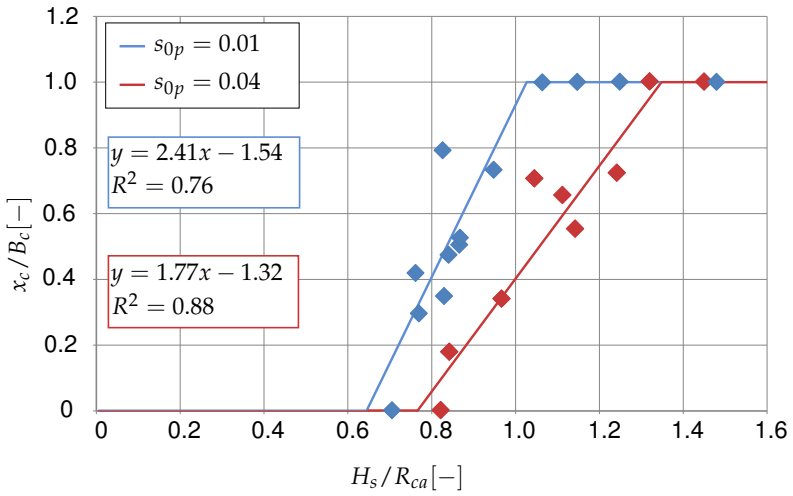

Figure 7.11: Wet part of base slab as function of dimensionless wave height for swell- and storm waves

Shape of upward pressure profile

In figures 7.12 and 7.13 vertical pressures at three time steps for swell and storm waves can be seen for zero freeboard. These pressure profiles represent the three maximum pressures during these records.
It is observed that each peak pressure within the same record exhibits more or less the same shape of envelope. On the front side of the base a relatively high pressure is found where after a considerable drop is noticed at 1/3 of the total length from the front.

It is observed that for each of the seven conditions maximum upward pressures do not show peculiarities in comparison to each other. From this, it is concluded that the extreme upward pressures are measured correctly.

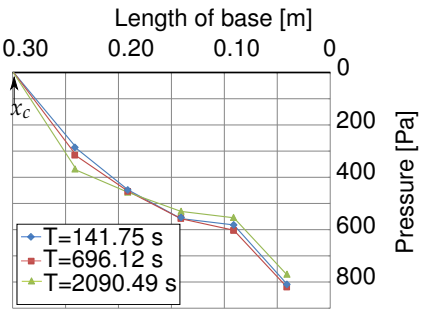

Figure 7.12: Extreme vertical pressures at three time steps for pressure record of test condition: A_{swell1}.

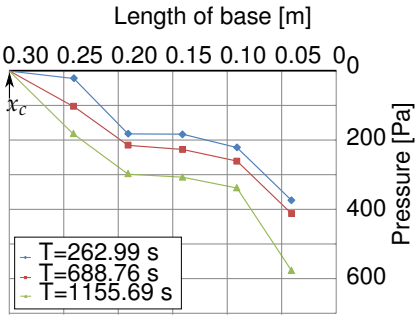

Figure 7.13: Extreme vertical pressures at three time steps for pressure record of test condition: A_{storm1}.

In figures 7.14 and 7.15 maximum pressure profiles are shown per test condition for swell and storm waves as function of wave height and freeboard.
In general it is observed that for larger values of H_s/R_{ca} the pressure is more or less S-shaped whereas it converts into a parabolic shape for decreasing H_s/R_{ca}. It is remarkable that for swell waves (figure 7.14) the magnitude of the pressure at the front side is especially determined by the absolute wave height, since the biggest upward pressure at the front is found for the largest wave height but also largest R_{ca}.

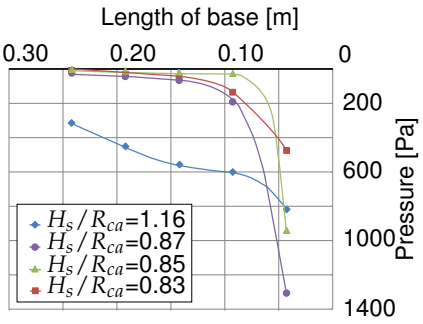

Figure 7.14: Maximum vertical pressures for each swell test condition.

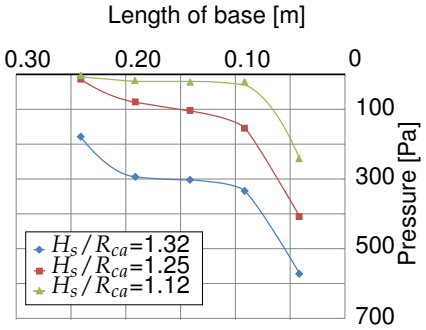

Figure 7.15: Maximum vertical pressures for each storm test condition.

Conclusion

In studies mainly assumptions have been made for the upward pressure distribution instead of using measured distributions. PEDERSEN [1996], MARTIN *et al.* [1999] and JUUL JENSEN [1984] assume a pressure distribution which is triangular and reaches zero at the rear end of the base slab, which does not depend on freeboard. The maximum pressure exists at the front side of the base and has the same value as the horizontal pressure at the bottom of the wall.

From findings of this research these assumptions seem to be conservative in two ways: Firstly the position at which the pressure becomes zero actually appears to be dependent on freeboard and wave height. The zero pressure point shifts to the front side for increasing freeboard.
From video analysis and pressure measurements relationships for both wave steepness are obtained in which the covered part of the base x_c/B_c is given as function of dimensionless wave height H_s/R_{ca}. Supposing a direct relationship between upward pressure and covered part of the base, conclusions can be drawn about the effect of upward pressure based on total coverage of the base, which is summarized in the tables below.

Swell waves $s_{0p} = 0.01$	
x_c/B_c [-]	Condition
1	$H_s/R_{ca} \geq 1.05$
0	$H_s/R_{ca} \leq 0.64$
$2.41 H_s/R_{ca}$	$0.64 < H_s/R_{ca} < 1.05$

Storm waves $s_{0p} = 0.04$	
x_c/B_c [-]	Condition
1	$H_s/R_{ca} \geq 1.35$
0	$H_s/R_{ca} \leq 0.77$
$1.72 H_s/R_{ca}$	$0.77 < H_s/R_{ca} < 1.35$

Secondly, the assumed shape of the upward pressure profile seems to be different according to the test results. For small freeboard (or large H_s/R_{ca}) a S-shaped profile is observed whereas it transforms into a more or less parabolic shape for decreasing H_s/R_{ca}.

The two ways in which current design methods are too conservative are summarized in figure 7.16. It can be seen that the maximum value for upward pressure is assumed to be equal to that of currently assumed upward pressure. This seems reasonable since it is observed that vertical loads found in this research are more or less equal to the predictions of PEDERSEN [1996] and NØRGAARD *et al.* [2013] when no base freeboard is considered ($R_b = 0$), this can be seen in figures 7.20 and 7.21. When freeboard increases the overprediction of vertical loads increases as well and the actual p_{max} should decrease, the magnitude of the maximum pressure remains merely an assumption.
The covered and uncovered part are indicated by x_c and x_u which are a function

of H_s / R_{ca} whereas according to PEDERSEN [1996], MARTIN *et al.* [1999] and JUUL JENSEN [1984] the covered length is constant and always equal to the full length of the base $B_c = x_u + x_c$.

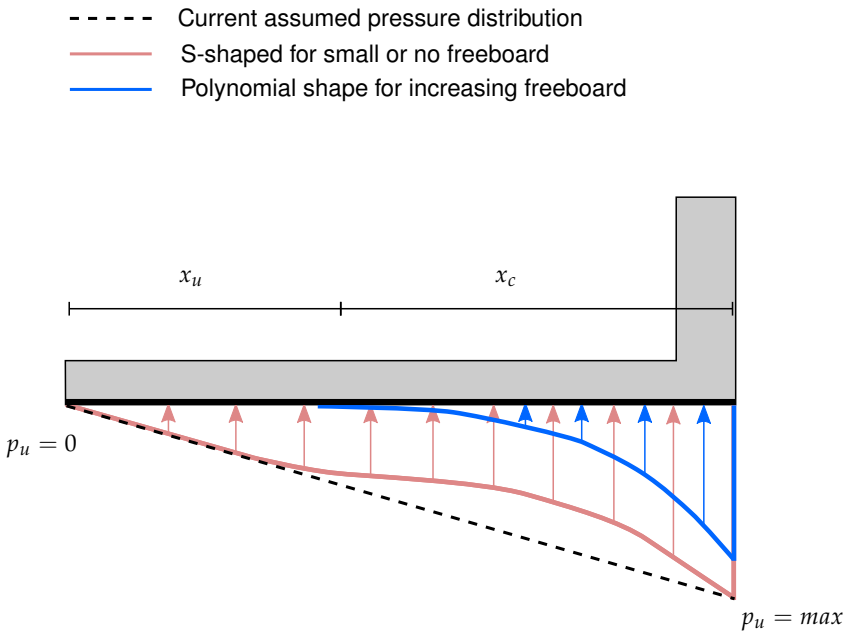

Figure 7.16: Summarize of upward pressure findings

7.4.2 Phase lag

To investigate whether phase lag is present between $F_{H,max}$ and $F_{V,max}$, the horizontal and vertical pressure profiles within the failure interval are considered at several time steps.
In figure 7.17 the vertical and horizontal pressure distribution on the crown wall can be seen for test condition A_{storm2}. Through the data points for horizontal pressure a best fit is drawn based on measurements of PEDERSEN [1996]. The data points corresponding to upward pressure are connected according to findings about the shape of upward pressure as function of freeboard (paragraph 7.4.1). Furthermore, the upward pressures at the front side of the base are based on the horizontal bottom pressure values. The effective length is indicated by a red arrow which is based on the findings in figure 7.11, as can be seen this corresponds to the pressure measurements.
The maximum horizontal pressure occurs at T=273.74 s (red line) whereas the maximum upward pressure occurs 0.11 s later (purple). When integrating the pressure profiles, point loads are obtained.
It can be concluded that after the maximum horizontal load is exerted the wave needs time to travel through the breakwater before collapsing with a maximum magnitude against the base, this phenomenon is known as 'phase lag'.
In table 7.3 results are shown for the test conditions in table A.01 of Appendix

A. It can be seen that in general no phase lag is present for swell waves except for relatively large freeboard. Whereas in the case of storm waves phase lag already occurs for $R_b = 0$ m and $R_b = 0.02$ m. It is remarkable that no phase lag is found for $R_b = 0.03$ m since it is expected that phase lag will increase with increasing freeboard.

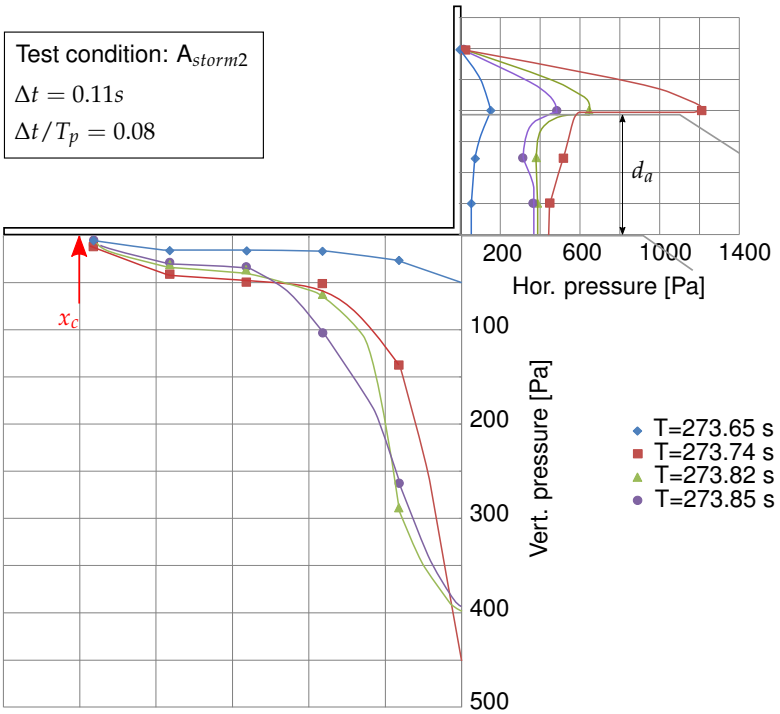

Figure 7.17: Horizontal and upward pressure for a storm wave in which phase lag is present.

Table 7.3: Results for phase lag

Test condition	Phase lag Δt [s]	Relative phase lag $\Delta t / T_p$ [-]
A$_{swell1}$	0	0
A$_{swell2}$	0	0
A$_{swell3}$	0	0
A$_{swell4}$	0.09-0.11	0.03
A$_{storm1}$	0.02	0.016
A$_{storm2}$	0.11	0.08
A$_{storm3}$	0	0

Conclusion

For stability against sliding CIRIA *et al.* [2007] proposes a criterion in which the horizontal- and vertical design loads occur simultaneously. This is the most unfavourable situation since the weight of the structure will decrease as much as possible while at the same moment the crown wall is maximal loaded in horizontal direction as well.

From the results it is concluded that phase lag is expected to occur, especially for steep waves. For increasing freeboard phase lag could also occur for swell waves.
However, no clear relationships are found and since pressures are filtered quite heavily, this has consequences for the reliability, especially for horizontal measured pressure since these are subjected to dynamic rapidly varying peak loads. The time span for dynamic peak loads are small, approximately 0.001-0.005 s based on figures 6.10 to 6.13. The considered failure interval in figure 7.17 is $\Delta T = 0.20$ s which is divided in 4 smaller time steps of $\Delta T \approx 0.05$ s. Due to filtering it might be possible that peak loads with time spans of the order 0.001-0.005 s are flattened and therefore not observed in the time steps of 0.05 s. Wrong conclusions may be drawn with respect to phase lag due to flattening of the peaks.
Therefore, more stable pressure sensors should be used, in which heavy filtering is not necessary, to obtain more reliable data with respect to a quantitative analysis of phase lag.

7.4.3 Vertical load

Based on the findings for vertical stability tests, vertical loads can be derived from the critical masses found in figure 7.6 with respect to vertical failure. Vertical loads will be derived according to figure 7.18 in which the following assumptions are important:

- The hinge does not exert a reaction force in the form of a moment;
- The foil which blocks a possible pressure loss exerts a negligible reaction force on the crown wall;
- Centre of gravity of the crown wall is constant for every test run, so x_G does not change (in fact $x_G = 0.177 \pm 0.001$ m);
- The upward pressure profile is assumed to be triangular in order to estimate the point of action of the vertical load, which is located at $2/3x_c$ from the zero pressure point $p_u = 0$;
- The measured values x_c and x_u are used to derive the vertical load;
- $F_V = F_G \cdot x_G / (x_u + \frac{2}{3}x_c)$

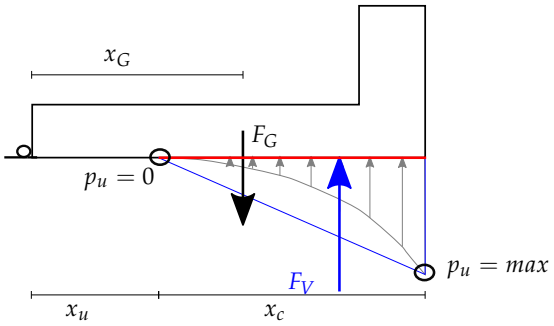

Figure 7.18: Loading diagram to derive vertical loads

Since freeboard plays an important role in the magnitude of loads it is chosen to make the significant wave height dimensionless by the armour crest freeboard. According to HUGHES [2003] the momentum of a wave is proportional to H^2, for that reason the dimensionless wave height is squared.
In figure 7.19 the vertical loads as function of dimensionless wave height for swell- and storm waves are shown. The blue and red points indicate the vertical load at which stability of the crown wall is critical, bigger loads lead to failure whether the crown wall remains stable for smaller loads. The green points with a red border represent vertical loads at which no failure occurred, apparently the loads are smaller then these points predict (red arrows). Therefore, they function as boundary since a linear fit must stay below these values.
From a physical point of view loading is by definition zero when $H_s/R_{ca} = 0$. This point is indicated by a blue bordered red circle.
Best fits are determined for the derived critical vertical loads in which swell and storm waves are separated. For swell- and storm waves no vertical loading is found when $H_s^2/R_{ca}^2 \leq 0.42$ or $H_s^2/R_{ca}^2 \leq 1.15$ which corresponds to $H_s/R_{ca} = 0.65$ and $H_s/R_{ca} = 1.07$.

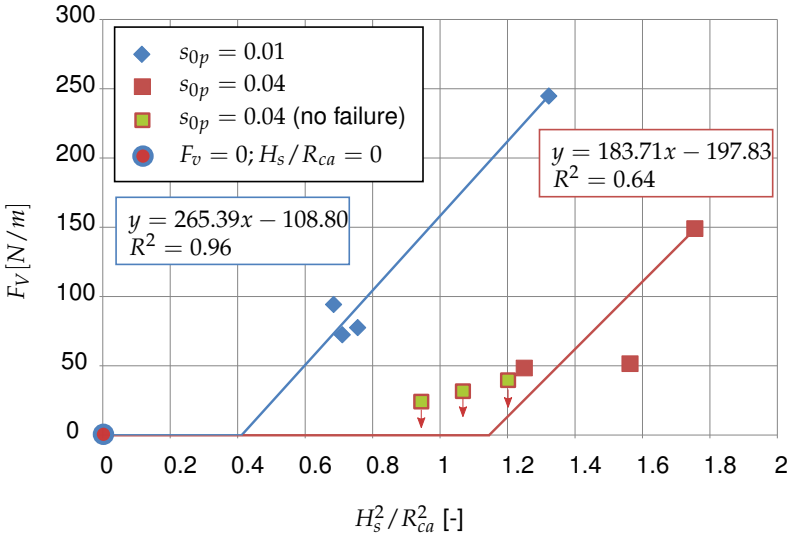

Figure 7.19: Vertical load as function of H_s/R_{ca} for $s_{0p} = 0.01$ and $s_{0p} = 0.04$

Conclusion

By comparing these findings to figure 7.11 the following conclusions can be made:

Swell waves $s_{0p} = 0.01$	
$F_V\,[N/m]$	Condition
0	$H_s^2/R_{ca}^2 < 0.42$
$265H_s^2/R_{ca}^2$	$H_s/R_{ca} \geq 0.42$

Storm waves $s_{0p} = 0.04$	
$F_V\,[N/m]$	Condition
0	$H_s^2/R_{ca}^2 < 1.15$
$184H_s^2/R_{ca}^2$	$H_s/R_{ca} \geq 1.15$

When comparing the results to calculated vertical loads for the same conditions using PEDERSEN [1996] and NØRGAARD *et al.* [2013], an over prediction is observed for both $s_{0p} = 0.01$ and $s_{0p} = 0.04$ when $R_{ca} > d_a$ and so $R_b > 0$ which causes a reduction in vertical load since the effective length x_c reduces ($x_c < B_c$).
In figures 7.20 and 7.21 these over predictions are shown. Best linear fits are drawn corresponding to the data points. Especially for swell waves a more reliable fit is drawn whereas the outlier in storm waves causes a less reliable fit. However, in general it can be concluded that vertical loads are over predicted

which corresponds to conclusions drawn with respect to upward pressure distribution in section 7.4.1.

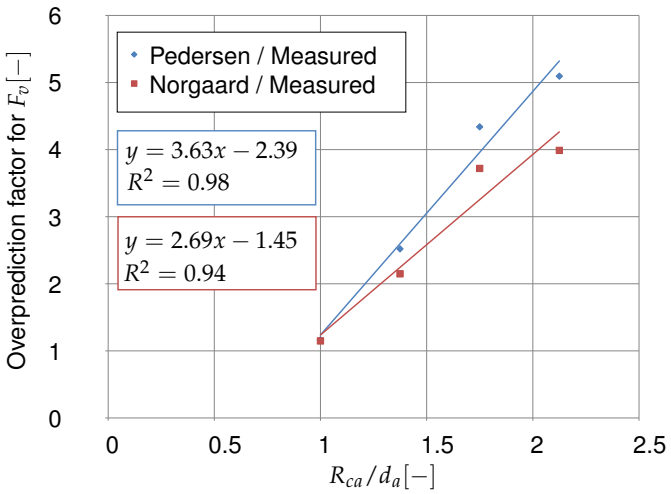

Figure 7.20: Overprediction of vertical load F_v by PEDERSEN [1996] and NØRGAARD *et al.* [2013] for $s_{0p} = 0.01$.

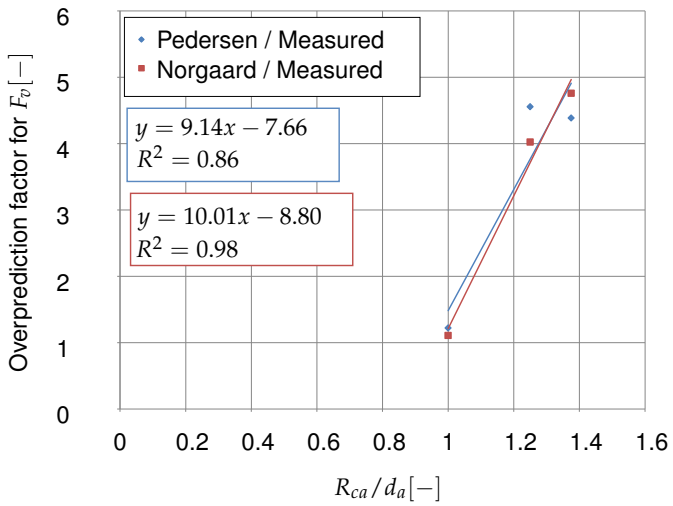

Figure 7.21: Overprediction of vertical load F_v by PEDERSEN [1996] and NØRGAARD *et al.* [2013] for $s_{0p} = 0.04$.

7.4.4 Overall stability

Overall stability of the crown wall depends on the resistance against sliding and the loads exerted on the structure.
Resistance against sliding could also be indicated as strength and is defined as the nett own weight multiplied by the static friction coefficient (which holds during loading conditions): $S = F_G \cdot \mu_s$.
Loading of the structure takes place due to an interaction between horizontal and vertical loads.

In this section overall stability is presented as critical weight as function of H_s, $H_{0.1\%}$ and R_{ca}. Critical weights, based on results given in section 7.3.3, are defined as: $W_{crit} = mg/\mu_s$. The relevant test conditions are given in table A.02 in Appendix A.

Stability as function of H_s

In figure 7.22 data is given of critical weights for the crown wall as function of H_s^2/R_{ca}^2. Six different kinds of data points can be distinguished which represent statistical average values of critical weights and corresponding upper- and lower boundaries based on a 95% confidence interval.
Based on linear regression, best fits are drawn through these points.

The solid lines give an estimate for the average expected critical weights given a significant wave height and armour crest freeboard. For values of $H_s^2/R_{ca}^2 = 0 - 0.5$ no measurements were done and therefore this extrapolation leads to uncertainties. The best fit for average critical weights considering swell waves crosses the y-axis at y=13.28 which implies that the crown wall should have a weight of 13.28 N/m to be stable while no loading is applied. From a physical point of view this could not be correct since zero wave height means no wave momentum and hence no loads exerted on the crown wall, however, the value of 13.28 N/m is relatively small in comparison to the tangent of the function from which it can be concluded that this physical contradiction can be neglected.

Stability as function of $H_{0.1\%}$

It is observed that for most of the test conditions the biggest wave $H_{0.1\%}$ causes sliding and thus failure of the crown wall. For each test condition the $H_{0.1\%}$ is found which can be seen in Appendix A.
The relative 0.1% wave height is defined as $H_{0.1\%}/R_{ca}$. The critical mass is plotted as function of $H_{0.1\%}^2/R_{ca}^2$ and is shown in figure 7.23. Upper- and lower boundaries are given based on a 95% confidence interval.

The solid lines give an estimate for the average expected critical weights given a significant wave height and armour crest freeboard. For values of $H_{0.1\%}^2/R_{ca}^2 = 0 - 0.5$ no measurements were done and therefore this extrapolation leads to uncertainties. The best fit for average critical weights considering swell waves crosses the y-axis at y=79.64 which implies that the crown wall should have a weight of 79.64 N/m to be stable while no loading is applied. From a physical point of view this could not be correct since zero wave height means no wave momentum and hence no loads exerted on the crown wall. The value of 79.64 N/m is relatively large in comparison to the tangent and therefore

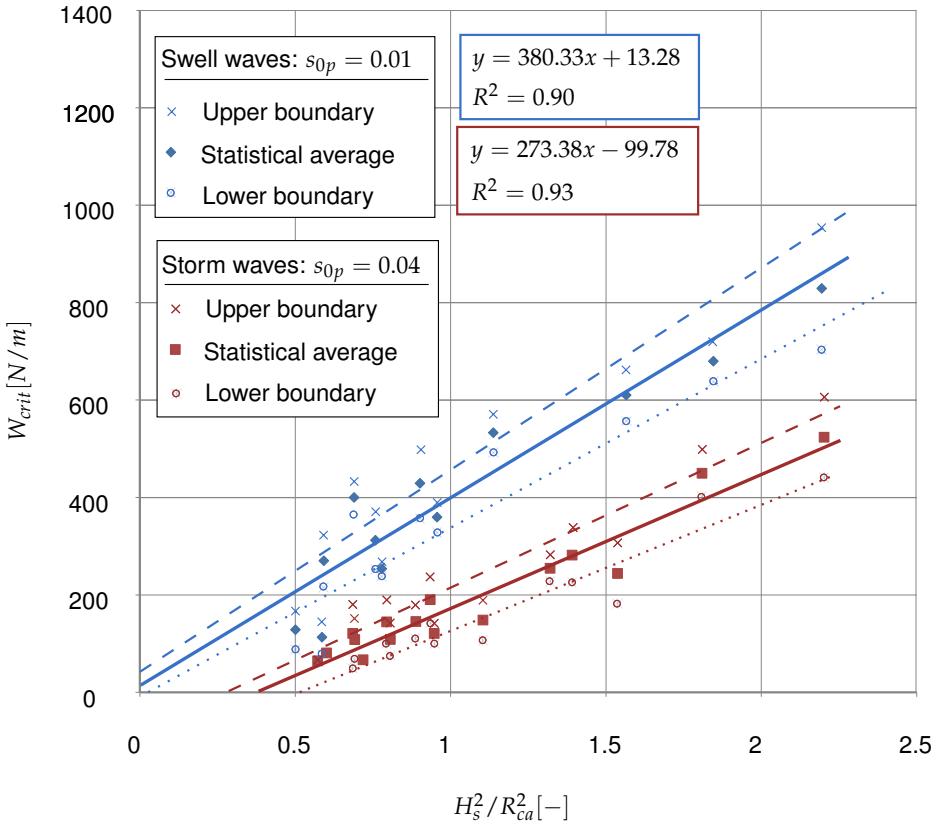

Figure 7.22: Best fits for critical weights as function of H_s^2/R_{ca}^2 for $s_{0p} = 0.01$ and $s_{0p} = 0.04$

it is concluded that the found equation is not reliable within the range of $H_{0.1\%}^2/R_{ca}^2 = 0 - 1.0$.

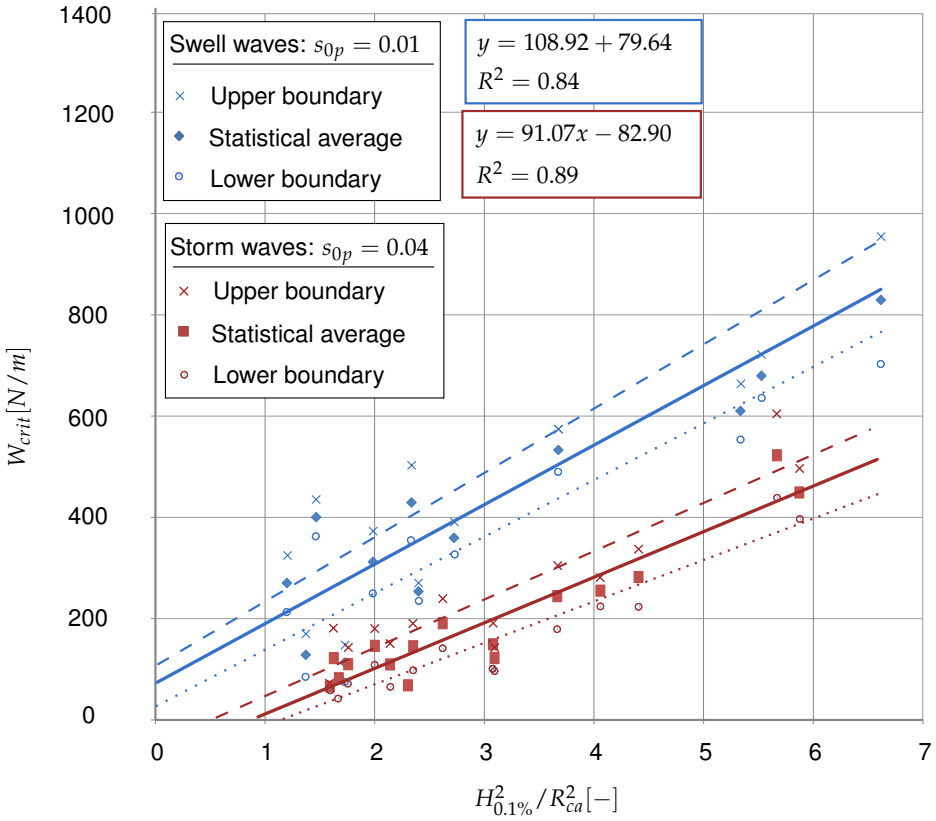

Figure 7.23: Best fits for critical weights as function of $H^2_{0.1\%}/R^2_{ca}$ for $s_{0p} = 0.01$ and $s_{0p} = 0.04$

7.4.5 Comparison to PEDERSEN [1996]

Since PEDERSEN [1996] is the mostly used wave load calculation method until now, a comparison will be made between the found data and the expected critical weights calculated by using the methods of PEDERSEN [1996] with and without using the extension of NØRGAARD *et al.* [2013].
These calculations are based on stability against sliding for which CIRIA *et al.* [2007] states that the maximum horizontal and vertical loads occur simultaneously. Since no clear relationship for phase lag is found stability calculations are made according to the criterion:

Stability against sliding: $F_{H,max} = \mu_s(F_G - F_{V,max})$

CIRIA *et al.* [2007] defines F_G as the nett own weight after buoyancy is taken into account for the complete volume of the crown wall. From video analysis it is observed that this assumption is much too conservative for the test conditions in this research. For that reason initially buoyancy is omitted which means that $F_G = W$ without considering a buoyancy force F_B which is done in CIRIA *et al.* [2007].

Conventional PEDERSEN [1996] and NØRGAARD *et al.* [2013]

In figures 7.24 and 7.25 predictions for the critical weight as function of significant wave height and freeboard by PEDERSEN [1996], NØRGAARD *et al.* [2013] and the best fit for the results are shown for both wave steepness.
It can be seen that for $s_{0p} = 0.01$ PEDERSEN [1996] is way too conservative in predicting the critical weight especially for increasing freeboard whereas NØRGAARD *et al.* [2013] proves that his extension approaches the fits better since the overprediction decreases for increasing freeboard in comparison to PEDERSEN [1996]. For larger values of H_s^2 / R_{ca}^2, or decreasing freeboard, NØRGAARD *et al.* [2013] predicts critical weights between the upper- and lower boundaries of the design equations.
In the case of $s_{0p} = 0.04$ PEDERSEN [1996] is still way to conservative. However, for low freeboard some critical weights are predicted below the lower boundary of the design equation. NØRGAARD *et al.* [2013] seems to predict the weight better than PEDERSEN [1996] but also for low freeboard predictions are below the lower boundary of the design equation.

From figures 7.24 and 7.25 it could be concluded that NØRGAARD *et al.* [2013] provides better predicitions than PEDERSEN [1996] does. In general overpredicitions tend to increase for increasing freeboard (decreasing H_s^2 / R_{ca}^2) whereas an decreasing freeboard (increasing H_s^2 / R_{ca}^2) sometimes lead to underprediction of the critical weight with respect to the fit.

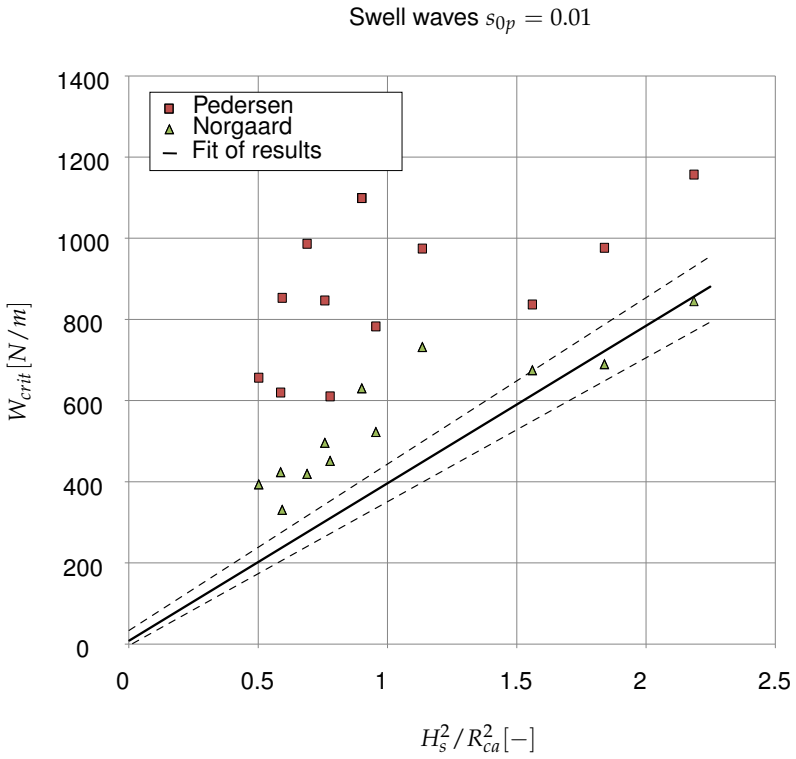

Figure 7.24: Critical weight predicted by conventional methods of PEDERSEN [1996] and NØRGAARD *et al.* [2013] compared to test results, for $s_{0p} = 0.01$

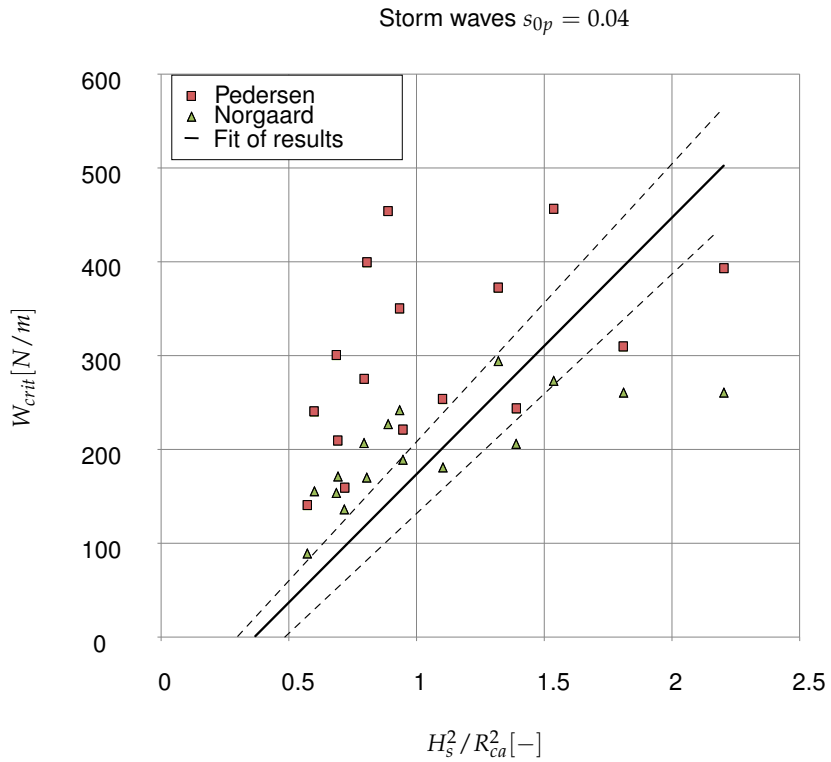

Figure 7.25: Critical weight predicted by conventional methods of PEDERSEN [1996] and NØRGAARD *et al.* [2013] compared to test results, for $s_{0p} = 0.04$

Adapted PEDERSEN [1996] and NØRGAARD *et al.* [2013]

A possible reason for these over- and under predictions is the effect of vertical load which varies based on varying effective length x_c, found in figure 7.11. This is not taken into account for the conventional methods of PEDERSEN [1996] and NØRGAARD *et al.* [2013].

The effective vertical load is equivalent to the integrated upward pressure which act over the effective length x_c, described in figure 7.11 for swell and storm waves. The effective length x_c leads to a reduction coefficient for the upward pressure and so the vertical load F_V. For example: $x_c/B_c = 0.4$ means an effective upward pressure of $0.4P_{U,0.1\%}$ instead of $P_{U,0.1\%}$ which is done in current design methods.
By taking the actual covered length x_c into account the predictions as shown in figures 7.26 and 7.27 are obtained. It can be seen that predictions by PEDERSEN [1996] for $s_{0p} = 0.01$ still gives a substantial overprediction. Meanwhile, NØRGAARD *et al.* [2013] gives more reliable estimates in comparison to the found fit although two substantial outliers are observed (indicated by a blue circle). This can be explained because $H_{0.1\%}/R_{ca}$ turns out to be very large for these 2 points in comparison to surrounding conditions and since NØRGAARD *et al.* [2013] describes run-up height as a function of $H_{0.1\%}$ this seems to be a logical explanation.
For stormwaves $s_{0p} = 0.04$ both methods seems to be more reliable since most of the predictions for both PEDERSEN [1996] and NØRGAARD *et al.* [2013] are within the upper- and lower boundaries of the 95% confidence-interval. However, some substantial outliers are found for the adapted method of NØRGAARD *et al.* [2013] for $H_s^2/R_{ca}^2 > 1.75$ (indicated by A blue square). In this measurement point $H_{0.1\%} = 1.60$ which is relatively small in comparison to surrounding data points where $H_{0.1\%} \approx 1.70 - 1.80$. Since the loads determined by NØRGAARD *et al.* [2013] are based on $H_{0.1\%}$ this could have substantial consequences.

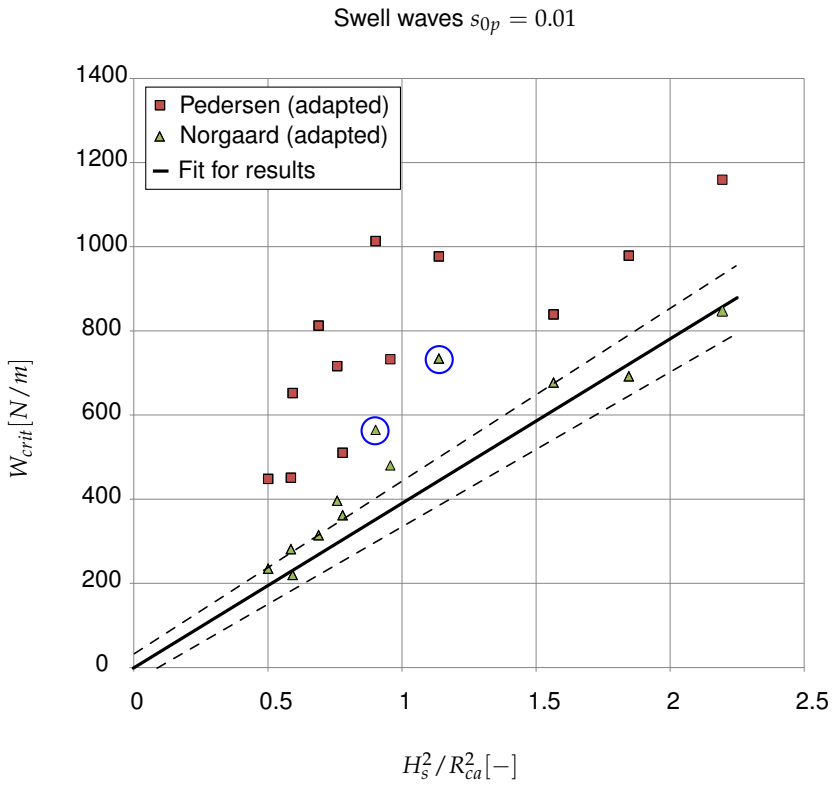

Figure 7.26: Critical weight predicted by adapted methods of PEDERSEN [1996] and NØRGAARD *et al.* [2013] compared to test results, for $s_{0p} = 0.01$

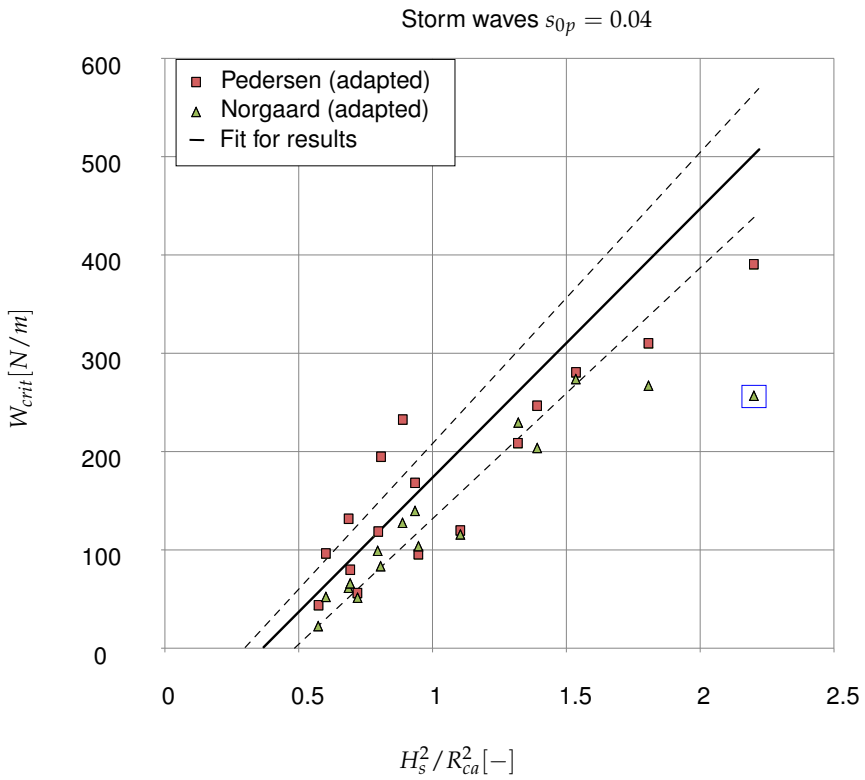

Figure 7.27: Critical weight predicted by adapted methods of PEDERSEN [1996] and NØRGAARD *et al.* [2013] compared to test results, for $s_{0p} = 0.04$

Conclusion

It can be concluded that the conventional methods of PEDERSEN [1996], even extended by NØRGAARD *et al.* [2013], is too conservative for large values of R_{ca}/H_s in comparison to the best fit for the results of the experiments.

Adapting the methods by bringing the effective length x_c/B_c of the upward pressures into account, seems to lead to better predictions. For swell waves ($s_{0p} = 0.01$) PEDERSEN [1996] is still too conservative since all the predictions lie outside the confidence interval, whereas NØRGAARD *et al.* [2013] gives results within the upper- and lower boundaries except for some outliers which may be caused due to a substantially larger ratio of $H_{0.1\%}/R_{ca}$ than surrounding points. For storm waves ($s_{0p} = 0.04$) most of the predictions by both methods lie within the confidence interval.

7.4.6 Design proposal

The critical weight is made dimensionless by using the density of water, gravity acceleration and the length and height of the crown wall, which are specific properties that provide the weight.
As a result, the dimensionless critical weight can be defined as $W^*_{crit} = W_{crit}/\mu_s \rho_w g B_c d_c$.
Design guidelines are given for critical weights at which stability against sliding is critical. When a crown wall is designed below its critical weight it is likely to fail whether it should remain stable when making the structure heavier than the indicated critical weight.

Design guidelines for critical weight as function of dimensionless wave height H_s^2/R_{ca}^2 are given in the table below and plotted in figure 7.28 for two wave steepness. They are also plotted as function of $H_{0.1\%}/R_{ca}$, which are shown in the table below and figure 7.29.
From a physical point of view the design guidelines for swell waves leads to a discrepancy since it intersects the y-axis above the origin, see figures 7.22 & 7.23. It is therefore advised to use these design guidelines within its range of application.

Swell waves ($s_{op} = 0.01$)		
$W^*_{crit} = 0.86 \frac{H_s^2}{R_{ca}^2} + 0.03$	for:	$0.50 \leq H_s^2/R_{ca}^2 \leq 2.20$
$W^*_{crit} = 0.25 \frac{H_{0.1\%}^2}{R_{ca}^2} + 0.18$	for:	$1.00 \leq H_{0.1\%}^2/R_{ca}^2 \leq 6.60$

Storm waves ($s_{op} = 0.04$)		
$W^*_{crit} = 0.62 \frac{H_s^2}{R_{ca}^2} - 0.23$	for:	$0.50 \leq H_s^2/R_{ca}^2 \leq 2.20$
$W^*_{crit} = 0.21 \frac{H_{0.1\%}^2}{R_{ca}^2} - 0.19$	for:	$1.00 \leq H_{0.1\%}^2/R_{ca}^2 \leq 6.60$

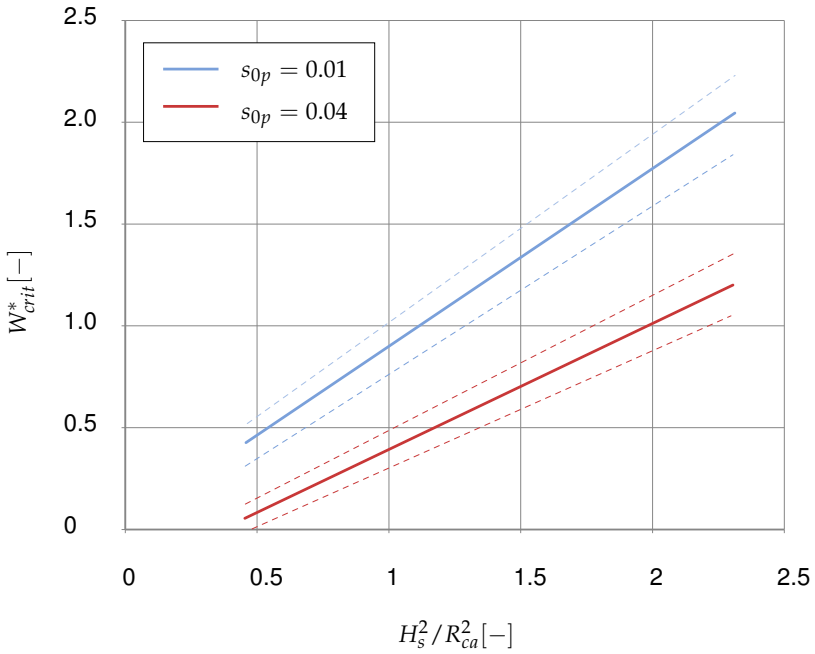

Figure 7.28: Proposed design equation for W^*_{crit} as function of H^2_s / R^2_{ca} for $s_{0p} = 0.01$ and $s_{0p} = 0.04$

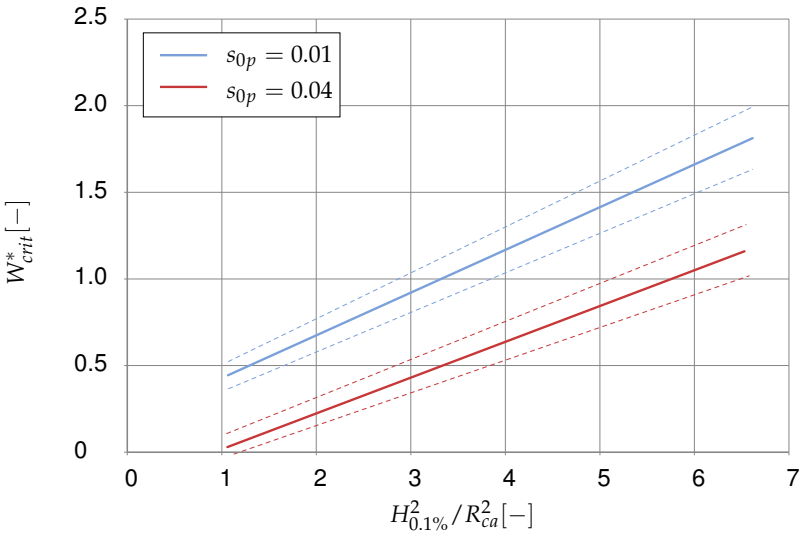

Figure 7.29: Proposed design equation for W^*_{crit} as function of $H^2_{0.1\%} / R^2_{ca}$ for $s_{0p} = 0.01$ and $s_{0p} = 0.04$

It is advised to use these design equations in combination with the extended method of NØRGAARD *et al.* [2013] in which the effect of vertical loading is taken into account. The equations in figure 7.11 lead to a reduction coefficient $\gamma_v = x_c/B_c$ for the upward pressure term $P_{U,0.1\%}$, used by NØRGAARD *et al.* [2013]. The upward pressure term used by NØRGAARD *et al.* [2013] must be multiplied with the reduction coefficient, according to table 7.4, for each loading case.

Table 7.4: Reduction coefficient γ_v for upward pressure $P_{U,0.1\%}$ used by PEDERSEN [1996] and NØRGAARD *et al.* [2013]

Swell waves ($s_{op} = 0.01$) (surging)		
$\gamma_v = 0$	for:	$H_s/R_{ca} \leq 0.64$
$\gamma_v = 2.41\frac{H_s}{R_{ca}} - 1.54$	for:	$0.64 \geq H_s/R_{ca} \leq 1.05$
$\gamma_v = 1$	for:	$H_s/R_{ca} > 1.05$
Storm waves ($s_{op} = 0.04$) (plunging/collapsing)		
$\gamma_v = 0$	for:	$H_s/R_{ca} \leq 0.75$
$\gamma_v = 2.41\frac{H_s}{R_{ca}} - 1.54$	for:	$0.75 \geq H_s/R_{ca} \leq 1.34$
$\gamma_v = 1$	for:	$H_s/R_{ca} > 1.34$

Range of application

This design proposal has been established within the ranges for parameters indicated in table 7.5. It is highly possible that wave steepness in practice will differ from $s_{0p} = 0.01$ or $s_{0p} = 0.04$. In this case, it is advised to compare the breaking type of the wave since this is assumed to be of importance in the exerted loads. When the breaker index indicates a plunging or collapsing breaker the equations for $s_{0p} = 0.04$ should be used, whereas the equation for $s_{0p} = 0.01$ should be used for surging breakers (less energy dissipation).

Table 7.5: Parametric ranges for this research

Parameter	Range
H_s / R_{ca}	0.71 - 1.48
H_s / L_{0p}	0.01 ; 0.04
B_a / d_a	1.88
d_c / d_a	1.88
$d_{50,c} / d_{50,a}$	0.40
$(d_{85} / d_{15})_c$	1.39
$(d_{85} / d_{15})_a$	1.45
cotα	2

7.4.7 Validation of design guidelines

In order to validate the design guidelines, the Constanţa design is compared to the proposed guidelines.

Constanţa design

According to the breakwater extension in the port of Constanţa in Romania, physical scaled model tests were executed by Artelia in Grenoble in order to verify stability calculations by making use of PEDERSEN [1996].
Model tests (scale 1:50) were done according to the configuration shown in figure 7.30. The corresponding physical dimensions are given in table 7.6. In table 7.7 hydraulic design conditions are presented in which H_s and T_p are given values whereas T_p is based on a first approximation of $T_m \approx 0.8T_p$ according to VERHAGEN *et al.* [2012], from which the fictitious wave steepness s_{0p} is determined.

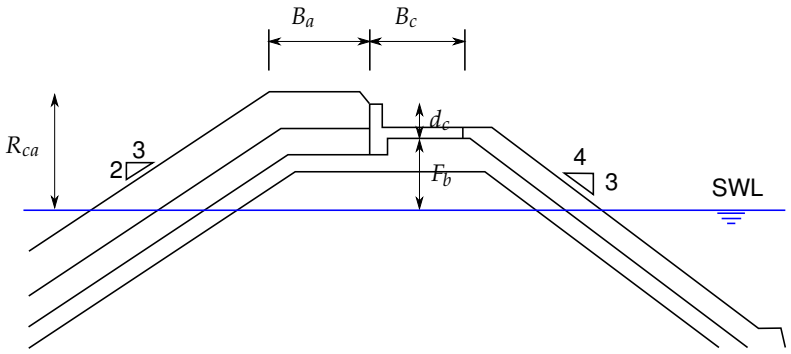

Figure 7.30: Cross- section of breakwater including crown in Constanta. Scale tests (1:50) by Artelia

Table 7.6: Physical dimensions Constanta breakwater

Parameter	Value	Unit
R_{ca}	8.8	m
B_a	8.50	m
B_c	8.00	m
d_c	3.00	m
F_b	4.8	m
$cot\alpha$	1.50	-

Table 7.7: Hydraulic parameters Constanta breakwater

Parameter	Value	Unit
H_s	7.5	m
T_m	10.7	s
T_p	13.4	s
s_{0p}	0.03	-
ξ_m	3.25	-

The own weight of the crown wall equals 281 kN/m that leads to a stable design which is revealed by Artelia.
Below, the critical weight according to the conventional and adapted method of NØRGAARD *et al.* [2013] is given and compared to current configuration. Furthermore, a critical weight according to the design guidelines is presented and compared to current configuration. A safety factor will be used whether safety or stability is expected. The stability factor against sliding is defined as follows: $SF = F_{G,actual}/(F_{H,max}/\mu_s + F_{V,max})$. A safety factor of SF=1 indicates critical stability.

Conventional method of NØRGAARD *et al.* [2013]

NØRGAARD *et al.* [2013] determines the run-up level by using $H_{0.1\%}$. This 1 in 1000 wave height is not known and therefore it is assumed that the following holds $H_{0.1\%} = 1.8H_s$, from which follows $H_{0.1\%} = 13.5$ m [VERHAGEN *et al.*, 2012].
The calculated design wave loads by NØRGAARD *et al.* [2013] are as follows:

$F_{H0.1\%} = 199.4$ kN/m

$F_{V0.1\%} = 384.5$ kN/m

Considering stability against sliding these loads would lead to a safety factor of: SF=0.38 which would be unstable as well.
The critical weight according to the conventional method of NØRGAARD *et al.* [2013] should be: 747.0 kN/m (for SF=1).

Adapted method of NØRGAARD *et al.* [2013]

The calculated design wave loads by making use of the method of NØRGAARD *et al.* [2013] in which the effective length over which upward pressures exert loads is taken into account, follows:

$F_{H0.1\%} = 199.4$ kN/m

$F_{V0.1\%} = 72.5$ kN/m

Considering stability against sliding these loads would lead to a safety factor of: SF=0.65 which would be unstable as well.
The critical weight according to the conventional method of NØRGAARD *et al.* [2013] should be: 435 kN/m (for SF=1).

Proposed design guidelines

The fictitious wave steepness $s_{0p} = 0.03$ deviates from the steepness $s_{0p} = 0.01$ and $s_{0p} = 0.04$ which were used during the tests.
However, from a physical point of view the breaking behaviour should be analysed. The breaker parameter $\xi_m = 3.25$ indicates a non breaking wave, since the transition between breaking and non- breaking waves lies around $\xi_m = 2.5 - 3$ according to VERHAGEN *et al.* [2012].
This type of wave could be compared to the swell waves $s_{0p} = 0.01$ and therefore the design guideline for swell waves will be followed.
In order to be able to use this design proposal the armour crest freeboard R_{ca} is assumed to be bounded by the height of the wall which means that R_{ca} =7.8 m (instead of 8.8 m).

This leads to a critical weight of $W_{crit} = 191.0$ kN/m, which lies substantially lower than predicted by the adapted method of NØRGAARD *et al.* [2013] but also in comparison to the actual weight of the prototype.
This predicted critical weight represents the total effective loading as well, since critical weight means just stable from which follows SF=1.
It could be concluded that judging from the found design guideline for swell waves, the crown wall is designed in a stable way in which the stability factor equals SF=281/191=1.47.

8

Conclusions and Recommendations

8.1 Conclusions

Current wave load calculation methods lead to designs which are too conservative especially when freeboard increases. In this research, physical scaled model tests were carried out to investigate the effect of freeboard on loads acting on the crown wall on top of a rubble mound breakwater.

8.1.1 Study steps

In order to be able to answer the research question, the predefined study steps are treated and answered.

1. Investigate the effect and shape of upward pressure distribution on the base as function of freeboard:

It can be concluded that current design methods are conservative in two ways. Firstly, it appears that the shape of the upward pressure distribution is more or less S-shaped for zero base freeboard whereas it converts into a more or less hyperbolic shape for increasing freeboard.
Secondly, the effective length x_c over which the upward pressure exerts a load, depends on wave height and freeboard. The point at which the pressure becomes zero shifts more to the front of the base for increasing freeboard.

2. Define a relationship between vertical loads on the crown wall as function of wave conditions and freeboard:

From the found vertical loads it is concluded that current design methods give reliable predictions for zero freeboard ($R_b = 0$), but substantially overpredictions occur for increasing freeboard. A linear relationship is found for these overprediction as function of dimensionless freeboard.

3. Describe any existing phase difference between the horizontal and vertical loads as function of freeboard:

From pressure measurements it is concluded that phase lag between maximum horizontal and vertical loads could occur at the moment when sliding of the crown wall occurs. However, no clear relationships were found to describe

the presence of phase lag properly. Filtering of the pressure records could lead to wrong conclusions with respect to observed phase lag since dynamic peak loads occur in very short time short time spans of approximately 0.001 - 0.005 s, whereas in this research, phase lag is analysed in time spans of 0.05 s. This means that some peak loads may be overlooked.
However, from a physical point of view, the proposed stability criteria in CIRIA *et al.* [2007] in which the maximum horizontal and vertical loads occur simultaneously seems to be somewhat conservative, though, further research is necessary.

4. Generate a dataset of critical weights as function of wave conditions and freeboard:

From comparing the methods of PEDERSEN [1996] and NØRGAARD *et al.* [2013] to the found dataset of critical weights for swell- and storm waves it is concluded that the conventional methods lead to conservative designs for increasing freeboard ($R_b > 0$). However, adapting these methods by taking into account the effective length x_c in the form of a reduction coefficient for vertical loads γ_v, better and more reliable predictions arise especially by NØRGAARD *et al.* [2013]. Design guidelines for critical weights are given as function of H_s and $H_{0.1\%}$. It is recommended to use these guidelines, within its range of application, in combination with the adapted method of NØRGAARD *et al.* [2013] in which vertical loads are multiplied by the reduction coefficient γ_v.

8.1.2 Research question

'What causes current design methods to be not accurate enough in the design of the crown wall on top of a rubble mound breakwater?'

Current wave load calculation methods neglect the decrease of effective length x_c over which the upward pressure exerts a load against the base for increasing freeboard. Taking into account this effective length as function of wave height and freeboard in the form of a reduction coefficient γ_v, predictions become substantially better in comparison to the found data set for critical weights.
The effect of ignoring highly possible phase lag between horizontal and vertical loads is not as large as supposed at the start of this study.

8.2 Recommendations

If one consideres to do further research into the stability of a crown wall on top of a rubble mound breakwater using a physical scaled model, the following recommendations could be useful:

8.2.1 Test subject

Further research should focus on extending the dataset for critical weights of the crown wall. Adapting the weight of a crown wall until failure occurs is robust since this way of testing always provides useful data.
Additionally, one should extend the dataset of effective lengths x_c over which upward pressures exert loads, e.g. by using a camera.

8.2.2 Test parameters

It is recommended to vary more parameters, which were kept constant in this research, to improve the proposed design guidelines and to extent its range of application. More specifically, it could be useful to extend the dataset for test conditions in which $0.70 > H_s/R_{ca} > 1.50$ since no measurements were done within that range.

The following geometrical parameters should be varied in further research:

- Slope of the structure α;
- Crown wall height d_c;
- Berm width B_a.

8.2.3 Instruments

In this research a camera with a frame rate of 25 frames per second is used. In principle, this is sufficient, however, an increase in frame rate will make the analysis more reliable. Furthermore, it is desirable to use a better contrast between the colour of basalt rubble mound and the water line since this makes it more easy to follow the water motion from camera footage, this could be done by painting the rubble mound breakwater in a lighter colour.

The pressure sensors which were used during this research have been useful in order to prove that the currently assumed pressure distribution is not correct and to check whether there is a direct relationship between the effective length x_c and pressures. However, because of the known sensitivity for vibrations of the complete system (known as noise), the records were filtered quite heavily which means that a qualitative analysis is still possible but a quantitative analysis would not be reliable. Besides that, base level shifts (highly) due to air inclusion make an analysis more complicated.
Therefore, phase lag should be investigated using pressure sensors which are less sensitive for air inclusion and surrounding noise, so that no heavy filters are required. Heavy filtering could make a phase lag analysis unreliable since relevant peaks are flattened. Secondly, it is desired to measure pressures at the front of the base and at the bottom of the wall. Lastly, it could be sensible to use more sensors to obtain more data.

Appendix A

Test conditions

Table A.01: Conditions 'Test series A'

Test condition	H_s [m]	T_p [s]	R_{ca} [m]	h [m]	s_{0p} [-]
A_{swell1}	0.09	2.56	0.08	0.65	0.01
A_{swell2}	0.09	2.56	0.11	0.62	0.01
A_{swell3}	0.12	2.91	0.14	0.59	0.01
A_{swell4}	0.15	3.18	0.17	0.56	0.01
A_{storm1}	0.11	1.26	0.08	0.65	0.04
A_{storm2}	0.13	1.44	0.10	0.63	0.04
A_{storm3}	0.12	1.50	0.11	0.62	0.04

Table A.02: Conditions 'Test series B'

Condition #	H_s [m]	$H_{0.1\%}$ [m]	T_p [s]	R_{ca} [m]	h [m]	s_{0p} [-]
B_{swell1}	0.1001	0.1848	2.49	0.08	0.65	0.01
B_{swell2}	0.1087	0.1881	2.54	0.08	0.65	0.01
B_{swell3}	0.1185	0.2058	2.67	0.08	0.65	0.01
B_{swell4}	0.0971	0.1704	2.44	0.11	0.62	0.01
B_{swell5}	0.1076	0.1816	2.54	0.11	0.62	0.01
B_{swell6}	0.1173	0.2109	2.65	0.11	0.62	0.01
B_{swell7}	0.1072	0.1840	2.55	0.14	0.59	0.01
B_{swell8}	0.1219	0.1973	2.65	0.14	0.59	0.01
B_{swell9}	0.1330	0.2140	2.80	0.14	0.59	0.01
$B_{swell10}$	0.1204	0.1992	2.65	0.17	0.56	0.01
$B_{swell11}$	0.1308	0.1862	2.77	0.17	0.56	0.01
$B_{swell12}$	0.1412	0.2060	2.77	0.17	0.56	0.01
B_{storm1}	0.0944	0.1679	1.23	0.08	0.65	0.04
B_{storm2}	0.1076	0.1936	1.25	0.08	0.65	0.04
B_{storm3}	0.1187	0.1903	1.33	0.08	0.65	0.04
B_{storm4}	0.0933	0.1675	1.22	0.11	0.62	0.04
B_{storm5}	0.1071	0.1938	1.25	0.11	0.62	0.04
B_{storm6}	0.1156	0.1933	1.26	0.11	0.62	0.04
B_{storm7}	0.1264	0.2216	1.45	0.11	0.62	0.04
B_{storm8}	0.1364	0.2108	1.53	0.11	0.62	0.04
B_{storm9}	0.1059	0.1778	1.26	0.14	0.59	0.04
$B_{storm10}$	0.1165	0.2057	1.39	0.14	0.59	0.04
$B_{storm11}$	0.1248	0.2154	1.47	0.14	0.59	0.04
$B_{storm12}$	0.1353	0.2272	1.53	0.14	0.59	0.04
$B_{storm13}$	0.1318	0.2214	1.53	0.17	0.56	0.04
$B_{storm14}$	0.1408	0.2184	1.60	0.17	0.56	0.04
$B_{storm15}$	0.1527	0.2269	1.63	0.17	0.56	0.04
$B_{storm16}$	0.1602	0.2417	1.72	0.17	0.56	0.04

Appendix B

Execution of the structure

Figure B.01: Top view: Mold in which centre part is constructed.

Figure B.02: Centre part of the core constructed in the mold

Figure B.03: Mold for total core, centre part is already placed

Figure B.04: Mold for total core, slope placed as well

Figure B.05: Centre part of the core is placed in the wave flume

Figure B.06: Centre part of the core is removed from the wave flume

Appendix C

Grading curves

In figure C.01 the grading curves for the stones in the core and armour are shown.

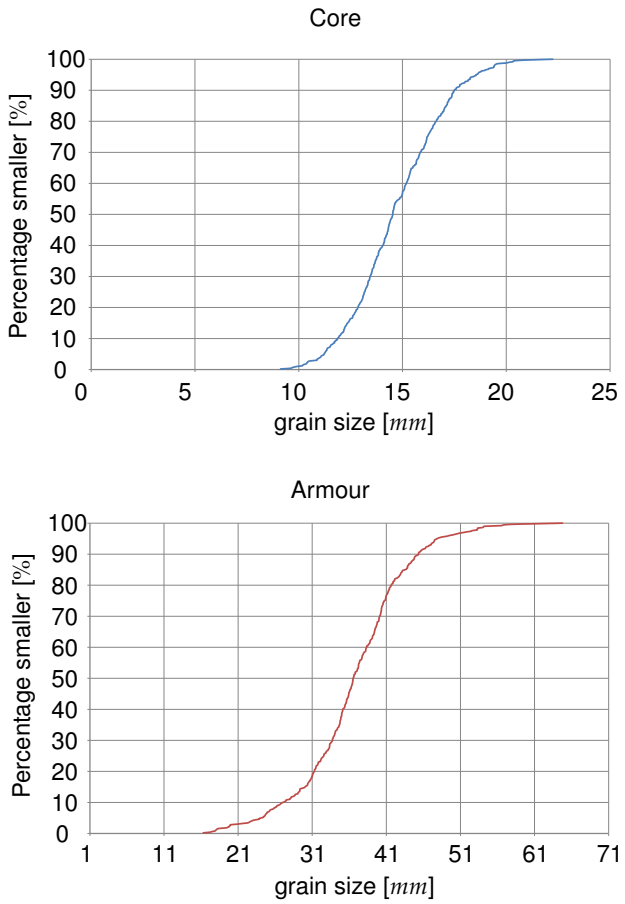

Figure C.01: Grading curve for stones in the core and armour layer

Appendix D

Location pressure sensors

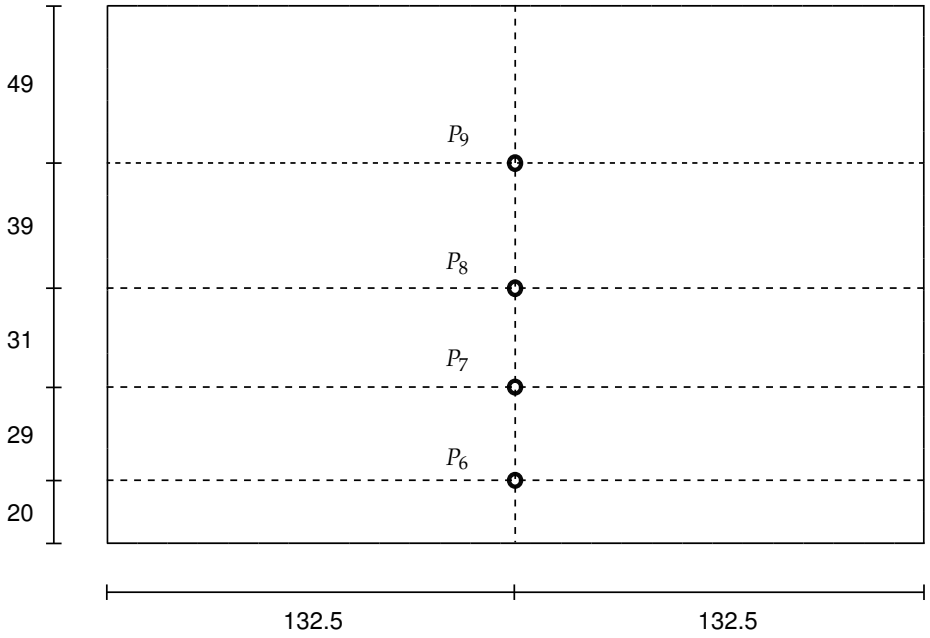

Figure D.01: Pressure sensors in the vertical wall of the crown wall

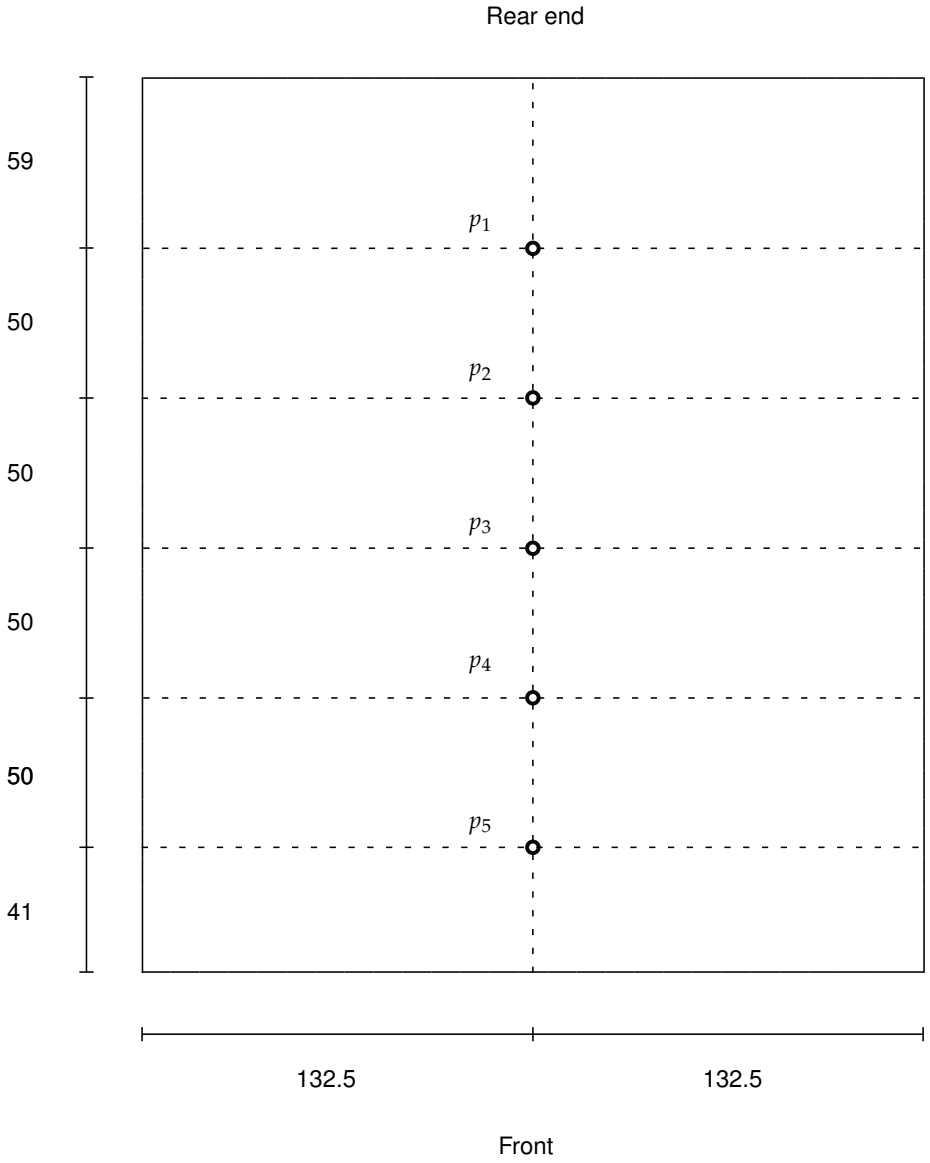

Figure D.02: Pressure sensors in the base slab of the crown wall

Appendix E

Calibration measurement instruments

E.1 Wave gauges

In table E.11 the calibration of the wave gauges is shown. The test conditions in Appendix A are obtained by gauges 4,5 and 6.

Table E.11: Calibration wave gauges

Wave gauge	Voltage [V] at $\Delta s = 0$ m	Voltage [V] at $\Delta s = 0.10$ m	$\Delta s / \Delta m$
1	-1.01	-2.83	0.026
2	-0.31	3.88	0.024
3	-0.61	3.62	0.024
4	-2.68	1.22	0.026
5	-1.27	2.83	0.024
6	-0.71	3.30	0.025

E.2 Pressure sensors

In table E.22 the calibration of the pressure sensors is shown.

Table E.22: Calibration pressure sensors

Sensor	Point 1 [mwc]	[V] at point 1	Point 2 [mwc]	[V] at point 2	$\frac{\Delta m}{\Delta V}$
P_1	0.057	1.698	0.209	7.61	2.57
P_2	0.069	1.698	0.209	7.61	2.37
P_3	0.081	2.232	0.205	7.45	2.38
P_4	0.085	2.141	0.207	7.63	2.22
P_5	0.10	2.745	0.208	7.70	2.18
P_6	0.085	2.171	0.193	6.93	2.27
P_7	0.076	1.612	0.198	6.79	2.36
P_8	0.098	2.630	0.202	7.07	2.34
P_9	0.097	3.007	0.206	8.02	2.17

E.3 Rangefinders

In figure E.31 the calibration curves of the rangefinders are shown. The relation between voltage and measured distance is described by the Boltzmann equation:

$y = 7.45 - 2.2ln(1/pV - 1)$

In this equation y is the distance measured between crown wall and rangefinder, whereas pV is the percentage of voltage, which is calculated by:

$pV = 0.11 * V - 0.22$

Total displacement is determined by: $y_{start} - y_{end}$, for which the following thresholds hold:

Sliding if: $\Delta V = 0.20 \rightarrow y_{start} - y_{end} \geq 0.2 - 0.3$ mm

Uplift if: $\Delta V = 0.10 \rightarrow y_{start} - y_{end} \geq 0.1 - 0.2$ mm

These equations only hold for a specific range of testing (in this study), therefore care must be taken by using these equations.

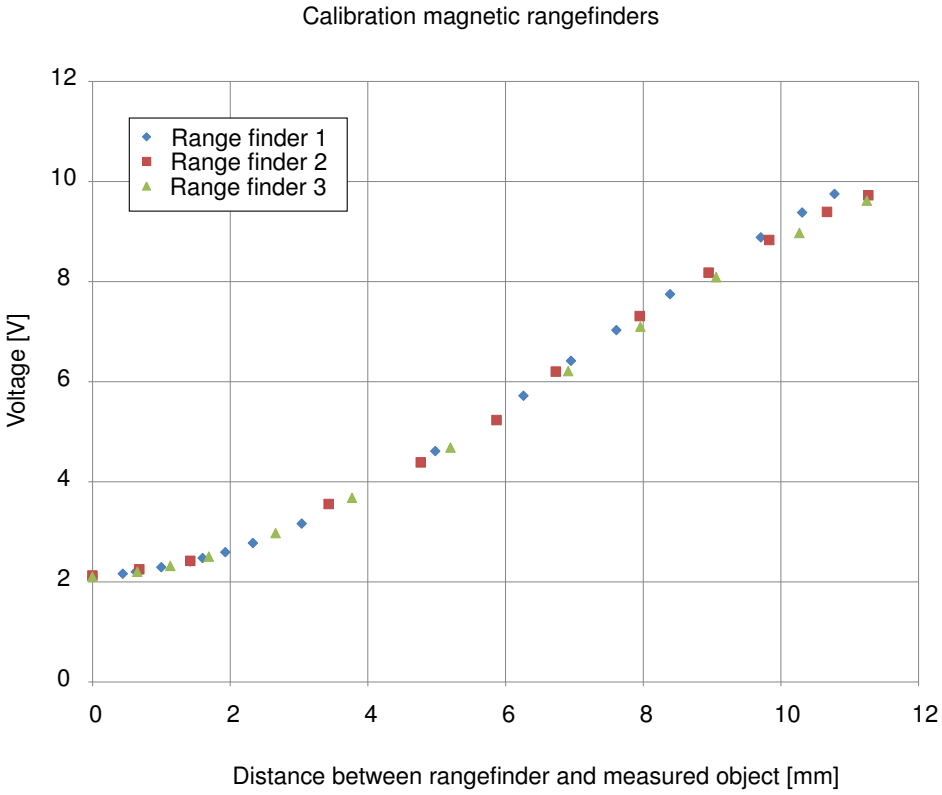

Figure E.31: Calibration rangefinders

E.4 Load cell

In figure E.42 the calibration of the load cell is shown.

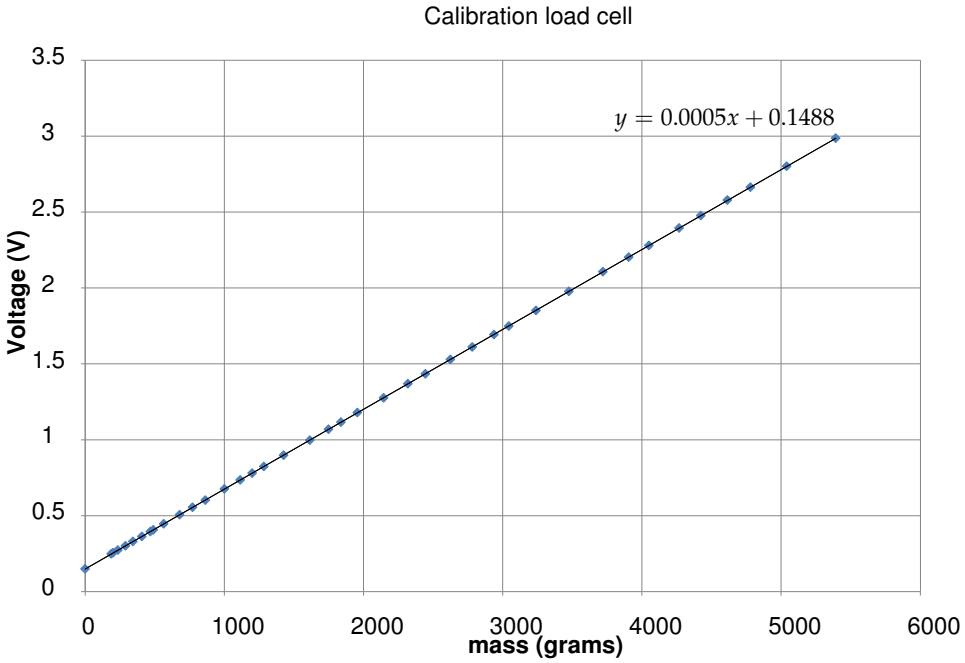

Figure E.42: Calibration loadcell

Appendix F

Technical properties/information instruments

Deltares

Enabling Delta Life

Instrument

Wave height meter

The wave height meter is developed for measurement of dynamically varying liquid levels, wave heights of water in particular. The wave height meter can be used as a standalone probe or combined with a control unit. The main difference when using a control unit is the ability to adjust the gain and zero shift of the output signal by means of dials. Furthermore, the control unit provides the probe with power. The output signal for the surface elevation is analogue for both the standalone version as the control unit.

Applications

The wave height meter is, amongst others, used for laboratory research in the fields of:

- wave penetration in harbours
- performance of breakwaters and dikes
- coastal protection
- load and stability of off-shore structures

Probe

The probe of the wave height meter is constructed of two parallel stainless steel rods, mounted underneath a small box. This box contains electronics for sensor excitation, signal detection, amplification and galvanic isolation. The rods act as the electrodes of an electric conduction meter. A platinum reference electrode is included to compensate the surface elevation measurement for the effect of varying electrical conductivity of the fluid. The analogue output signal is linearly proportional to the liquid level between the sensor rods.

Features

- fast dynamic response
- wide range 0.5 m, other ranges optional
- automatic compensation for conductivity variation
- high linearity
- easy installation
- analogue output indication on control unit

Technical specifications

Wave height electrodes	• rods, stainless steel, type 316, 4 mm diameter • electrode spacing 24.3 mm • electrode length 590 mm (other lengths optional)
Reference electrode	platinum
Other materials exposed to liquid	PVC-U
Liquid medium	• medium conductive liquids non-aggressive to mentioned materials • minimum required conductivity 0.1 mS/cm • sensitivity variation < 1 % for 0.1 to 2.0 mS/cm
Accuracy	0.5 % of measuring range, best straight line
Output	0.4 V/cm level variation (standard: -10 to +10 VDC for 50 cm liquid level change)
Frequency response	> 15 Hz
Dimensions	incl. electronics 675 mm long (standard length)
Cable	25 m (optional up to 100 m)

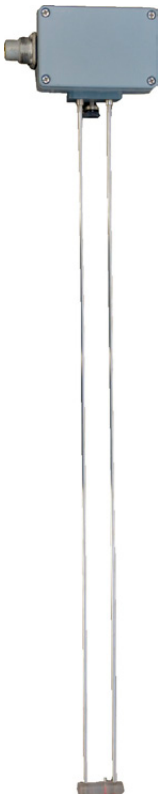

probe

Control unit

The control unit supplies the wave height meter with power and provides a way to adjust the wave height meter to the desired calibration. Four switch selectable ranges are available to adjust the gain of the output signal. The zero level is adjustable by a dial. One universal carrying case (UCC) can support two control units.

Features

- output indication
- switch selectable ranges
- adjustable zero level
- can be used with probes of various length

Technical specifications

Probes available	standard probe 0.5 m range special probe 1.0 m range other lengths on request
Ranges	0.05, 0.1, 0.2, 0.5 m for standard probe 0.1, 0.2, 0.4, 1.0 m for special probe
Frequency response	> 15 Hz
Output	+/- 10 VDC
Dimensions cassette	standard eurostyle cassette

Control unit front view

Control unit rear view

Several configurations can be built on request. One example is a setup where a number of wave height meters without control units are powered by one electronics box. For each wave height meter the analogue output signal is available on a BNC connector. Furthermore, there is the possibility to include data output over USB or Ethernet.

More information: instrumentation@deltares.nl

Deltares

PO Box 177
2600 MH Delft, The Netherlands
T +31 (0)88 335 82 73
info@deltares.nl
www.deltares.nl

Deltares is an independent institute for applied research in the field of water, subsurface and infrastructure. Throughout the world, we work on smart solutions, innovations and applications for people, environment and society.
Deltares is based in Delft and Utrecht.

Induktiver Näherungsschalter
Détecteur de proximité inductif
Inductive Proximity Switch

DW - A□ - 509 - M30

Durchmesser / Diamètre / Diameter	Schaltabstand / Portée / Operating distance	Einbau / Montage / Mounting
M30	**0...20mm**	**quasi-bündig / quasi noyable / quasi-embeddable**

Ausführung mit Analogausgang

Wichtigste Eigenschaften:

- Erfassungsbereich 0 ... 20 mm
- Betriebsspannung 10...30 VDC
- Spannungsausgang 0 ... 5 V
- Stromausgang 1 ... 5 mA
- Kurzschlussschutz, Induktionsschutz, Verpolungsschutz eingebaut
- Nicht linearisierte Ausführung
- Anschluss über Kabel oder Stecker S12

Appareil à sortie analogique

Caractéristiques principales:

- Domaine de détection 0 à 20 mm
- Tension de service 10 ... 30 VDC
- Tension de sortie 0 à 5 V
- Courant de sortie 1 à 5 mA
- Protections contre les courts-circuits, les surtensions induites et l'inversion de tension incorporées
- Version non linéarisée
- Raccordement par câble ou par connecteur S12

Analog output model

Main features:

- Sensing range 0 to 20 mm
- Supply voltage 10 ... 30 VDC
- Output voltage 0 to 5 V
- Output current 1 to 5 mA
- Protections against short-circuits, induced overvoltages and power supply reversal built-in
- Non-linearized version
- Cable and S12 connector versions

Technische Daten (gemäss IEC 60947-5-2)	**Caractéristiques techniques:** (selon CEI 60947-5-2)	**Technical data:** (according to IEC 60947-5-2)	
Erfassungsbereich s_d	Domaine de détection s_d	Sensing range s_d	0 ... 20 mm
Normmessplatte	Cible normalisée	Standard target	60 x 60 x 1 mm
Wiederholgenauigkeit (gemäss IEC 60947-5-2)	Reproductibilité (selon CEI 60947-5-2)	Repeat accuracy (according to IEC 60947-5-2)	0,3 mm (U_B = 20 ... 30 VDC, T_A = 23 °C ± 5 °C)
Wiederholgenauigkeit (T_A = konstant)	Reproductibilité (T_A = constant)	Repeat accuracy (T_A = constant)	± 0,05 mm
Auflösung	Résolution	Resolution	≤ 5 µm
Betriebsspannungsbereich U_B	Tension de service U_B	Supply voltage range U_B	10 ... 30 VDC
Zulässige Restwelligkeit	Ondulation admissible	Max. ripple content	≤ 20% U_B
Ausgangsspannung an A1 s = 0 mm	Tension de sortie à A1 s = 0 mm	Output voltage at A1 s = 0 mm	0 V / - 0 + 0,2 V (23 °C)
s = 10 mm	s = 10 mm	s = 10 mm	+ 2,6 V / ± 0,2 V (23 °C)
s = 20 mm	s = 20 mm	s = 20 mm	+ 5 V / ± 0,2 V (23 °C)
Laststrom am Spannungsausgang A1	Charge à la sortie tension A1	Load at voltage output A1	≤ 10 mA
Ausgangsstrom an A2 s = 0 mm	Courant de sortie à A2 s = 0 mm	Output current at A2 s = 0 mm	1 mA / ± 0,2 mA (23 °C)
s = 20 mm	s = 20 mm	s = 20 mm	5 mA / ± 0,2 mA (23 °C)
Max. Last am Stromausgang A2	Charge max. à la sortie courant A2	Max. load at current output A2	1 kΩ (U_B=10 V) / 5 kΩ (U_B=30 V)
Leerlaufstrom	Courant hors-charge	No-load supply current	≤ 10 mA
Bandbreite	Bande passante	Bandwidth	200 Hz (-3 dB bei / à / at s=10mm)
Bereitschaftsverzögerung	Retard à la disponibilité	Time delay before availability	≤ 50 msec
Umgebungstemperaturbereich T_A	Plage de température ambiante T_A	Ambient temperature range T_A	-25 ... + 70 °C
Temperaturdrift von s_r	Dérive en température de s_r	Temperature drift of s_r	≤ 10%
Kurzschlussschutz	Protection contre les courts-circuits	Short-circuit protection	eingebaut / intégrée / built-in
Verpolungsschutz	Protection contre les inversions	Induction protection	eingebaut / intégrée / built-in
Schocks und Schwingungen	Chocs et vibrations	Shocks and vibration	IEC 60947-5-2 / 7.4
Leitungslänge	Longueur du câble	Cable length	300 m max.
Gewicht (Kabel / Stecker)	Poids (câble / connecteur)	Weight (cable / connector)	215 g / 155 g; -120: 190 g / 135 g
Schutzart	Indice de protection	Degree of protection	IP 67
EMV - Schutz:	Protection CEM:	EMC protection:	
IEC 60255-5	CEI 60255-5	IEC 60255-5	5 kV
IEC 61000-4-2	CEI 61000-4-2	IEC 61000-4-2	Level 2
IEC 61000-4-3	CEI 61000-4-3	IEC 61000-4-3	Level 3
IEC 61000-4-4	CEI 61000-4-4	IEC 61000-4-4	Level 2
Gehäusematerial	Matériau du boîtier	Housing material	Messing cr/laiton cr/cr-plated brass
Aktive Fläche	Face sensible	Sensing face	PBTP
Anschlusskabel (andere Längen auf Anfrage)	Câble de raccordement (autres longueurs sur demande)	Connection cable (other lengths on request)	PUR 4 x 0,25mm² / 128 x 0,05mm Ø 2m

Anschlussschema
Schéma de raccordement
Wiring diagram

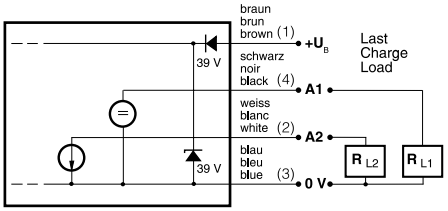

Steckerbelegung (Gerät)
Attribution des pins (appareil)
Pin assignment (device)

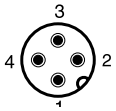

S12

CONTRINEX AG Industrial Electronics
route André Piller 50 - CH 1762 Givisiez - Switzerland - **Tel:** +41 26 460 46 46 - **Fax:** +41 26 460 46 40 - **Internet:** www.contrinex.com - **E-mail:** info@contrinex.com

Abmessungen / Dimensions / Dimensions:

Diese Zeichnungen lassen sich aus dem Internet (www.contrinex.com) herunterladen.
Ces dessins peuvent être téléchargés depuis Internet (www.contrinex.com).
These drawings can be downloaded from Internet (www.contrinex.com).

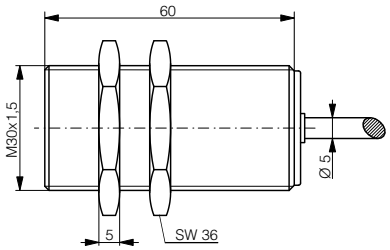

DW-AD-509-M30

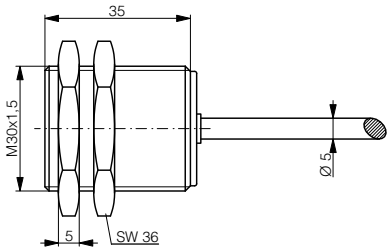

DW-AD-509-M30-120

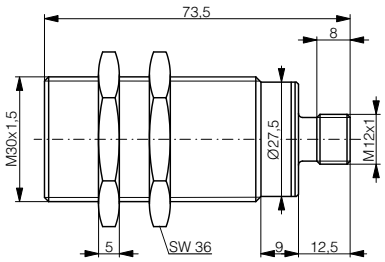

DW-AS-509-M30-002

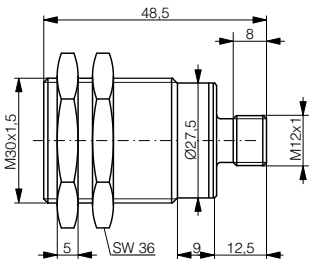

DW-AS-509-M30-120

* typische Werte / valeurs typiques / typical values

Ansprechkurve* / Courbe de réponse* / Response diagram*:

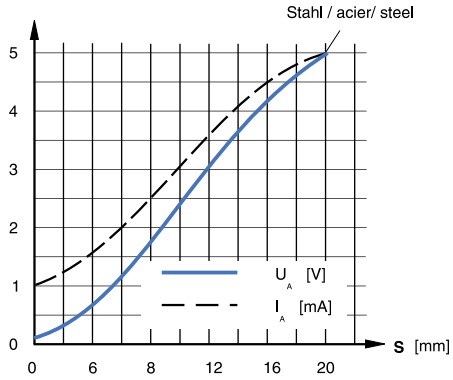

Einbau / Montage / Installation:

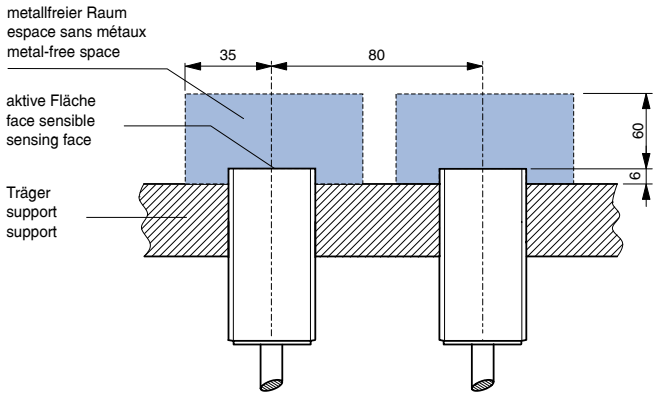

Reduktionsfaktoren* / Coefficients de réduction* / Correction factors*

Stahl FE 360 Acier FE 360 Steel FE 360	**1,0**	Kupfer cuivre copper	**0,17**	Aluminium aluminium aluminum	**0,2**	Messing laiton brass	**0,3**	Edelstahl V2A acier INOX V2A stainless steel V2A	**0,65**

Typenspektrum / Types disponibles / Available types:

Artikelnummer Numéro article Part number	Typenbezeichnung désignation part reference	Anschluss raccordement connection	Ausgang sortie output
320 020 108	DW-AD-509-M30	Kabel / câble / cable	Spannung und Strom / tension et courant / voltage and current
320 020 109	DW-AS-509-M30-002	Stecker / connecteur / connector S12	Spannung und Strom / tension et courant / voltage and current
320 020 114	DW-AD-509-M30-120	Kabel / câble / cable	Spannung und Strom / tension et courant / voltage and current
320 020 115	DW-AS-509-M30-120	Stecker / connecteur / connector S12	Spannung und Strom / tension et courant / voltage and current

Der Einsatz dieser Geräte in Anwendungen, wo die **Sicherheit von Personen** von deren Funktion abhängt, ist **unzulässig**. Änderungen und Liefermöglichkeiten vorbehalten. Ces détecteurs **ne peuvent être utilisés** dans des applications où la **protection** ou la **sécurité** de **personnes** est concernée. Sous réserve de modifications et de possibilités de livraison. These proximity switches **must not be used** in applications where the **safety of people** is dependent on their functioning. Terms of delivery and rights to change design reserved.

CONTRINEX AG Industrial Electronics
route André Piller 50 - CH 1762 Givisiez - Switzerland - **Tel:** +41 26 460 46 46 - **Fax:** +41 26 460 46 40 - **Internet:** www.contrinex.com - **E-mail:** info@contrinex.com

Induktiver Näherungsschalter
Détecteur de proximité inductif
Inductive Proximity Switch

DW - A□ - 509 - M30 - 3□0

Durchmesser / Diamètre / Diameter	Schaltabstand / Portée / Operating distance	Einbau / Montage / Mounting
M30	**0...20mm**	**quasi-bündig / quasi noyable / quasi-embeddable**

Ausführung mit Analogausgang

Wichtigste Eigenschaften:

- Erfassungsbereich 0 ... 20 mm
- Betriebsspannung 15...30 VDC
- Spannungsausgang 0 ... 10 V
- Stromausgang 4 ... 20 mA
- Kurzschlussschutz, Induktionsschutz, Verpolungsschutz eingebaut
- Nicht linearisierte Ausführung
- Anschluss über Kabel oder Stecker S12

Appareil à sortie analogique

Caractéristiques principales:

- Domaine de détection 0 à 20 mm
- Tension de service 15 ... 30 VDC
- Tension de sortie 0 à 10 V
- Courant de sortie 4 à 20 mA
- Protections contre les courts-circuits, les surtensions induites et l'inversion de tension incorporées
- Version non linéarisée
- Raccordement par câble ou par connecteur S12

Analog output model

Main features:

- Sensing range 0 to 20 mm
- Supply voltage 15 ... 30 VDC
- Output voltage 0 to 10 V
- Output current 4 to 20 mA
- Protections against short-circuits, induced overvoltages and power supply reversal built-in
- Non-linearized version
- Cable and S12 connector versions

Technische Daten: (gemäss IEC 60947-5-2)	**Caractéristiques techniques:** (selon CEI 60947-5-2)	**Technical data:** (according to IEC 60947-5-2)	
Erfassungsbereich s_d	Domaine de détection s_d	Sensing range s_d	0 ... 20 mm
Normmessplatte	Cible normalisée	Standard target	60 x 60 x 1 mm
Wiederholgenauigkeit (gemäss IEC 60947-5-2)	Reproductibilité (selon CEI 60947-5-2)	Repeat accuracy (according to IEC 60947-5-2)	0,3 mm (U_B = 20 ... 30 VDC, T_A = 23 °C ± 5 °C)
Wiederholgenauigkeit (T_A = konstant)	Reproductibilité (T_A = constant)	Repeat accuracy (T_A = constant)	± 0,05 mm
Auflösung	Résolution	Resolution	≤ 5 µm
Betriebsspannungsbereich U_B	Tension de service U_B	Supply voltage range U_B	15 ... 30 VDC
Zulässige Restwelligkeit	Ondulation admissible	Max. ripple content	≤ 20% U_B
Ausgangsspannung an A1 s = 0 mm	Tension de sortie à A1 s = 0 mm	Output voltage at A1 s = 0 mm	0 V / - 0 + 0,4 V (23 °C)
s = 10 mm	s = 10 mm	s = 10 mm	+ 5,2 V / ± 0,4 V (23 °C)
s = 20 mm	s = 20 mm	s = 20 mm	+ 10 V / ± 0,4 V (23 °C)
Laststrom am Spannungsausgang A1	Charge à la sortie tension A1	Load at voltage output A1	≤ 10 mA
Ausgangsstrom an A2 s = 0 mm	Courant de sortie à A2 s = 0 mm	Output current at A2 s = 0 mm	4 mA / ± 0,8 mA (23 °C)
s = 20 mm	s = 20 mm	s = 20 mm	20 mA / ± 0,8 mA (23 °C)
Max. Last am Stromausgang A2	Charge max. à la sortie courant A2	Max. load at current output A2	0,5 kΩ (U_B=15V) / 1 kΩ (U_B=30V)
Leerlaufstrom	Courant hors-charge	No-load supply current	≤ 12 mA
Bandbreite	Bande passante	Bandwidth	200 Hz (-3 dB bei/à/at s=10 mm)
Bereitschaftsverzögerung	Retard à la disponibilité	Time delay before availability	≤ 50 msec
Umgebungstemperaturbereich T_A:	Plage de température ambiante T_A:	Ambient temperature range T_A:	
A1 belastet, A2 unbelastet	A1 chargé, sans charge sur A2	load at A1, no load at A2	-25 ... +70°C
A1 unbelastet, A2 belastet	sans charge sur A1, A2 chargé	no load at A1, load at A2	gemäss / selon / acc. to Fig. 2
Temperaturdrift von s_r	Dérive en température de s_r	Temperature drift of s_r	≤ 10%
Kurzschlussschutz	Protection contre les courts-circuits	Short-circuit protection	eingebaut / intégrée / built-in
Verpolungsschutz	Protection contre les inversions	Voltage reversal protection	eingebaut / intégrée / built-in
Schocks und Schwingungen	Chocs et vibrations	Shocks and vibration	IEC 60947-5-2 / 7.4
Leitungslänge	Longueur du câble	Cable length	300 m max.
Gewicht (Kabel / Stecker)	Poids (câble / connecteur)	Weight (cable / connector)	-390: 215/155 g, -320: 190/135g
Schutzart	Indice de protection	Degree of protection	IP 67
EMV - Schutz:	Protection CEM:	EMC protection:	
IEC 60255-5	CEI 60255-5	IEC 60255-5	5 kV
IEC 61000-4-2	CEI 61000-4-2	IEC 61000-4-2	Level 2
IEC 61000-4-3	CEI 61000-4-3	IEC 61000-4-3	Level 3
IEC 61000-4-4	CEI 61000-4-4	IEC 61000-4-4	Level 2
Gehäusematerial	Matériau du boîtier	Housing material	Messing cr/laiton cr/cr-plated
Aktive Fläche	Face sensible	Sensing face	brass
Anschlusskabel (andere Längen auf Anfrage)	Câble de raccordement (autres longueurs sur demande)	Connection cable (other lengths on request)	PBTP
			PUR 4x0,25mm² / 128x0,05mm Ø 2 m

Anschlussschema
Schéma de raccordement
Wiring diagram

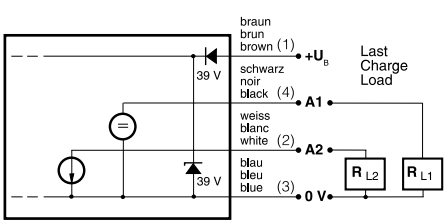

Steckerbelegung (Gerät)
Attribution des pins (appareil)
Pin assignment (device)

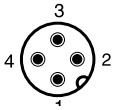

S12

CONTRINEX AG Industrial Electronics
route André Piller 50 - CH 1762 Givisiez - Switzerland - **Tel:** +41 26 460 46 46 - **Fax:** +41 26 460 46 40 - **Internet:** www.contrinex.com - **E-mail:** info@contrinex.com

Abmessungen / Dimensions / Dimensions:

Diese Zeichnungen lassen sich aus dem Internet (www.contrinex.com) herunterladen.
Ces dessins peuvent être téléchargés depuis Internet (www.contrinex.com).
These drawings can be downloaded from Internet (www.contrinex.com).

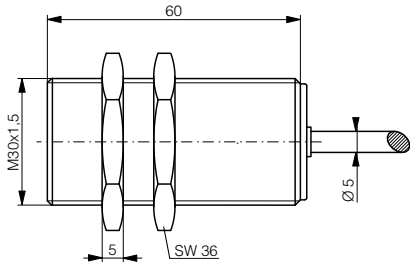

DW-AD-509-M30-390

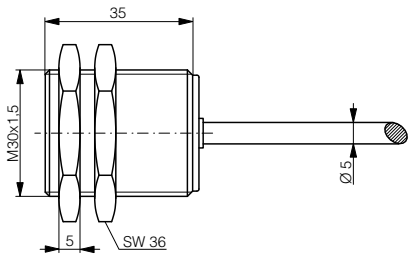

DW-AD-509-M30-320

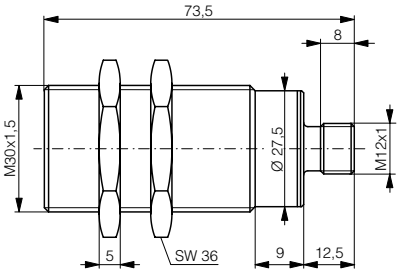

DW-AS-509-M30-390

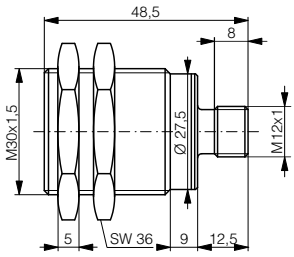

DW-AS-509-M30-320

Ansprechkurve* / Courbe de réponse* / Response diagram*:

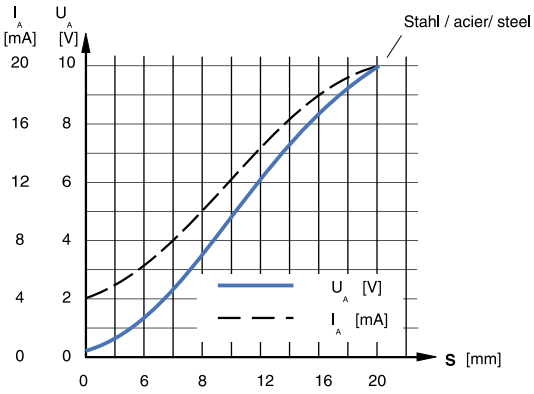

Fig. 2: Temperaturminderung / Réduction de température Temperature derating

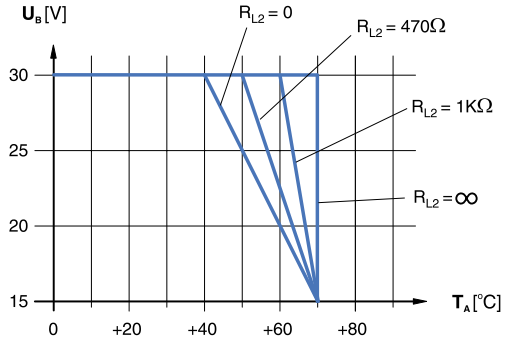

Fig. 3: Einbau / Montage / Installation

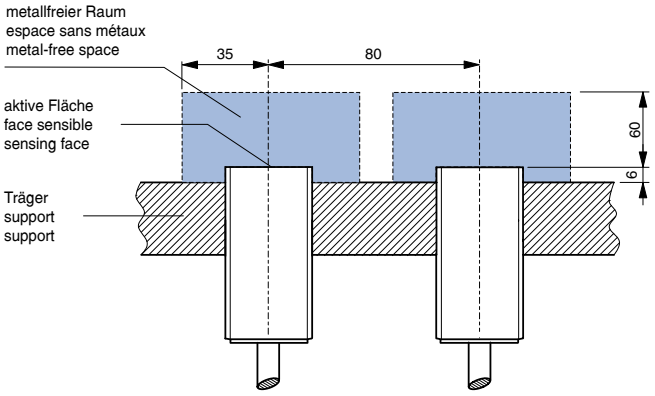

* typische Werte / valeurs typiques / typical values

Reduktionsfaktoren* / Coefficients de réduction* / Correction factors*

Stahl FE 360 Acier FE 360 Steel FE 360	**1,0**	Kupfer cuivre copper	**0,17**	Aluminium aluminium aluminum	**0,2**	Messing laiton brass	**0,3**	Edelstahl V2A acier INOX V2A stainless steel V2A	**0,65**

Typenspektrum / Types disponibles / Available types:

Artikelnummer Numéro article Part number	Typenbezeichnung désignation part reference	Anschluss raccordement connection	Ausgang sortie output
320 020 117	DW-AD-509-M30-390	Kabel / câble / cable	Spannung und Strom / tension et courant / voltage and current
320 020 118	DW-AS-509-M30-390	Stecker / connecteur / connector S12	Spannung und Strom / tension et courant / voltage and current
320 020 123	DW-AD-509-M30-320	Kabel / câble / cable	Spannung und Strom / tension et courant / voltage and current
320 020 124	DW-AS-509-M30-320	Stecker / connecteur / connector S12	Spannung und Strom / tension et courant / voltage and current

Der Einsatz dieser Geräte in Anwendungen, wo die **Sicherheit von Personen** von deren Funktion abhängt, ist **unzulässig**. Änderungen und Liefermöglichkeiten vorbehalten. Ces détecteurs **ne peuvent être utilisés** dans des applications où la **protection** ou la **sécurité** de **personnes** est concernée. Sous réserve de modifications et de possibilités de livraison. These proximity switches **must not be used** in applications where the **safety of people** is dependent on their functioning. Terms of delivery and rights to change design reserved.

CONTRINEX AG Industrial Electronics
route André Piller 50 - CH 1762 Givisiez - Switzerland - **Tel:** +41 26 460 46 46 - **Fax:** +41 26 460 46 40 - **Internet:** www.contrinex.com - **E-mail:** info@contrinex.com

Instruction Leaflet
Bedienungsanleitung
Feuille d'instructions

Uncompensated Pressure Transducers (GB)

Nichtkompensierte Druckmeßumformer (D)

Trasduttori di pressione non compensati (I)

Figures / Abbildung / Figura

①

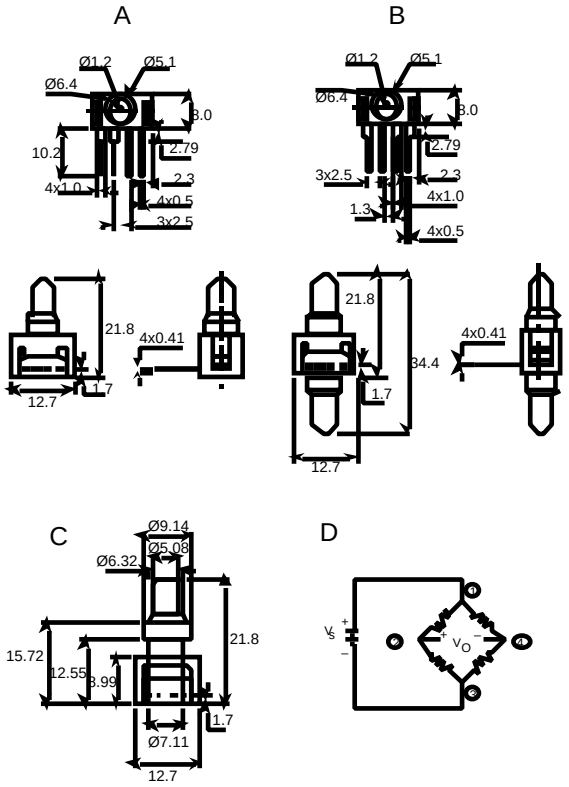

GB

Mounting dimensions

A. Gauge style-
Pressure is applied to port P2.
Port P1 vents to ambient pressure.
Pin 1 is notched, and is shown at the right of the package.
Pin 2 is next to pin 1, etc.
B. Differential style-
Port 1 is near terminals
C. Gauge style, 100 & 250psi only.
¼-28 UNF Thread
D. Electrical connections
Both types

Notes:-
1. Circled numbers refer to sensor terminals
2. Vo increases with pressure change P2>P1

Terminals:-
1. Pin 1 = Vs (+)
2. Pin 2 = Output (+)
3. Pin 3 = Ground (-)
4. Pin 4 = Output (-)
Pin 1 is notched, labeled on plastic.
Pin 2 next to Pin 1, etc.

D

Einbaumaße

A. Manometerausführung-
Der Druck wird auf den Anschluß P2 angelegt.
Der Anschluß P1 sorgt für den Umgebung-sdruck.
Stift 1 ist eingekerbt und auf derechten Seite dieser Ausführung abgebildet.
Stift 2 befindet sich in der Nähe von Stift 1 usw.
B. Differentialausführung
Anschluß 1 befindet sich in der Nähe der Klemmen.
C. Manometerausführung nur 100 & 250psi.¼ -28 UNF Gewinde
D. Elektrische Anschlüsse
Beide Ausführungen

Hinweise:

1. Die eingekreisten Ziffern beziehen sich auf Sensoranschlüsse.
2. Vo steigt bei Druckänderung P2>P1 an.

Anschlüsse:

1. Stift 1 = VS (+)
2. Stift 2 = Ausgang (+)
3. Stift 3 = Erde (-)
4. Stift 4 = Ausgang (-)
Stift 1 ist eingekerbt, auf Kunststoff markiert.
Stift 2 in der Nähe von Stift 1 usw.

I

Dimensioni di montaggio

A. Modello a indicatore-
La pressione viene applicata alla porta P2,
Porta P1 per lo sfogo alla pressione ambiente.
Il piedino 1 è intagiato ed è mostrato sulla destra della confezione.
Il piedino 2 è accanto al piedino 1, ecc.
B. Modello a differenziale -
La porta 1 è vicina ai terminali
C. Modello a indicatore, solo 100 e 250psi.
Filettatura UNF ¼-28
D. Collegamenti elettrici
Entrambi i modelli

Note:-

1. i numeri nei cerchietti si riferiscono i terminali del sensore
2. Vo aumenta con il cambiamento di pressione P2>P1

Terminali:-

1. Piedino 1 = Vs (+)
2. Piedino 2 = Uscita (+)
3. Piedino 3 = Massa (-)
4. Piedino 4 = Uscita (-)
Il piedino 1 è intagliato ed è etichettato su plastica.
Il piedino 2 è accanto al piedino 1, ecc.

GB **RS Stock No.**

Gauge 235-5762, 235-5784, 235-5807
235-5829, 235-5841, 235-5863, 235-5891
Differential 235-5778, 235-5790, 235-5813
235-5835, 235-5857, 235-5885, 235-5908

General

These pressure transducers are available in either a gauge or differential package. They are all based on a four active element piezo resistive bridge construction.
The gauge sensors use atmospheric pressure as a reference whereas the differential sensors will accept two independent pressure sources simultaneously.
Most sensors are supplied complete with steel lockring, however, the gauge versions of 100psi and 250psi have threaded parts (¼ - 28UNF) to assist in pipeline connections.

Measurand

Input media are limited to those media which will not attack polyethermide, fluorosilicone, or silicon.

Soldering

Limit soldering temperature to 315°C for 10 seconds duration maximum.

Cleaning

Apply cleaning fluids appropriate to the contaminants to be removed.

Selection chart

Type	**RS** stock no.
Gauge	
0.5psi	235-5762
1.0psi	235-5784
5.0psi	235-5807
15psi	235-5829
30psi	235-5841
100psi (1/4 - 28 unf)	235-5863
250psi (1/4 - 28 unf)	235-5891
Differential	
0.5psi	235-5778
1.0psi	235-5790
5.0psi	235-5813
15psi	235-5835
30psi	235-5857
100psi	235-5885
250psi	235-5908

Technical Specification

(All figure are typical unless otherwise stated)

	0.5psi	1.0psi	5.0psi	15psi	30psi	100psi	250psi
Full scale output;mV	35	45	115	225	330	225	212
Sensitivity per psi, mV	70	45	23	15	11	2.25	0.85
Overpressure (max)	20	20	20	45	60	200	500
Recommended Excitation	10v	10v	10v	10v	10v	10v	10v
Input resistance ohms	5k	5k	5k	5k	5k	5k	5k
Media Compatibility	Limited to those which will not attacpolyethermide, silicon or fluorosilicone						

RS Components shall not be liable for any liability or loss of any nature (howsoever caused and whether or not due to RS Components'negligence) which may result from the use of any information provided in **RS** technical literature.

D **RS Best-Nr.**

Manometer 235-5762, 235-5784, 235-5807
235-5829, 235-5841, 235-5863, 235-5891
Differential 235-5778, 235-5790, 235-5813
235-5835, 235-5857, 235-5885, 235-5908

Allgemeines

Diese Meßwertumformer sind entweder in Manometer- oder Differentialausführung erhältlich. Die Basis dieser Umformer bildet eine aus vier aktiven Elementen bestehende piezoresistive Meßbrückenkonstruktion.
Die Manometersensoren benutzen atmosphärischen Druck als Referenz, während die Differentialsensoren gleichzeitig zwei unabhängige Druckquellen akzeptieren.
Die meisten Sensoren werden komplett mit Sicherungsring aus Stahl geliefert. Die Manometerausführungen 100psi und 250psi haben Gewindeteile (¼ - 28UNF), was ihren Einsatz in Pipeline-Verbindungen ermöglicht.

Medienverträglicheit

Es dürfen nur Mittel eingelassen werden, die weder Polyethermid noch Siliziumfluor oder Silizium angreifen.

Löten

Die Löttemperatur ist auf 315°C für die Dauer von max. 10 Sekunden begrenzt.

Reinigen

Je nach Art der Verschmutzung entsprechende Reinigungsmittel auftragen.

Bestelltabelle

Typ	**RS** Best Nr.
Manometer	
0.5psi	235-5762
1.0psi	235-5784
5.0psi	235-5807
15psi	235-5829
30psi	235-5841
100psi (1/4 - 28 unf)	235-5863
250psi (1/4 - 28 unf)	235-5891
Differential	
0.5psi	235-5778
1.0psi	235-5790
5.0psi	235-5813
15psi	235-5835
30psi	235-5857
100psi	235-5885
250psi	235-5908

Technische Daten

(Gelten für alle Bestnummern, wenn nichts anderes angegeben ist)

	0.5psi	1.0psi	5.0psi	15psi	30psi	100psi	250psi
Vollbereichendwert;mV	35	45	115	225	330	225	212
Empfindlichkeit nach psi, mV	70	45	23	15	11	2.25	0.85
Überdruck (max.)	20	20	20	45	60	200	500
Empfohlene Versorgung	10v	10v	10v	10v	10v	10v	10v
Eingangswiderstand in Ohm	5k	5k	5k	5k	5k	5k	5k
Medienkompatibilität	Ist auf diejenigen begrenzt, die Polyethermid, Silizium oder Siliziumfluor nicht angreifen.						

RS Components haftet nicht für Verbindlichkeiten oder Schäden jedweder Art (ob auf Fahrlässigkeit von RS Components zurückzuführen oder nicht), die sich aus der Nutzung irgendwelcher der in den technischen Veröffentlichungen von **RS** enthaltenen Informationen ergeben.

I

RS Codici.

Indicatore 235-5762, 235-5784, 235-5807
235-5829, 235-5841, 235-5863, 235-5891
Differenziale 235-5778, 235-5790, 235-5813
235-5835, 235-5857, 235-5885, 235-5908

Informazioni generali

Questi trasduttori di pressione sono disponibili nel formato indicatore o differenziale. Sono tutti basati su una costruzione a ponte piezo-resistiva a quattro elementi attivi.
I sensori a indiactore utilizzano la pressione atmosferica come riferimento, mentre i sensori a differenziale accettano due fonti indipendenti di pressione simultaneamente.
La maggior parte dei sensori viene fornita con un anello di bloccaggio in acciaio, anche se le versioni a indicatore di 100psi e 250psi presentano parti filettate (¼ - 28UNF) per consentire le connessioni a tubazioni.

Compatibilità dei supporti

I supporti d'ingresso sono limitati a quelli che non attaccano polietermide, fluorosilicone o silicono.

Saldatura

Limitare la temperatura di saldatura a 315°C per 10 secondi massimo.

Pulizia

Usare detergenti liquidi adatti per i contaminanti da eliminare.

Tabella di selezione

Modello	Codice **RS**
Indicatore	
0.5psi	235-5762
1.0psi	235-5784
5.0psi	235-5807
15psi	235-5829
30psi	235-5841
100psi (1/4 - 28 unf)	235-5863
250psi (1/4 - 28 unf)	235-5891
Differential	
0.5psi	235-5778
1.0psi	235-5790
5.0psi	235-5813
15psi	235-5835
30psi	235-5857
100psi	235-5885
250psi	235-5908

Specifiche tecniche

(Tutti i valori sono tipici, salvo diversamente specificato)

	0.5psi	1.0psi	5.0psi	15psi	30psi	100psi	250psi
Uscita a fondo scala;mV	35	45	115	225	330	225	212
Sensibilità per psi, mV	70	45	23	15	11	2.25	0.85
Sovrapressione (max.)	20	20	20	45	60	200	500
Eccitazione consigliata	10v	10v	10v	10v	10v	10v	10v
Resistenza d'ingresso Ohm	5k	5k	5k	5k	5k	5k	5k
Compatibilità con supporti	Limitata a quei supporti che non attaccano polietermide, silicone o fluorosilicone						

La RS Components non si assume alcuna responsabilità in merito a perdite di qualsiasi natura (di qualunque causa e indipendentemente dal fatto che siano dovute alla negligenza della RS Components), che possono risultare dall'uso delle informazioni fornite nella documentazione tecnica.

UTILCELL
LOAD CELLS - WÄGEZELLEN

MODEL 190

15kg ... 400kg

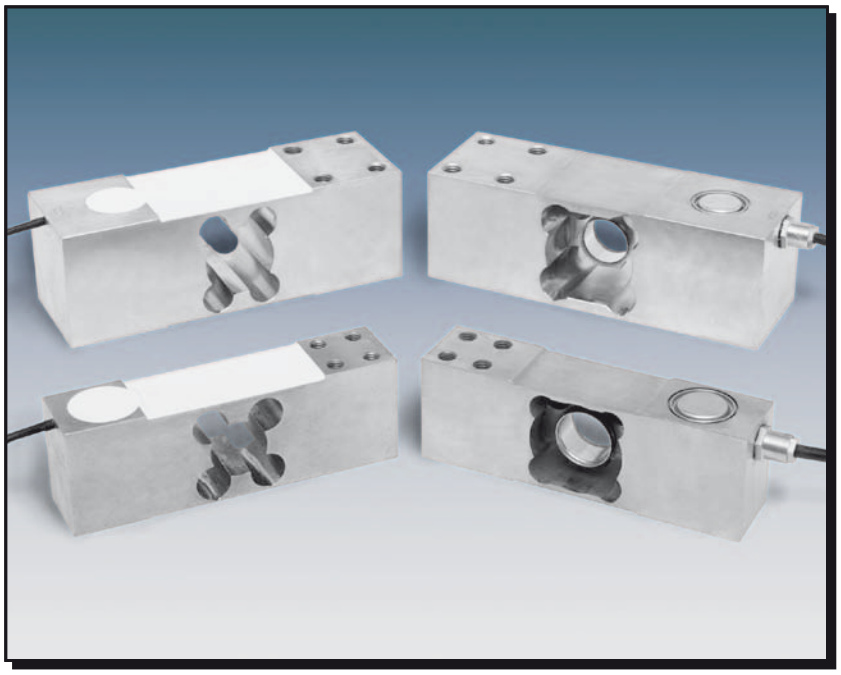

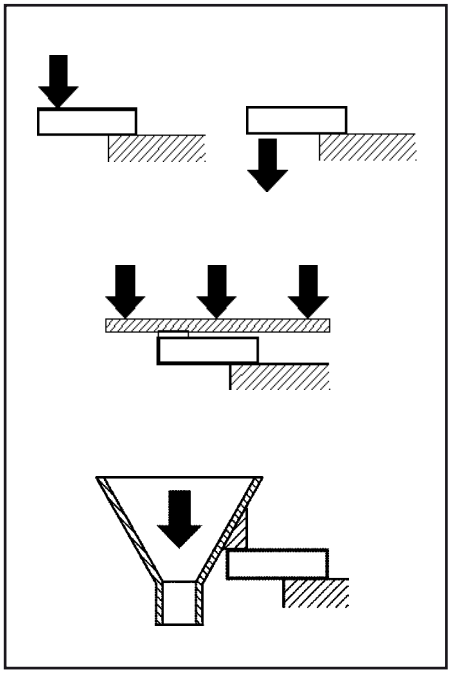

- Double bending beam load cell
- Versions:
  - **190 a** (50...400kg): Nickel-plated Steel alloy Silicone sealing, IP 66 (EN 60529), 4000 divisions O.I.M.L. R60 class C
  - **190i** (15...400kg): Fully Stainless Steel construction Hermetically sealed, fully welded, IP 68 (EN 60529) and IP 69K (ISO 20653), 3000 div. O.I.M.L. R60 class C
- High accuracy with off-center loads
- Available in ATEX version (optional) Zone 0-1-2 (gas) and 20-21-22 (dust)
- Applications: direct platform up to 600 x 600 mm or 800 x 800 mm; filling scales

- Doppelbiegebalkenprinzip
- Ausführungen:
  - **190 a** (50...400kg): Vernickelter Stahl, vergossen, IP 66 (EN 60529), 4000 Teile O.I.M.L. R60 Klasse C
  - **190i** (15...400kg): Edelstahl, hermetisch dicht, verschweißt, IP 68 (EN 60529) und IP 69K (ISO 20653), 3000 Teile O.I.M.L. R60 Klasse C
- Hohe Genauigkeit bei exzentrischer Lasteinleitung
- Erhältlich in ATEX -Ausführung (optional) Zone 0-1-2 (Gas) und 20-21-22 (Staub)
- Anwendungen: Plattformwaagen mit nur 1 Wägezelle, 600 x 600 mm oder 800 x 800 mm; Behälterwaagen

Model Modell	Nominal capacity Nennlast Ln	Accuracy class Genauigkeitsklasse n. OIML	Minimum division Kleinster Teilungswert vmin	Service load Gebrauchslast 150 % Ln	Platform Plattform A x B mm	Accuracy Genauigkeit 1/3 Ln
		a / i				
190 15 kg	15 kg	- / 3000	1.5 g	22.5 kg	600 x 600	3000 v
190 20 kg	20 kg	- / 3000	2 g	30 kg	600 x 600	3000 v
190 30 kg	30 kg	- / 3000	3 g	45 kg	600 x 600	3000 v
190 50 kg	50 kg	4000 / 3000	5 g	75 kg	600 x 600	3000 v
190 75 kg	75 kg	4000 / 3000	7.5 g	112.5 kg	600 x 600	3000 v
190 120 kg	120 kg	4000 / 3000	12 g	180 kg	600 x 600	3000 v
190 200 kg	200 kg	4000 / 3000	20 g	300 kg	600 x 600	3000 v
190 350 kg	350 kg	4000 / 3000	35 g	525 kg	600 x 600	3000 v
190 250 kg	250 kg	4000 / 3000	25 g	375 kg	800 x 800	3000 v
190 400 kg	400 kg	4000 / 3000	40 g	600 kg	800 x 800	3000 v

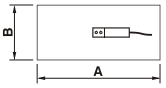

MODEL 190

Mod. 190a (50...400kg)

Mod. 190i (15...400kg)

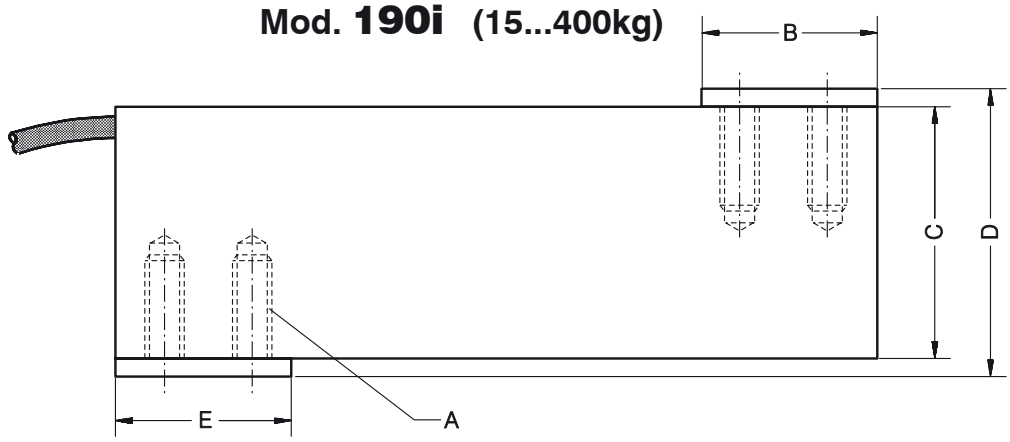

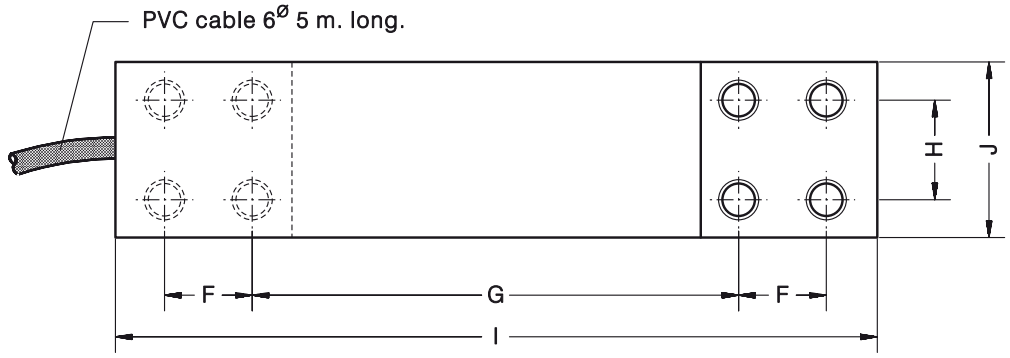

Nominal load (kg) Nennlast (kg)	A	B	C	D	E	F	G	H	I	J	Transport weight Transportgewicht
15-20-30-50-75-120-200-350	8 x M8 x 1.25 x 14	35	50	56	35	17	96	20	150	35	1.8 kg
250-400	8 x M10 x 1.5 x 20	50	60	66	50	30	100	40	180	60	4.3 kg

Dimensions in mm. *Abmessungen in mm.*

SPECIFICATIONS			TECHNISCHE DATEN
Nominal capacities (Ln)	15-20-30-50 75-120-200 350-250-400	kg	Nennlasten (Ln)
Accuracy class a / i	4000/3000	n. OIML	Genauigkeitsklasse a / i
Minimum dead load Service load Safe load limit	0 150 200	%Ln %Ln (1) %Ln (1)	Minimale Vorlast Gebrauchslast Grenzlast
Total error Repeatability error	< ±0.017 < ±0.01	%Sn (2) %Sn	Zusammengesetzter Fehler Wiederholgenauigkeit
Temperature effect: on zero on sensitivity	 < ±0.01 < ±0.006	 %Sn/5°K %Sn/5°K	Temperaturfehler: Nullpunkt Kennwert
Creep error (30 minutes)	< ±0.016	%Sn	Kriechfehler (30 min)
Temperature compensation Temperature limits	-10...+40 -20...+70	°C °C	Nenntemperaturbereich Arbeitstemperaturbereich
Nominal sensitivity (Sn) Nominal input voltage Maximum input voltage Input impedance Output impedance No load output Insulation resistance	2 ±10% 10 15 400 ±20 350 ±3 < ±2 > 5000	mV/V (3) V V Ω Ω %Sn MΩ	Nennkennwert (Sn) Nom. Speisespannung Max. Speisespannung Eingangswiderstand Ausgangswiderstand Nullsignaltoleranz Isolationswiderstand
Maximum deflection (at Ln)	0.3-0.5	mm	Nennmessweg (bei Ln)

(1) Only central loads on the load cell. Not for off-center loads
Nur bei zentrischer Belastung. Nicht bei exzentrischer Last
(2) Total error: Non Linearity and Hysteresis / Zusammengesetzter Fehler: Nichtlinearität und Hysterese
(3) 2 ±0.1% mV/V optional

ELECTRICAL CONNECTION
ELEKTRISCHER ANSCHLUSS:

MOD. 190a

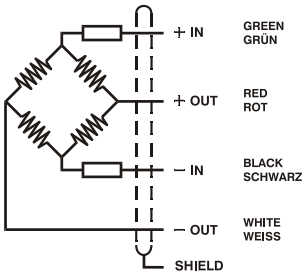

MOD. 190i

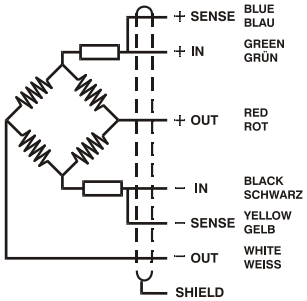

1347

MICRO-EPSILON

optoNCDT 1700 Intelligent sensor with integrated controller for industrial applications

The optoNCDT 1700 series is truly a world leading laser displacement sensor. Featuring Real Time Surface Compensation (RTSC), remote software programming and excellent linearity & resolution the optoNCDT 1700 is difficult to match at this price level. Integrated conditioning electronics allows the sensor to have a very unique and compact design.

Model		ILD 1700-2	ILD 1700-10	ILD 1700-20	ILD 1700-40	ILD 1700-50	ILD 1700-100	ILD 1700-200	ILD 1700-250VT	ILD 1700-500	ILD 1700-750
Measuring range		2mm	10mm	20mm	40mm	50mm	100mm	200mm	250mm	500mm	750mm
Start of measuring range	SMR	24mm	30mm	40mm	175mm	45mm	70mm	70mm	70mm	200mm	200mm
Midrange	MMR	25mm	35mm	50mm	195mm	70mm	120mm	170mm	195mm	450mm	575mm
End of measuring range	EMR	26mm	40mm	60mm	215mm	95mm	170mm	270mm	320mm	700mm	950mm
Linearity		2µm	8µm	16µm	32µm	40µm	80µm	200µm	630µm	400µm	750µm
	FSO	≤0.1%	≤0.08%					≤0.1%	≤0.25%	≤0.08%	≤0.1%
Resolution (at 2.5kHz without averaging)		0.1µm	0.5µm	1.5µm	4µm	3µm	6µm	12µm	50µm	30µm	50µm
Measuring rate		2.5kHz / 1.25kHz / 625Hz / 312.5Hz (adjustable)									
Light source		semiconductor laser <1mW, 670nm (red)									
Permissable ambient light	at 2.5kHz	10,000lx							15,000lx	10,000lx	
Laser safety class		class 2 acc. DIN EN 60825-1 : 2001-11									
Spot diameter	SMR	80µm	110µm	320µm	230µm	570µm	740µm	1300µm	1500µm	1500µm	1500µm
	MMR	35µm	50µm	45µm	210µm	55µm	60µm	1300µm	1500µm	1500µm	1500µm
	EMR	80µm	110µm	320µm	230µm	570µm	700µm	1300µm	1500µm	1500µm	1500µm
Temperature stability*		0.025% FSO/°C	0.01 % FSO/°C						0.025% FSO/°C	0.01 % FSO/°C	
Operation temperature		0 ...+50°C							0 ...+55°C	0 ...+50°C	
Storage temperature		-20 ... +70°C									
Output	measurements	selectable: 4 ... 20mA / 0 ... 10V / RS 422 / USB (optional with cable PC1700-3/USB)									
	switching outputs	1 x error or 2 x limit (each pogrammable)									
Switch Input		laser ON-OFF / zero									
Operation		via touch screen on sensor or via PC with ILD 1700 tool									
Power supply		24VDC (11 ... 30VDC), max. 150mA									
Electromagnetic compatibility (EMC)		EN 61000-6-3 EN 61000-6-2									
Sensor cable length (with connector)		0.25m (integrated cable with connector) option: 3m or 10m									
Synchronisation		possible for simultaneous or alternating measurements									
Protection class		IP 65									
Vibration		2g / 20 ... 500Hz									
Shock		15g / 6ms									
Weight (with 0.25m cable)		~ 550g			~ 600g		~ 550g			~ 600g	

FSO = Full Scale Output All specifications apply for a diffusely reflecting white ceramic target
*based on digital output
SMR = Start of measuring range MMR = Midrange EMR = End of measuring range

optoNCDT 1700 Dimensions and Accessories

optoNCDT 1700 (2/10/20/50/100/200/250VT)

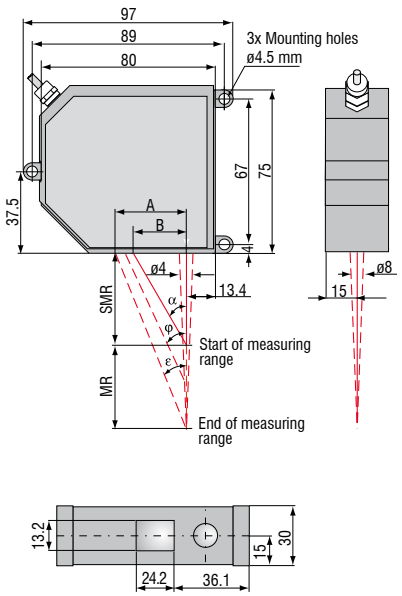

optoNCDT 1700 (40/500/750)

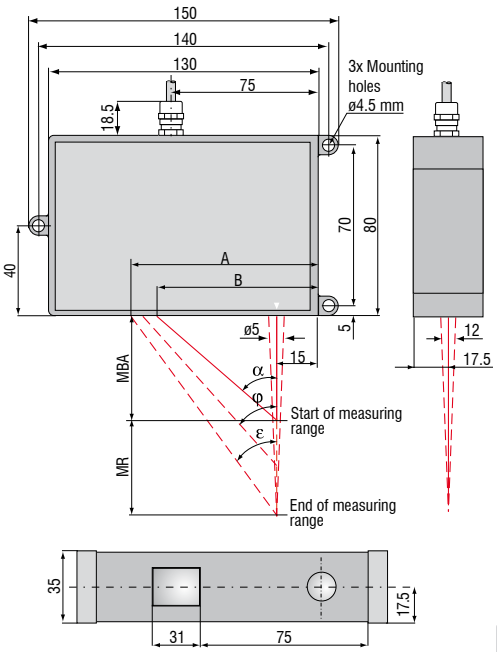

Connector (sensor side)
Article Number: 0323243

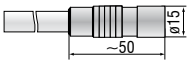

Connector (sensor cable)
Article Number: 0323272

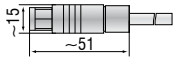

MR	SMR	α	φ	ε	A	B
2	24	35°	40°	44.8°	25.8	16.8
10	30	34.3°	35.2°	35.6°	28.7	20.5
20	40	28.8°	27.5°	26.7°	30.1	22.0
50	45	26.5°	23.0°	18.3°	31.5	22.5
100	70	19.0°	15.4°	10.9°	32.6	24.1
200	70	19.0°	9.78°	6.97°	33.1	24.1
250VT	70	19.0°	8.4°	6.0°	33.5	24.1
40	175	22.1°	21.9°	21.8°	101	86
500	200	19.3°	9.8°	7.0°	101	85
750	200	19.3°	7.7°	5.0°	101	85

Accessories optoNCDT 1700

Supply and output cable

PC 1700-3 (3 m)
PC 1700-10 (10 m)
PC 1700-10/3/IF2004 (10 m, for use with interface-card IF2004)
PC 1700-10/D-Sub/9-pol.
PC 1700-3/3/USB/BNC/US (power supply converter)
PC 1700-3/USB (3 m, with USB-RS422-converter, supply 90 ... 230 VAC)
PC1700-3/3/USB/OE/US (3 m, with USB-RS422-converter,supply 90 ... 230 VAC)

Power supply

PS 2010 (for top-hat rail mounting; L/W/H 120x120x40 mm Input 115 / 230 VAC selectable; output 24 VDC / 2.5 A)

Protective housing

SGx 1800 (for models ILD 1700-2/10/20/50/100/200/250VT)
SGx 2200-200 (for models ILD 1700-40/500/750)
SGxF 1800 (option with compressed air clean setup)
SGxF 2200-200 (option with compressed air clean setup)

Interface-card

IF2004 (RS422 PCI-interface-card for PC for 1-4 sensors optoNCDT or 3 sensors and 1 encoder)

External Trigger

Triggerbox 1700 (Electronics for triggering optoNCDT 1700 sensors. Acceptable trigger levels are from +2.4 VDC to +24 VDC, L/W/H 98x64x34 mm)

Display

CSP301 (digital processing and readout unit, pro grammable for two analog outputs)

Micro-Epsilon

info@micro-epsilon.com
www.micro-epsilon.com

info@micro-epsilon.co.uk
www.micro-epsilon.co.uk

info@micro-epsilon.us
www.micro-epsilon.us

certified DIN EN ISO 9001 : 2000
modifications reserved / Y9761161-C030059DGO

Bibliography

BAGNOLD, R. (1939) Interim report on wave-pressure research. *Tech. rep.*, Institution of Civil Engineeris

BERENGUER, J. AND BAONZA, A. (2006) Rubble mound breakwater crown wall design. In Proceedings of the National Conference of the Port and Coastal Technical Association, Algeciras, Spain (in Spanish)

BRADBURY, A. AND ALLSOP, N. (1988) P5. Hydraulic effects of breakwater crown walls. In Design of breakwaters, Thomas Telford Publishing. 385–396

BRAÑA, P.C. AND GUILLÉN, J.F. (2005) Wave forces on crown walls: evaluation of existing empirical formulations. In Coastal Engineering 2004: (In 4 Volumes), World Scientific. 4087–4099

BRUUN, P. (2013) Design and construction of mounds for breakwaters and coastal protection, vol. 37. Elsevier

BURCHARTH, H. (1992) Introduction of partial coefficients in the design of rubble mound breakwaters. *Coastal structures and breakwaters*

BURCHARTH, H.F., LIU, Z. AND TROCH, P. (1999) Scaling of core material in rubble mound breakwater model tests. In Fifth International Conference on Coastal and Port Engineering in Developing Countries. COPEDEC

CHEN, X., HOFLAND, B., ALTOMARE, C. AND UIJTTEWAAL, W. (2014) Overtopping flow impact on a vertical wall on a dike crest. *Coastal Engineering Proceedings*, 1(34), 4

CIRIA, C. *et al.* (2007) The rock manual. CIRIA London

GÜNBAK, A. AND GÖKCE, T. (1984) Wave screen stability of rubble-mound breakwaters. In International symposium of maritime structures in the Mediterranean Sea. Athens, Greece. 99–112

HUGHES, S.A. (2003) Estimating irregular wave runup on smooth, impermeable slopes. *Tech. rep.*, DTIC Document

IRIBARREN, R. AND NOGALES, C. (1964) Obras marítimas. *Ed. Dossat SA, Madrid*

JUUL JENSEN, O. (1984) A monograph on rubble mound breakwaters. *Tech. rep.*, Danish Hydraulic Institute (DHI)

LOSADA, I.J., DALRYMPLE, R.A. AND LOSADA, M.A. (1993) Water waves on crown breakwaters. *Journal of waterway, port, coastal, and ocean engineering*, 119(4), 367–380

LOSADA, M., MARTIN, F. AND MEDINA, R. (1995) Wave kinematics and dynamics in front of reflective structures. *Wave Forces on Inclined and Vertical Wall Structures*, 282–310

MANSARD, E.P. AND FUNKE, E. (1980) The measurement of incident and reflected spectra using a least squares method. In Coastal Engineering 1980. 154–172

MARTIN, F. (1995) Estudio hidrodinámico de la interacción de ondas de gravedad con estructuras reflejantes. Ph.D. thesis, Tese Doctoral, Universidad de Cantabria, Escuela Técnica Superior de Ingenieros de Caminos, Canales y Puertos

MARTIN, F.L., LOSADA, M.A. AND MEDINA, R. (1999) Wave loads on rubble mound breakwater crown walls. *Coastal Engineering*, 37(2), 149–174

NEGRO VALDECANTOS, V., LÓPEZ GUTIÉRREZ, J.S. AND POLVORINOS FLORS, J.I. (2013) Comparative study of breakwater crown wall–calculation methods. In Proceedings of the Institution of Civil Engineers-Maritime Engineering. Thomas Telford (ICE Publishing), vol. 166, 25–41

NØRGAARD, J.Q.H., ANDERSEN, T.L. AND BURCHARTH, H.F. (2013) Wave loads on rubble mound breakwater crown walls in deep and shallow water wave conditions. *Coastal Engineering*, 80, 137–147

OUMERACI, H., KLAMMER, P. AND PARTENSCKY, H. (1993) Classification of breaking wave loads on vertical structures. *Journal of waterway, port, coastal, and ocean engineering*, 119(4), 381–397

PEDERSEN, J. (1996) Wave forces and overtopping on crown walls of rubble mound breakwaters. *Phd*

PULLEN, T., ALLSOP, N., BRUCE, T., KORTENHAUS, A., SCH, H., VAN DER MEER, J. *et al.* (2007) Wave overtopping of sea defences and related structures: assessment

RAMACHANDRAN, K., GENZALEZ, R.R., OUMERACI, H., SCHIMMELS, S., KUDELLA, M., VAN DOORSLAER, K., DE ROUCK, J., VERSLUYS, T. AND TROUW, K. (2012) Loading of vertical walls by overtopping bores using pressure and force sensors-a large scale model study. *Coastal Engineering Proceedings*, 1(33), 44

VAN DER MEER, J.W. (1988) Rock slopes and gravel beaches under wave attack. Ph.D. thesis, TU Delft, Delft University of Technology

VAN DER MEER, J.W. AND STAM, C.J.M. (1992) Wave runup on smooth and rock slopes of coastal structures. *Journal of Waterway, Port, Coastal, and Ocean Engineering*, 118(5), 534–550

VERHAGEN, H., D'ANGREMOND, K. AND VAN ROODE, F. (2012) Breakwaters and closure dams. VSSD